University of California
Los Angeles

Kinetic Monte Carlo Simulations of Defect Nano-mechanics with Applications to Dislocation Dynamics in Irradiated α-Iron

A dissertation submitted in partial satisfaction
of the requirements for the degree
Doctor of Philosophy in Mechanical Engineering

by

Ming Wen

2005

The dissertation of Ming Wen is approved.

D.C.H. Yang

J.-W. Ju

G.P. Carman

N.M. Ghoniem, Committee Chair

University of California, Los Angeles

2005

To my parents and my wife . . .

for their love and support

TABLE OF CONTENTS

List of Figures

LIST OF TABLES

ACKNOWLEDGMENTS

VITA

1974	Born, Jianshi County, Hubei Province, China.
1991-1996	B.S., Engineering Mechanics, Tsinghua University, Beijing, China.
2000-2005	PhD, Mechanical and Aerospace Engineering, University of California, Los Angeles, USA.

PUBLICATIONS

Ming Wen, Nasr M. Ghoniem and Bachu N. Singh, ”Dislocation Decoration and Raft Formation in Irradiated Materials”, *Philosophical Magazine A*, 85(22): (2005) 2561-2580.

Nasr M. Ghoniem, Shih-Hsi Tong, Jianming Huang, Bach N. Singh and Ming Wen, ”Mechanisms of Dislocation-Defect Interactions in Irradiated Metals Investigated by Computer Simulations”, *Journal of Nuclear Materials*, 307-311: (2002) 843-851.

Ming Wen, C.H. Woo and Hanchen Huang, ”Atomistic Studies of Stress Effects on Self-Interstitial Diffusion in α-Titanium”, *Journal of Computer-Aided Materials Design*, 7(2): (2000) 97-110.

Ming Wen, Quan-Shui Zheng, and Danxu Du, "Some Basic Problems in Numerically Simulating Effective Properties and Local Fields of Composite Materials", *Acta Mechanica Solida Sinica*, 12(4): (1999) 328-339.

Abstract of the Dissertation

Kinetic Monte Carlo Simulations of Defect Nano-mechanics with Applications to Dislocation Dynamics in Irradiated α-Iron

by

Ming Wen

Doctor of Philosophy in Mechanical Engineering
University of California, Los Angeles, 2005
Professor N.M. Ghoniem, Chair

Experimental observations of dislocation decoration with Self Interstitial Atom (SIA) clusters, and of SIA cluster rafts are analyzed to establish the mechanisms controlling these phenomena in bcc metals. The elastic interaction between SIA clusters, and between clusters and dislocations is included in Kinetic Monte Carlo (KMC) simulations of damage evolution in irradiated bcc metals. The results indicate that SIA clusters, which normally migrate by 1-D glide, rotate due to their elastic interactions, and that this rotation is necessary to explain experimentally-observed dislocation decoration and raft formation in neutron-irradiated pure iron. The critical dose for raft formation in iron is shown to depend on the intrinsic glide/ rotation characteristics of SIA clusters. The model is compared with experimental observations for the evolution of defect cluster densities (sessile SIA clusters and nano-voids), dislocation decoration characteristics, and the conditions for raft formation.

need additional material for last part

CHAPTER 1

INTRODUCTION

1.1 EFFECTS OF NEUTRON IRRADIATION ON MECHANICAL PROPERTIES OF MATERIALS

With the ~~constant~~ continuous increase in energy consumption, nuclear power has been regaining ~~stature~~ recognition as a serious alternative energy source ~~other than~~ to replace fossil fuel based sources. Among all the debates surrounding nuclear energy, the safety issue is no doubt one of the biggest concerns. Most materials experience dramatic mechanical and physical property changes when irradiated by energetic particles, such as fission or fusion neutrons [1]. Radiation damage plays a decisive role in the lifetime and safety of components used in current fission power plants, and thus indirectly affects the economy of fission power. For proposed future fusion reactors, radiation damage caused by the interaction of fusion plasma ions and neutron-induced recoils with the first walls, structures, and other functional materials is a major challenge in the realization of fusion power [2, 3, 4, 5, 6, 7].

It is well established that neutron irradiation causes a substantial amount of hardening and changes significantly the deformation behavior of metals and alloys, particularly at irradiation temperatures below the recovery stage V (i.e. $< 0.4\ T_m$ where T_m is the melting temperature). Since the early investigation of irradiation hardening by McReynolds et al. [10] and Bleweitt et al. [11], the effect of irradiation on mechanical properties has been a subject of extensive

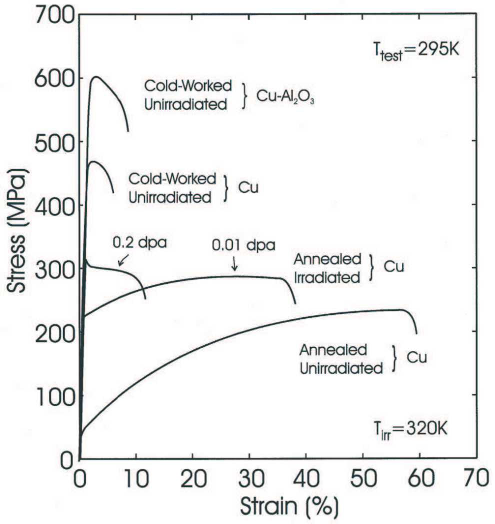

Figure 1.1: Experimental stress-strain curves for irradiated and unirradiated copper. Specimens were irradiated in the DR-3 reactor at Risø National Laboratory at 320 K, and tensile tested at 295 and 320K [8].

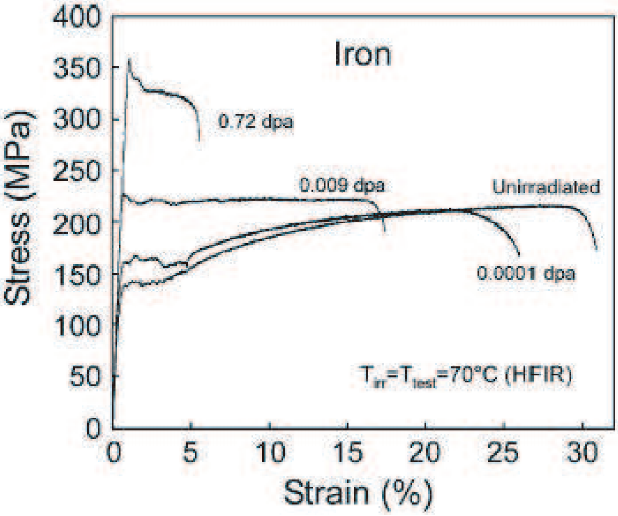

Figure 1.2: Experimental stress-strain curves for irradiated and unirradiated pure iron. Irradiations were conducted in the High Flux Isotope Reactor (HFIR) at Oak Ridge National Laboratory (ORNL) at about 70 °C, and tensile tested at 70 °C. [9].

investigation for more than 40 years. The post-irradiation deformation experiments (i.e. tensile tests) with measurements of the stress-strain curve and the yield stress have consistently illustrated the three significant changes induced by neutron irradiation. First, it is noted that the yield strength of metals and alloys increases with increasing neutron dose level. These effects are ~~quite~~ very considerabl~~y~~le; for example, the yield stress for 0.2 displacements per atom (dpa) was increased by a factor of more than 6 in figure 1.1 [8]. Second, it is observed that materials irradiated to a displacement dose beyond a certain level exhibit the phenomenon of a sharp and prominent yield drop, and that the magnitude of yield drop increases with increasing dose level. Third, the irradiation causes almost a complete loss of work hardening ability and a severe reduction in uniform plastic elongation (i.e. ductility) as measured in a uniaxial tensile test. The decrease in tensile ductility associated with low temperature neutron irradiation was the topic of an overwhelming amount of studies performed in the the 1950s and 1960s, and the phenomenon was commonly referred to as low temperature radiation embrittlement. A more appropriate term for the low uniform elongation typically observed following low temperature irradiation is the loss of strain hardening capacity. Under these conditions, in many cases ~~the~~ specimens show a clear sign of plastic instability immediately beyond the yield drop. It is interesting to note that these plastic deformation characteristics such as yield drop, lack of work hardening and increase in yield stress with increasing dose levels observed in copper (figure 1.1) are not isolated observations for particular crystal structures. In fact, these characteristics are common to all three crystal structures, fcc, bcc and hcp (see Ref. [12] for a review). Figure 1.1 and 1.2 demonstrate the similar deformation behavior reported for fcc copper irradiated at 320 K [8] and bcc iron irradiated at 70 °C [9].

One of the most striking microstructural features emerging from post-irradiation

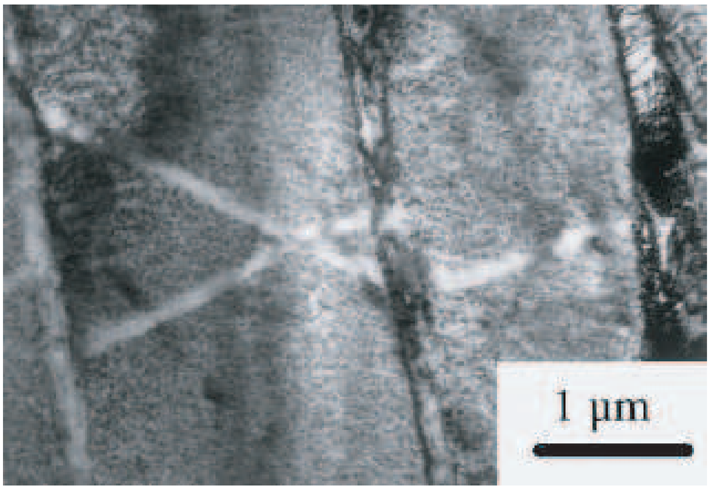

Figure 1.3: Example of cleared dislocation channels formed in pure iron irradiated at 320 K to 3.75×10^{-1} dpa and tensile tested at 320 K [13].

investigations is the observation of 'cleared' dislocation channels, narrow bands of material (∼50-200 nm in width) often completely cleared of the defects produced during irradiation by the successive passage of dislocations generated from some dislocation source within the material. The post-deformation microstructure of irradiated materials displaying a prominent yield drop clearly indicates that the plastic deformation is initiated in a very localized fashion and confined almost exclusively to the 'cleared' channels (see Ref. [14] for a review). An example of localized plastic flow in irradiated pure iron is shown in figure 1.3. Plastic flow localization will eventually lead to loss of ductility and premature failure. It is this prospect of irradiation induced drastic decrease in ductility and the possibility of initiation of plastic instability that has given rise to a serious concern regarding the mechanical performance and lifetime of materials used in structural components of a fission or a fusion reactor. The changes in mechanical properties result from corresponding changes in the material microstructure. Therefore, the key to understanding and predicting mechanical behavior changes during irradiation relies on having a detailed understanding of both the materials microstructure evolution during irradiation and the connection between microstructure and mechanical properties.

1.2 DEFINITIONS AND TERMINOLOGY

A number of important physical phenomena take place when energetic particles penetrate through solids. Those macroscopic, observable, and often technologically significant results induced by the bombarding particles are collectively known know as **radiation effects**.The area of radiation damage and effects is concerned with the investigation of microscopic and macroscopic phenomena resulting from the immediate interaction of high-energy particle s with solid materials. The microstructure of irradiated materials evolves over a wide range of length and time scales, making radiation damage an inherently multiscale phenomenon.

In a fission or fusion reactor, neutrons will transfer substantial energy to a stationary lattice atom in a collision, which is of the order of hundreds to thousands of kiloelectron volts (KeV). This amount of energy is so much greater than the energy binding the atom in its lattice site, namely the **displacement threshold energy**, that the struck atom is permanently displaced from its equilibrium lattice site. The empty lattice site left behind by the displaced atom is called a **vacancy**. The displaced atom which is situated between the normal sites of the lattice is referred to as an **interstitial**. If an interstitial atom is of the same nature with the atoms of the matrix lattice, it is said to be a **self-interstitial atom** (SIA). The combination of an interstitial and a vacancy is termed a **Frenkel pair**.

The lattice atom first stuck and displaced by the incident particle possesses is called the **primary knock-on atom**, or PKA. A PKA can possesses enough energy to impart a fraction of its energy to neighboring lattice atoms, and therefore create additional lattice displacements. These subsequent generation of displaced lattice atoms are known as **secondary ~~order~~ knock-on atoms** (SKAs) or recoil atoms. The recoils can become energetic particles in their own right and are capable of resulting in more recoils as long as their energy is above the displacement threshold. The collection of point defects of both interstitial or vacancy types generated by a single primary knock-on atom is defined as a **collision cascade**. In addition, higher-energy cascades may be expected to break up into several local damage zones called **subcascades**.

A cascade exhibits two main stages as it evolves with time. The first is a ballistic or collision phase lasting a few tenths of a picosencond, during which the energy of the PKA is distributed by multiple collisions among many atoms, with the result that they leave their lattice sites. This creates a central disordered core surrounded by regions of crystal displaced outwards. ~~In~~ During the second phase, ~~in addition to the displaced atoms~~ the atomic collisions of ~~the nucleons~~ displaced atoms generate sufficient thermal agitation that the highly disrupted core region of atoms may be considered to have been raised to a temperature above the melting point, producing what is referred to as a **thermal spike**. The Thermal-spike phase lasts several ps and the hot disordered core initially acquires some liquid-like characteristics. During this phase, the majority of the displaced atoms in the outer regions return by athermal relaxation to lattice sites in less than one ps, but strong disorder persists in the core for a longer time (several ps). This process can be viewed as a short term local melting followed by a rapid **quenching** of the liquid phase to form a damaged solid structure in the bombardment affected region. The atoms that are unable to regain lattice sites during this final stage become self-interstitial atoms at the periphery of the core and, together with the vacant sites produced when the core crystallizes, form the **primary damage state** - ‘primary’ in the sense that damage is produced directly in displacement cascade - of irradiation during this short time frame [15]. Following the quenching stage of the thermal spike, further rearrangement and interaction of the surviving defects take place by normal, thermally-activated diffusion of mobile defects.

Radiation damage is not restricted to ~~the~~ isolated point defects produced by the incident particles. Actually, vacancies and interstitials can be produced so close to each other that clustering of ~~the~~ point defects takes place spontaneously within the short time frame of the primary damage state. ~~The~~ Point defect **clusters** created in displacement cascades can be thermally stable and behave very differently from ~~the~~ component individual point defects in a kinematic sense.

Because of the proximity of point defects in a displacement cascade, a large portion of ~~the~~ point defects produced by ~~the~~ high-energy collisions are almost instantaneously annihilated by the spontaneous recombination of unstable Frenkel pairs within their nascent cascade. In fact, the fraction of point defects, which actually survives a cascade and is capable of producing observable radiation effects, is of the most interest. ~~The~~ Point defects and some of their clusters become mobile by thermal activation at elevated temperatures. Therefore, soon after production in cascades, some defects will be able to escape their nascent cascade and migrate long distances in the matrix, thus contributing to the formation and evolution of the microstructure by interactions between themselves, as well as with extended microstructures, such as dislocations and grain boundaries. These dynamic processes that occur after the primary stage are diffusional, involving much longer length and time scales than that of the primary damage state.

1.3 SCOPE OF THIS THESIS

The defects created in cascades form the primary damage state and their subsequent evolution gives rise to important changes in the mechanical properties of metals. The primary objective of this thesis is to develop numerical simulation techniques to investigate the evolution of microstructure in irradiated bcc metals and its effects on the motion of dislocations. In Chapter 2, we review the experimental evidence of microstructure features under neutron irradiation, including dislocation decoration and formation of SIA loop rafts. In Chapter 3, the general Kinetic Monte Carlo (KMC) scheme and related subjects are briefly described. In the following chapter, a general elastic model, which is capable of evaluating the elastic interaction between atomic-size defects is introduced. An application of the model to perfect defect clusters is also presented. In Chapter 5, using the elastic model described in ~~the previous~~ Chapter 4, we developed a KMC-based approach describing ~~the~~ microstructure evolution under displacement cascades, damage, ~~with~~ and incorporating the elastic interaction between defects. The main features of the model are provided as well. In what follows we use the ~~new~~ developed KMC model to investigate the mechanisms of dislocation decoration and raft formation, as well as the kinetics of damage accumulation under low doses ~~of cascade-producing~~ irradiation in bcc iron at room temperature. Results of the model and comparison with experiments are also described in the same chapter. The dynamics of individual dislocations, their inertial mass, as well as interactions with radiation-induced microstructures are then investigated in Chapter 7. Finally, Chapter 8 concludes the present dissertation on ~~the~~ modeling ~~of~~ microstructure evolution in neutron-irradiated materials as well as the dynamics of dislocation interaction with radiation-induced defects. ~~The~~ Finally, related future research is briefly discussed.

CHAPTER 2

EVIDENCE OF DISLOCATION DECORATION AND RAFTS

Because of the rich variety of physical phenomena and the technological importance associated with these phenomena,

The microstructure evolution in both fcc and bcc metals produced by neutron irradiation has been extensively studied ~~for a long period of time~~. Under neutron irradiation, primary defect clusters, which are directly produced in displacement ~~cascade,~~ cascades play an important role in microstructure evolution and changes in properties of irradiated materials. Evidence for the existence of self-interstitial atom (SIA) and vacancy clusters within the cascade volume has been provided by experimental observations as well as by computer simulations. For example, Diffuse X-ray scattering on fast neutron irradiated metals at temperatures below stage I provide evidence for spontaneous SIA cluster formation in cascades [16, 17, 18]. Molecular dynamics (MD) studies have also established the fact that SIA clusters are produced directly in high energy cascades without the need for diffusion during the cooling down phase of the cascade [15, 19, 20, 21, 22, 23, 24, 25, 26]. Small interstitial loops can further organize to make up patches or *rafts* at elevated temperatures [27, 28, 29], and dislocations are often heavily decorated by SIA clusters in the form of small interstitial loops [12, 28, 30]. Under some conditions, say a high temperature for instance, a raft of small closely spaced loops becomes unstable ~~due to easy proceeding of glide and climb~~, and can eventually ~~result in~~ agglomerate into a large dislocation loop [27].

2.1 EXPERIMENTAL OBSERVATIONS

Using Foreman and Eshelby's [31] calculation of the elastic interaction of prismatic dislocation loops, Barnes [32] presented a primary discussion on the migration of point defects by slip or climb or by both processes, and suggested a "rafts" configuration of loops which resulted from loops interacting elastically with others on neighbouring basal plane and thereby adjusting their positions and orientations to take up low energy positions. The experimental observation of rafts of loops was provided for graphite irradiated at 150 °C and subsequently annealed as well [32]. A comprehensive and systematic investigation of the development of microstructure as a function of irradiation temperature was later executed by Brimhall and Mastel [27] for molybdenum in 1970. Even though the formation of rafts of small interstitial clusters/loops is one of the most striking features under cascade damage conditions and has been found for quite some time, this phenomenon has not been investigated systematically in the past. Brimhall and Maslel's ~~Masterl's~~ work still remains to be the most recognized on the mechanism of raft formation so far. They were the first to report the observation of raft formation in Mo. Through use of transmission electron microscopy (TEM), it was found that at low irradiation temperatures, ∼ 50 °C, existing small dislocation loops, presumably interstitial, grow by point defect addition. At intermediate temperatures, 400 to 600 °C, small interstitial loops can migrate and agglomerate into rafts. At high temperatures, 600 to 800 °C, the loops are highly mobile to form large loops, and eventually interact with each other to produce a coarse dislocation network. They discussed the possible mechanisms of formation of loops rafts and dislocation decoration by loops and attributed them to loop glide combine with self-climb, though their treatment was limited to higher temperatures where both prismatic glide and conservative climb were both operative. Eyre, Maher and Bartlett [33] have carried out experimental observations and theoretical calculations on the damage structures in molybdenum irradiated by neutrons, and concluded that the growth of interstitial loops during post-irradiation annealing also occurs by a combined glide and climb mechanism.

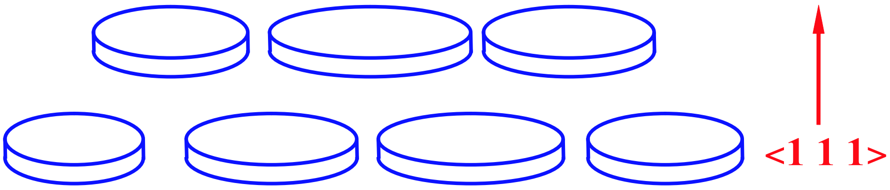

Figure 2.1: Idealized representation of ~~an~~ a side view of prismatic edge dislocation loops comprising a raft

Brimhall and Mastel [27] assumed that prismatic gliding of loops did not occur at 323 K. However, recent molecular dynamics simulations have demonstrated that small SIA loops glide rapidly via correlated diffusion of SIAs in the clusters/loops [20], and furthermore, Trinkaus et al. [30] have shown that the decoration of dislocation and formation of rafts are attributed to the one-dimensional glide of SIA clusters to a great extent. An idealized configuration for a raft [27] was also proposed with using the elastic calculations by Foreman and Eshelby [31]. The edge-on representation of the configuration for this idealized raft is shown in figure 2.1. Elastic analysis shows that loops lying at 42.4° with respect to one another render a minimum interaction energy and form a stable configuration. It was believed that rafts formed by loops having identical Burgers vectors gliding together as a result of the elastic interaction between the loops, but being prevented from complete coalescence by the limiting process of self climb [29]. Since then, more subsequent experimental observation of raft formation in Mo and TZM (Mo-0.5Ti-0.1Zr) have been reported [34, 29, 35, 36, 37, 38]. The

compare to page 78

single crystal

formation of rafts of interstitial loops in the ~~monocrystalline~~ Mo was observed to occurring at a relatively low dose level of 5.4×10^{-3} dpa [38]. The segregation of the microstructure into rafts of loops and isolated loops eventually leads to a very heterogeneous microstructure at a dose level of 0.16 dpa. Eldrup and his co-workers [9] investigated the difference in defect accumulation behavior, mainly concerned about void nucleation and growth, between fcc Cu and bcc Fe under neutron irradiation to fluences in the range of 10^{-4} to 0.8 dpa. TEM observations show that the density of SIA clusters both in Fe and Cu first increases with dose. At doses higher than $\simeq 0.01$ dpa, the clusters begin to segregate and form rafts of SIA clusters. The formation of the rafts-like structures is significantly more efficient in bcc Fe than in fcc Cu. A TEM photograph of formation of rafts of loops in Fe irradiated to a dose of 0.72 dpa was presented, the engineering stress-strain curve by tensile test for the iron specimen irradiated to 0.72 dpa exhibited a strong yield drop as well. In their experimental observations on void formations in nickel 270 irradiated from 1×10^{18} to 1.5×10^{22} neutrons/cm^2 at various temperatures, Stiegler and Bloom [28] also reported rafts of small, perfect dislocation loops, which they presumed as interstitial, were dispersed throughout the specimens. Most experimental results suggest that a raft is made up of a bunch of clusters of small interstitial loops, all having the same Burgers vector, the raft as a whole having a clear $< 111 >$ habit plane identical to the Burgers vector of the loops. The size and distribution of rafts are heavily depended on the material purity, irradiation temperature and irradiation dose, and the size spectrum may range from ~100 Å to more than 1000 Å [27, 29].

In many microstructural studies of neutron irradiated metals and alloys segregation of small dislocation loops of SIA type is often observed in the vicinity of grow-in dislocations in form of a ‘Cottrell-like’ atmosphere [39]. Figure 2.2 shows the structure of a coarse dislocation network with a high concentration of small

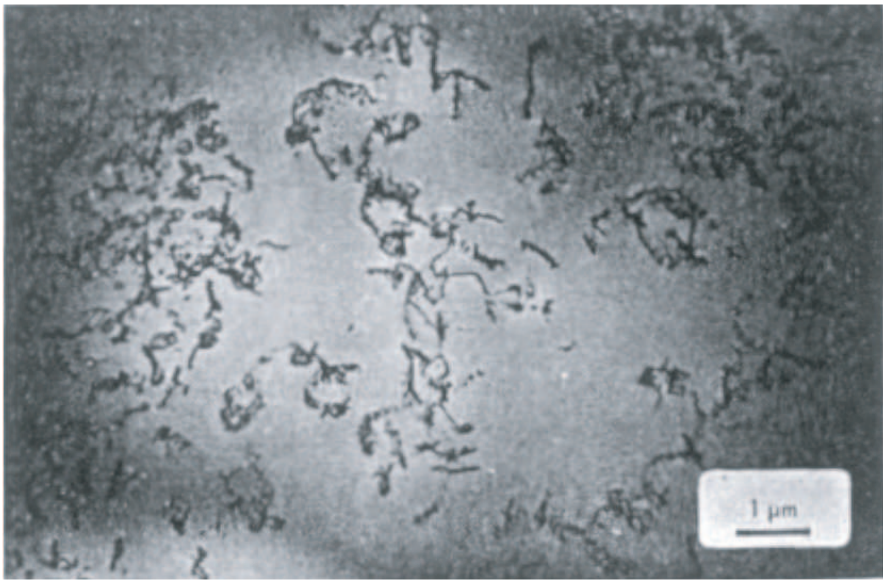

Figure 2.2: Dislocation structure in Nickel 270 irradiated to a fluence of 3.2×10^19 neutron/cm^2 [28].

loops located on or near the dislocation lines in Nickel 270 irradiated to a fluence of 3.2×10^{19} neutrons/cm^2 [28]. The phenomenon of decoration of dislocations by small interstitial loops under cascade damage conditions have been observed in a wide range of metals and alloys, for instance, pure nickel irradiated with 14 MeV neutrons at 300 K [40] and 560 K [41], Ni$-$2 at.% Cu and Ni$-$2 at.% Ge alloys irradiated with 14 MeV neutrons at 563K [41], pure copper and copper alloys irradiated with 14 MeV neutrons at 473 K [42], molybdenum irradiated at 500 ^{O}C to a fluence of 5.7 $\times 10^{19}$ neutrons/cm^2[27], and pure single crystal of molybdenum irradiated with fission neutrons to a dose level of 1.6×10^{-1} dpa at 320 K [38].

2.2 THE ~~THEORETICAL ANALYSIS ON~~ MECHANISMS OF DISLOCATION DECORATION AND RADIATION HARDENING

Being associated with post-irradiation deformation behavior and post-deformation microstructures, properties of clusters of vacancies and SIAs have received considerable attentions because of their significant effects on microstructure evolution~~s~~. Deeper ~~The escalation of~~ understanding of the mechanisms of the production, migration, and ~~characters~~ characteristics of an ~~the~~ SIA clusters has lead to the development of dislocation- and production-bias [43] theories in terms of defect production and reaction kinetics to explain long-term damage accumulation and microstructure evolution in irradiated materials. In ~~in~~ particular, the heterogeneous and segregated features of microstructure under cascade damage conditions are now clearly established. The production of stable SIA clusters in cascades in combination with the decay of vacancy clusters in the ~~at~~ void swelling temperature range provides a remarkable driving force for void swelling, which has been called 'production bias'. ~~on the condition that~~ On the other hand, a considerably large number of stable SIA clusters are ~~were~~ annihilated preferentially at extend sinks such as dislocations, grain boundaries and surfaces, leading to the accumulation of vacancies into voids and driving further volumetric swelling.

Of particular interest here is the ~~already-mentioned microstructure features~~ ~~of~~ the formation of rafts of small dislocation loops, and the decoration of dislocation sources by loops. The available evidences on dislocation decoration ~~could be~~ date ~~dated~~ back to ~~as~~ early ~~as~~ the discovery of raft formation (see Section 2.1), but it is rather limited and scattered in the literature~~s~~. No attempt was made to systematically study the phenomenon of dislocation decoration until Trinkaus, Singh and Foreman [30] took the first step to define ~~leap on~~ the mechanisms for decoration of dislocations by small SIA loops. One earlier mechanism, which was suggested by Makin[44] that the decoration of a dislocation by loops might result from the sweeping of glissile SIA loops during the motion of the dislocation, was first ruled out by examining the fact that the accumulation of SIAs near the dislocation continues even when the dislocations are ~~locked~~ sessile. Calculations also show~~s~~ that strain enhanced clustering of single three-dimensionally migrating SIAs is unlikely to produce the observed decoration phenomena, so is the metastable one-dimensionally migrating crowdion. The model proposed by Trinkaus et al.[30] concludes that the trapping and accumulation of glissile SIA loops in terms of one-dimensional motion is the dominant mechanism corresponding to the occurrence of dislocation decoration and raft formation. A concept of stand-off distance is introduced such that SIA clusters approaching the dislocation within the range of the stand-off distance get absorbed into the dislocation by spontaneously Burgers vector changes or climb and the loop accumulation can take place only outside this region[12]. Based on the analysis of experimental measurements of plastic deformation in metals irradiated with fission neutrons, in conjunction with the microstructure feature of dislocation decoration, Singh et al.[12] proposed the so-called 'cascade-induced source hardening'(CISH) model to explain the characteristic features in the deformation behavior of metals and alloys under cascade damage conditions, such as the increase ~~of~~ the upper yield stress without dislocation generation and followed by a yield drop and plastic instability. In the model, it is postulated that a dislocation decorated with interstitial loops is confined by the surrounding atmosphere of interstitial loops and thus unable to move ~~as supposed~~ until the applied resolved stress reaches a high level so that the dislocation can be released from cluster atmospheres in the vicinity of the dislocation glide plane. The CISH model was used to estimate the stress necessary to unlock trapped dislocations from the atmosphere of loops surrounding them, so that these detrapped dislocations can operate as dislocation sources. The increase in the critical resolved shear stress (CRSS), $\Delta\tau$, was shown by Singh et al.[12] to be given by

$$\Delta\tau \simeq 0.1\mu(b/l)(d/y)^2 \tag{2.1}$$

where μ is the shear modulus, b is the magnitude of the Burgers vector, l is the average separation of obstacles, and d and y are the defect diameter and stand-off distance, respectively.

In addition to the ~~recent~~ CISH model, there are ~~some~~ other theories of radiation hardening used for experimental data interpretation. In those models, the hardening and embrittlement (decrease~~s~~ in tensile ductility and fracture toughness) that occur in irradiated metals are considered to be controlled by interactions between dislocations and defect clusters. In an early effort to explain the observed increase in the yield stress of plastic deformation due to neutron irradiation, Seeger proposed the so-called ‘Zone Theory’of radiation hardening[45]. It was deemed that the increase in the critical shear stress was attributed to dislocation interaction with radiation-induced obstacles, which were referred to as depleted zones formed during neutron irradiation. This is similar to the model used to compute matrix hardening by barriers to dislocation motion ~~was~~ developed by Orowan[46] for the ‘by-passing’of impenetrable obstacles by bowing of dislocation segments around them. Based on Orowan’s model, the most commonly ~~express~~ expression for the change in shear stress induced ~~in~~ on the dislocation glide plane by a regular array of defects is ~~shown in the following equation~~: is given by

$$\Delta\tau = \alpha\mu b/l \tag{2.2}$$

where α is a parameter representing the obstacle strength. In principle, α is determined by the angle between adjacent dislocation segments at the point where the dislocation breaks free of the obstacle[47]; if the critical angle is ϕ, $\alpha = \cos(\phi/2)$. For the case of a random array of obstacles of diameter d and volume density N, $l = 1/\sqrt{Nd}$. Thus Equation 2.2 becomes

$$\Delta\tau = \alpha\mu b\sqrt{Nd} \tag{2.3}$$

Hirsch

This model is most appropriate for strong obstacles. An alternative obstacle-controlled strengthening was developed by Friedel-Kroupa-~~Hirsck~~ (FKH) for weak obstacles[48, 49], e.g. prismatic loops[49, 50], where the effective inter-particle spacing is increased compared to the planar geometric spacing due to less extensive dislocation bowing prior to obstacle breakaway. A simple estimation for the increase of the critical shear stress is given by the following equation:

$$\Delta\tau = \frac{1}{8}\mu b d N^{2/3} \tag{2.4}$$

For many radiation-induced small defect clusters, which are weak obstacles to dislocation motion, the FKH model (Equation 2.4) may be more appropriate than the widely used dispersed barrier hardening (DBH) model (Equation 2.3)[51]. However, these obstacle-controlled strengthening models are unable to provide a rational explanation for the observed yield drop during tensile testing of irradiated materials.

Huang and Ghoniem[52] investigated the interaction dynamics between sessile SIA clusters and dislocations in terms of elastic interactions with various SIA cluster densities, the spatial and size distributions of cluster, and the orientation distribution of individual Burgers vectors by using the method of parametric dislocation dynamics (PDD) simulations. A considerably smaller CRSS was found ~~compar~~ing with the results of the FKH model[50] based on dislocation-defect cluster interaction, and its extension by Trinkaus et al.[30], which were based on calculations of elastic interaction forces between dislocations and defect clusters in rigid and static configurations.

Both raft formation and dislocation decoration heavily depend on an impor-

compared

tant process, namely the production and migration of SIA clusters. Theoretically, there are two main mechanisms which could result in the formation and growth of interstitial loops: (1) ~~the~~ acquiring single SIA s one at a time, and (2) the migration and aggregation of interstitial clusters. In most of the studied cases, the first mechanism is concluded to play an insignificant role in terms of the fact that the coexistence and simultaneous growth of vacancy and interstitial clusters[32]. If the first mechanism dominate s the growth of clusters, it is necessary that an interstitial loop mainly acquires interstitial atoms and rejects vacancies. The efficiency of the growth process is predicably ~~to be~~ much lower than when the second mechanism of loop~~s~~ migration is ~~are~~ involved. Barnes[32] presented ~~a~~ an illustrative discussion on the direction of migration, magnitude of the driving force, and migration distance by considering two interacting simple prismatic edge dislocation loops in aluminium. In reality the situation is much more complex than in the two-interacting-loop~~s~~ case. When we ~~it~~ is considere~~d~~ that the vacancy and interstitial loops each have all ~~the~~ possible Burgers vectors, are not simple edge dislocations, have various sizes, and in addition, the interactions are not between two loops but with all those nearby, the situation becomes overwhelmingly complex. On the other hand, these atomic-scale cluster processes such as migration, agglomeration, recombination etc., are difficult to observe *in situ*. The difficulties encountered in the studies by experimental and analytical methods ~~meaning~~s make large scale numerical simulations a practical and necessary option in investigating the mechanisms of formation of rafts and dislocation decoration in neutron irradiated materials.

CHAPTER 3

REVIEW OF THE KINETIC MONTE CARLO METHOD

3.1 INTRODUCTION

In the study of radiation damage, MD simulations using the semi-empirical embedded-atom method (EAM) interatomic potentials have played a very important role in understanding the details of defect production in displacement cascades, and in helping to study the dynamics of point defects and defect cluster diffusion. Comprehensive reviews of recent developments in MD simulations of radiation damage have been given by Diaz de la Rubia [53] and Osetsky et al.[54]. Radiation damage, however, includes a vast range of irradiation effects, such as production and diffusion of point defects, and their interaction with other microstructure features, which take place over time and length scales that span many orders of magnitude. From a simulation perspective, although MD techniques can be used to study the structure and the initial evolution of ~~the~~ damage, the computational time becomes prohibitive beyond the first few nanoseconds, even with recent impressive advances in computers and algorithms. To overcome these limitations, ~~a~~ ways of connecting ~~the~~ MD simulation results to other simulation methods, such as rate theory (~~for example~~ e.g. [55], [56] and [23]) or Kinetic Monte Carlo simulations (for example [57], [58] and [59]) ~~is~~ are required. In particular, KMC simulations appear very promising because they provide the ability to perform atomic-level simulations of ~~the~~ defect kinetics and microstructure evolution over relevant length and time scales, and can account for the spatial heterogeneities of the microstructure!

The Monte Carlo (MC) method refers to any stochastic technique~~s~~, which investigat~~e~~s problems by sampling from random numbers and ~~using~~ use probability statistics. It is generally believed that the widespread use of the Monte Carlo concept began with the Metropolis algorithm in the calculation ~~for~~ of a rigid-sphere system [60]. The MC method is simply a statistical method for solving deterministic or probabilistic problems. It is a physics experiment carried out numerically. This technique can be readily used to study equilibrium properties of a system of atoms. Since the kinetic path of microstructure evolution is physically meaningless in this scheme, it is not suitable for treating defect distribution process in radiation damage.

This chapter gives a detailed account of the Kinetic Monte Carlo (KMC) method which is suitable for simulating kinetic evolution process. The n-fold way algorithm [61] is first introduced which is believed to be the earliest form of the current KMC concept. A formal KMC procedure specifically designed for simulating cascade-induced damage evolution in this thesis is next described.

3.2 THE N-FOLD WAY ALGORITHM

In Metropolis MC methods we decide whether to accept a move by considering the energy difference between the states. In KMC methods, we use rates that depend on the energy barrier between the states. The term "Kinetic Monte Carlo" was initiated by Horia Metiu, Yan-Ten Lu and Zhenyu Zhang in a 1992 Science paper [62]. The paper first pointed out the demands on atomic level control of modern electronic and photonic devices and the importance of *in situ* STM observations of small atomic "clusters" to a theorist who wants to understand growth and segregation, It then elaborated upon the usefulness of KMC simulations in reproducing these experimental observations. The basic feature of their model was to move atoms site-to-site on a square lattice terrace. They postulated rates for all of the elementary processes involved, such as ~~the~~ site-to-site jumps, the jumps to leave or join a step or an existing adsorbate cluster, and so forth. The atoms were deposited on the surface and moved from site to site with a frequency proportional to the rate of the respective moves. If the rate constant of the i-th kinetic process was r_i, the largest rate was chosen as a reference and denoted r_r. The probability $P_i = r_i/r_r$ was then used in ~~a~~ an MC ~~program~~ algorithm as the probability that the atom performed a jump i. The work used Voter's transition state theory [63] to monitor the simulation time. The ~~essence through the references~~ procedure can be traced to Bortz, Kalow, and Lebowitz's n-fold way algorithm [61, 64, 65].

The n-fold way idea was created to replace the standard MC algorithm in generating new configurations in simulating Ising spin systems. In or near the equilibrium state, the standard MC scheme using a Boltzmann kinetic factor, exp(-$\Delta E/kT$), where ΔE is the system energy change, k is the Boltzmann constant and T the absolute temperature, becomes very inefficient since the Boltzmann factor is usually very small in comparison with a random number over the interval $[0, 1]$ [61]. On the other hand, the n-fold way chooses a spin site from the entire ensemble based upon its probability of flipping. Once a site was selected, the flipping was guaranteed and could be immediately performed. The n-fold way also provided a new simulation time concept. At each flip, the time was incremented by a stochastic variable, Δt, whose expectation value is proportional to Q^{-1} (where Q is the number of spins times the average ~~probability~~ frequency that an attempt will produce a flip for a given configuration). Mathematically,

$\Delta t = -(\tau/Q)\ln\xi$, where ξ is a random fraction and τ a system dependent time. This choice reflects properly the distribution of time intervals between flips for a reasonable physical model. The cumulative time thus summed is approximately proportional to real time. The n-fold way reduced computation time by an order of magnitude or more for many applications [61]. A similar concept was used in Voter's 1987 transition state theory [63].

3.3 The KINETIC MONTE CARLO (KMC) METHOD

Molecular dynamics is probably the most accurate atomistic simulation technique. However, due to the fact that it simulates all ~~the~~ lattice atoms, and, most importantly, that it uses an almost constant time step on the order of femtoseconds (10^{-15} s), it cannot simulate the timescales involved in typical technological processing steps (seconds to hours). The kinetic Monte Carlo method, on the contrary, is an event-driven technique, i.e., simulates events at random with probabilities according to the corresponding event rates. In this way it self-adjusts the timestep as the simulation proceeds, depending on the fastest event present at that time.

If an Arrhenius-like relationship is assumed to describe the diffusional processes of clusters, the jump frequency (or the probability per unit time) for a possible jump of a cluster, i, to take place is given by:

$$r_i = \omega_0 \exp(-\frac{E_i}{k_B T}) \tag{3.1}$$

where ω_0 is the pre-exponential factor of the defect cluster, k_B the Boltzmann constant, E_i the 'effective' activation energy for jumps of the cluster, and T is the absolute temperature. Although the values of E_i for interstitials and vacancies are well known from experiments, the values of E_i for small clusters and glissile dislocation loops and of ν_0 for all kinds of defects have not been obtained experimentally. In the present work, we will use results of MD calculations for these values.

In many applications of the MC method, such as the equilibration of atomic positions in a defected crystal, the space of possible configurations that the system can assume is continuous. Therefore, there exists (in theory) an infinite number of new configurations available to the system at any MC step. However, since we are simulating defects in a volume of *finite* size, which evolves according to a *finite* set of physical or mechanical mechanisms, the number of new configurations available at any MC step is *finite* and *enumerable*. This configuration space is discrete. In other words, at each MC step, we can determine all ~~of the~~ potential changes that the system can possibly undergo. Therefore, instead of attempting a random change to the system at each simulation step and then accepting or rejecting that change based on some criterion, we choose and execute one change from the list of all possible changes at each simulation step. The choice is made based on the relative rates at which each change can occur (i.e., the probability of choosing one particular reaction instead of another is proportional to the rate at which the reaction occurs relative to the rates of the other reactions).

Thus the microstructure evolution of ~~the~~ cascade-induced defect clusters is accomplished by a KMC procedure in which one reaction is executed at one site during each time step. The first step in KMC simulations is to tabulate the rate at which an event (i) will take place anywhere in the system, r_i. The probability of selecting an event is simply equal to the rate at which the event occurs relative to the sum of all possible event rates. Once an event is chosen, the system is changed appropriately, and the list of events that can occur at the next KMC step is updated. Therefore, at each KMC step, one event denoted by

m is randomly selected from all possible M events, as follows:

$$\frac{\sum_{i=0}^{m-1} r_i}{\sum_{i=0}^{M} r_i} < \overset{\xi_m}{\xi_1} < \frac{\sum_{i=0}^{m} r_i}{\sum_{i=0}^{M} r_i} \tag{3.2}$$

ξ_m

where r_i is the rate at which event i occurs ($r_0 = 0$) and ξ_1 is a random number uniformly distributed in the range [0, 1]. The way in which the M events are labeled (i.e., by specifying which events correspond to $i = 1, 2, 3, \ldots, m, \ldots, M$) is arbitrary. After an event is chosen and executed, the total number of possible events, M, and the sequence in which the events are labeled, will change.

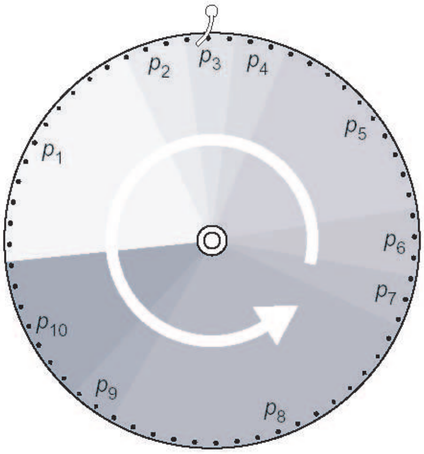

Circumference = Σp_i
where
$p_i = n_0 \exp(-E_i/k_BT)$

Figure 3.1: Schematic representation of various competing thermally activated diffusional processes. The large sectors represent jump paths with large jump rates and vice versa.

The essence of the first step for a diffusion problem can be illustrated by a pie chart, Fig. 3.1. Consider a system with numerous potential jump paths. Allow the big sectors to denote high probability jump paths and the small sectors to

as shown in

with

denote low probability paths. To faithfully execute the KMC process, any one of them, no matter ~~it~~ is a high or low probability jump, should have a chance to be selected. This can be accomplished by allowing every point on the perimeter of the pie-chart to have an equal chance to be selected. This automatically takes into account the weighting process. For the present work, since the number of mobile defects is not very large, we used the simple linear search algorithm.

The reciprocal of an atomic jump probability per unit time is a residence time for a defect cluster that moves by that specific type of jump. Since the jump probabilities of all ~~the~~ different types of jumps are independent, the overall probability per unit time for the system to change its state by any type of jump step is just the sum of all the possible specific jump type probabilities, and so the residence time that would have elapsed for the system in a specific configuration is the reciprocal of this overall jump probability

$$\tau_R \quad \cancel{\Delta t} = \frac{1}{\sum\limits_{i=0}^{M} r_i} \tag{3.3}$$

which is independent of the chosen transition. It may also be important to include the appropriate distribution of escape times. For random uncorrelated processes, this is a Poisson distribution. If ξ_2 is a random number from 0 to 1, the elapsed time for a particular transition is given by

$$\Delta t = \frac{-\ln \xi_2}{\sum\limits_{i=0}^{M} r_i} = -\tau_R \ln \xi_2 \tag{3.4}$$

The system is then advanced to the final state of the chosen transition and the process is repeated. By following the ensuing discrete jump path for the system, accumulating the residence time of the system along the path, and linking this history to the cascade arrival interval (or the damage rate), the diffusion process can be realistically simulated. The expression for Δt in Eqn. 3.4 is rigorous[61], and a derivation is also provided by Battaile[66].

CHAPTER 4

ELASTIC REPRESENTATION OF DEFECTS

4.1 KRÖNER'S DESCRIPTION OF POINT DEFECTS BY FORCE MULTIPOLES

Although the interaction between atomic-size defects requires extensive MD or even *abinitio* calculations, the theory of elasticity can be utilized to simplify such calculations. Defect-defect interaction does not generally result in significant local deformation, and hence linear elasticity is expected to give accurate results. This approach has been successfully used to describe static defect-defect interactions [50, 67, 68, 69]. Following Kröner [70] and Teodosiu [71], nano-scale defects exert forces on the atoms in ~~theirs~~ their vicinity, which are different from those acting on these atoms in a perfect lattice. Let $\mathbf{P}^v$ denote the additional forces at $\vec{x}' + \vec{l}$ exerted by a nano-defect centred at $\mathbf{x}'$ on the atom situated ~~at $\mathbf{x}' + \mathbf{l}^v$~~ x. According to the definition of Green's function, the force system $\mathbf{P}^v$ generates in an infinite elastic medium the displacement field (see Figure 4.1)

use bold for vectors

$$u_m(\mathbf{x}) = \sum_{v=1}^{N} G_{ms}(\mathbf{x} - \mathbf{x}' - \mathbf{l}^v) P_s^v \tag{4.1}$$

where $\mathbf{G}$ is Green's tensor function of the elastic medium, while N is the number of atoms on which extra forces are exerted. Theoretically, $N = \infty$, but, as $\mathbf{P}^v$ decays very rapidly when $\|\mathbf{l}^v\| \to \infty$, it is usually sufficient to take into account only the forces employed on the first and second nearest neighbors. Expanding

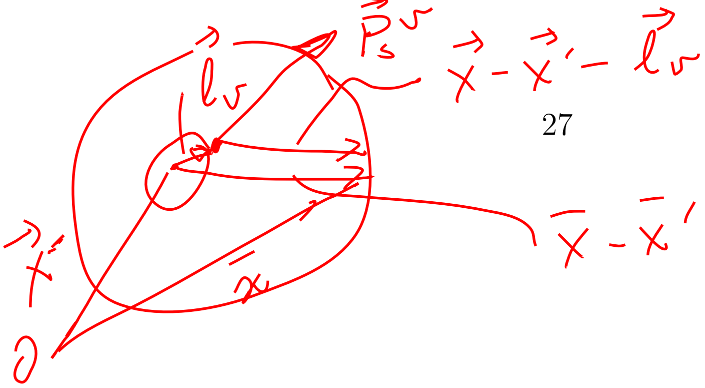

need better diagram

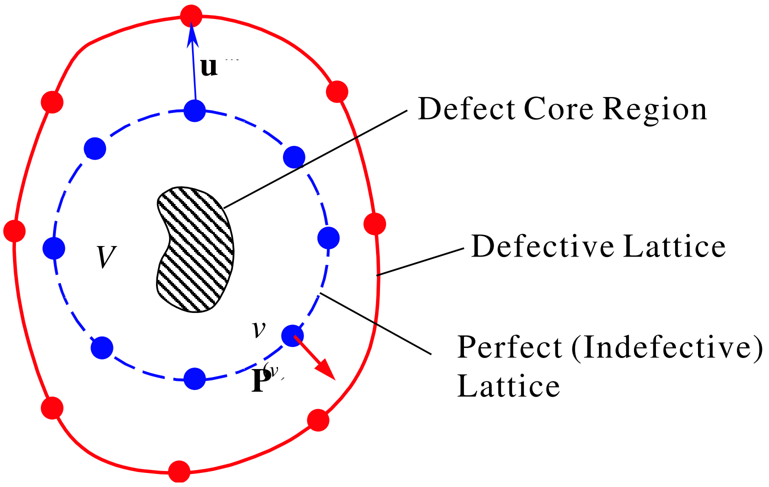

Figure 4.1: Schematic representation of lattice deformation induced by the occurrence of a defect, as well as the point forces approximation.

$\mathbf{G}(\mathbf{x} - \mathbf{x}' - l^v)$ in a Taylor series about $\mathbf{x} - \mathbf{x}'$ leads to

$$G_{ms}(\mathbf{x} - \mathbf{x}' - \mathbf{l}^{\mathbf{v}}) = \sum_{k=0}^{\infty} \frac{1}{k!} G_{ms,q_1'q_2'\ldots q_k'}(\mathbf{x} - \mathbf{x}') l_{q_1}^v l_{q_2}^v \ldots l_{q_k}^v \tag{4.2}$$

where $(\cdot)_{,m'} = \frac{\partial(\cdot)}{\partial x_m'}$. The expansion (4.2) converges only for sufficiently small values of $\|\mathbf{l}^v\|$, i.e. only if the application points of the forces $\mathbf{P}^v$ are sufficiently close to the nano-defect.

Substituting (4.2) into (4.1), we have

$$u_m(\mathbf{x}) = \sum_{k=0}^{\infty} \frac{1}{k!} G_{ms,q_1'q_2'\ldots q_k'}(\mathbf{x} - \mathbf{x}') P_{q_1 q_2 \ldots q_k s}^{(k)} \tag{4.3}$$

where

$$\mathbf{P}^{(0)} = \sum_{v=1}^{N} \mathbf{P}^v, P_s^{(0)} = \sum_{v=1}^{N} P_s^v, \tag{4.4}$$

is the resultant force, and

$$\mathbf{P}^{(k)} = \sum_{v=1}^{N} \underbrace{\mathbf{l}^v \mathbf{l}^v \ldots \mathbf{l}^v}_{k} \mathbf{P}^v, \qquad P_{q_1 q_2 \ldots q_k s}^{(k)} = \sum_{v=1}^{N} l_{q_1}^v l_{q_2}^v \ldots l_{q_k}^v P_s^v \tag{4.5}$$

is the multipolar moment of the k-th order, $k = 1, 2, ...$, of the system of additional forces $\mathbf{P}^v$ exerted by the nano-defect on its surroundings. In particular, the following tensors are called dipole moment, quadrupole moment and octopole moment, respectively,

$$\mathbf{P}^{(1)} = \sum_{v=1}^{N} \mathbf{l}^v \mathbf{P}^v, \qquad \mathbf{P}^{(2)} = \sum_{v=1}^{N} \mathbf{l}^v \mathbf{l}^v \mathbf{P}^v, \qquad \mathbf{P}^{(3)} = \sum_{v=1}^{N} \mathbf{l}^v \mathbf{l}^v \mathbf{l}^v \mathbf{P}^v, \tag{4.6}$$

Applying the differential operator

$$\frac{1}{k!} P^{(k)}_{q_1 q_2 \ldots q_k s} \frac{\partial^k}{\partial x'_{q_1} \partial x'_{q_2} \ldots \partial x'_{q_k}} \tag{4.7}$$

to the equilibrium equation of a unit point force

$$C_{ijmn} G_{ms,jn}(\mathbf{x} - \mathbf{x}') + \delta_{is} \delta(\mathbf{x} - \mathbf{x}') = 0 \tag{4.8}$$

where C_{ijmn} is the elastic tensor and δ_{is} is the Kronecker δ, and comparing the results with (4.3), we can see that the action of a nano-defect on the elastic medium is equivalent to that of a body force field, which consists of force dipoles, quadrupoles, octopoles, etc. applied at the center of the defect, namely:

$$f_i(\mathbf{x}) = \sum_{k=0}^{\infty} \tilde{P}^{(k)}_{q_1 q_2 \ldots q_k i} \delta_{,q'_1 q'_2 \ldots q'_k}(\mathbf{x} - \mathbf{x}') \tag{4.9}$$

where

$$\tilde{P}^{(k)}_{q_1 q_2 \ldots q_k s} = \frac{1}{k!} P^{(k)}_{q_1 q_2 \ldots q_k s} \tag{4.10}$$

the strengths of the multipolar forces, $f_i(\mathbf{x})$, being completely determined through (4.10) by the multipolar moments associated with the nano-defect [71]. It should be noted that the resultant force and couple exerted by a nano-defect on its surroundings are zero. Thus, the equilibrium condition implies

$$\sum_{v=1}^{N} \mathbf{P}^v = \mathbf{0}, \qquad \sum_{v=1}^{N} \mathbf{l}^v \times \mathbf{P}^v = \mathbf{0} \tag{4.11}$$

The last relation may be rewritten as

Use $\in_{kns}$

$$\sum_{v=1}^{N} \epsilon_{kns} l_n^v P_s^v = \epsilon_{kns} P_{ns}^{(1)} = 0 \tag{4.12}$$

where ϵ_{kns} is so called permutation tensor. The dipole moment $\mathbf{P}^{(1)}$ must be a symmetric tensor, and conditions (4.11) are equivalent to:

$$\mathbf{P}^{(0)} = \mathbf{0}, \qquad \mathbf{P}^{(1)} = (\mathbf{P}^{(1)})^{\mathrm{T}} \tag{4.13}$$

Introducing (4.13) into (4.3), we obtain:

$$u_m(\mathbf{x}) = \sum_{k=0}^{\infty} \frac{(-1)^k}{k!} G_{ms,q_1q_2\ldots q_k}(\mathbf{x}-\mathbf{x}') P^{(k)}_{q_1q_2\ldots q_k s} \tag{4.14}$$

Equation (4.14) shows that the elastic field produced by a nano-defect in an infinite elastic medium is completely determined by the multipolar moments $\mathbf{P}^{(k)}$, $k = 1, 2, \ldots$, provided that Green's tensor functions of the medium are known.

For an isotropic material this function is

$$G_{ms}(\mathbf{x}-\mathbf{x}') = \frac{1}{16\pi\mu(1-\nu)} \left[\delta_{ms}(3-4\nu)\frac{1}{r} + \frac{(x_m - x'_m)(x_s - x'_s)}{r^3} \right] \tag{4.15}$$

where $r = \|\mathbf{x}-\mathbf{x}'\|$. By substituting (4.15) into (4.14), we see that $\mathbf{u}(\mathbf{x})$ is of the order $O(r^{-2})$ as $r \to \infty$, in agreement with the results obtained in modeling point defects by rigid spherical inclusions in an infinite isotropic medium. Assuming that the elastic medium is isotropic, we obtain from (4.15) that

$$\frac{\partial G_{ms}(\mathbf{x}-\mathbf{x}')}{\partial x_s} = -\frac{1-2\nu}{8\pi\mu(1-\nu)} \frac{x_m - x'_m}{r^3} \tag{4.16}$$

As already mentioned, the elastic field of a nano-defect is characterized by its multipolar moments. The main procedure for evaluating these quantities is to solve the equation system (4.14) with the displacement field $\mathbf{u}(\mathbf{x})$ acquired by MD simulation. As a rough approximation, we can only consider the force system $\mathbf{P}^v$ exerted on the first nearest neighbors and the first term in the Taylor expansion (4.14).

4.1.0.1 The elastic interaction between nano-defects

In this section we will study the elastic interaction between nano-defects which are simulated by force multipoles acting in an infinite elastic medium. It should be noted that this description of nano-defects provides a good approximation only if the separation distance between defects is large enough. Otherwise, a semi-discrete or fully atomic model of the interacting defects must be adopted.

The elastic interaction energy between a nano-defect located at $\mathbf{x}$ and an elastic displacement field $\mathbf{u}$ is given, according to elastic theory, by the work done against the forces $\mathbf{P}^v$ exerted by the point defect on ~~the~~ neighboring atoms, i.e.

$$\Phi_{\text{int}} = -\sum_{v=1}^{N} \mathbf{P}^v \cdot \mathbf{u}(\mathbf{x} + \mathbf{l}^v) \tag{4.17}$$

By expanding $\mathbf{u}(\mathbf{x} + \mathbf{l}^v)$ in a Taylor series around $\mathbf{x}$, we obtain

$$\begin{aligned} u_m(\mathbf{x} + \mathbf{l}^v) &= \sum_{n=0}^{\infty} \frac{1}{n!} u_{m,j_1 j_2 \dots j_n}(\mathbf{x}) \mathbf{l}^v_{j_1 j_2 \dots j_n} \\ &= u_m(\mathbf{x}) + u_{m,i}(\mathbf{x}) l_i^v + \frac{1}{2!} u_{m,ij}(\mathbf{x}) l_i^v l_j^v + \frac{1}{3!} u_{m,ijk}(\mathbf{x}) l_i^v l_j^v l_k^v + \dots \end{aligned} \tag{4.18}$$

Substituting this expansion into (4.17) and considering (4.4), (4.5), and (4.13) yields

$$\begin{aligned} \Phi_{\text{int}} &= -\sum_{n=0}^{\infty} \frac{1}{n!} u_{m,j_1 j_2 \dots j_n}(\mathbf{x}) P^{(n)}_{j_1 j_2 \dots j_n m} \\ &= -\left[P^{(1)}_{im} u_{m,i}(\mathbf{x}) + \frac{1}{2!} P^{(2)}_{ijm} u_{m,ij}(\mathbf{x}) + \frac{1}{3!} P^{(3)}_{ijkm} u_{m,ijk}(\mathbf{x}) + \dots \right] \end{aligned} \tag{4.19}$$

In a homogeneous strain field we have $u_{m,i}(\mathbf{x}) = \text{const.}$ and (4.19) reduces to

$$\Phi_{\text{int}} = -P^{(1)}_{im} u_{m,i} = -P^{(1)}_{im} E_{im} \tag{4.20}$$

i.e. only the dipole moments contribute to the interaction energy. Returning to the general case, we recall that the force employed on the nano-defects by the elastic state which generates the displacement field $\mathbf{u}$ is

$$\mathbf{F} = -\mathrm{grad}_{\mathbf{x}} \Phi_{\mathrm{int}} \tag{4.21}$$

Hence, by taking into account (4.19), we have

$$\begin{aligned} F_s = -\frac{\partial \Phi_{\mathrm{int}}}{\partial x_s} &= \sum_{n=1}^{\infty} \frac{1}{n!} u_{m,j_1 j_2 \ldots j_n s}(\mathbf{x}) P^{(n)}_{j_1 j_2 \ldots j_n m} \\ &= P^{(1)}_{im} u_{m,is}(\mathbf{x}) + \frac{1}{2!} P^{(2)}_{ijm} u_{m,ijs}(\mathbf{x}) + \frac{1}{3!} P^{(3)}_{ijkm} u_{m,ijks}(\mathbf{x}) + \ldots \end{aligned} \tag{4.22}$$

We can now easily derive the elastic interaction energy of two point defects situated at points $\mathbf{x}$ and $\mathbf{x}'$ in an infinite elastic medium and having the multipolar moments $\mathbf{P}^{(1)}, \mathbf{P}^{(2)}$, ..., and respectively $\tilde{\mathbf{P}}^{(1)}, \tilde{\mathbf{P}}^{(2)}$, ..., by substituting the expression (4.14) of the displacement field produced by one of the defects into (4.19). The results reads

$$\Phi_{\mathrm{int}} = -\sum_{n=0}^{\infty} \frac{1}{n!} P^{(n)}_{j_1 j_2 \ldots j_n m} \sum_{k=1}^{\infty} \frac{(-1)^k}{k!} \tilde{P}^{(k)}_{q_1 q_2 \ldots q_k s} G_{ms,q_1 q_2 \ldots q_k j_1 j_2 \ldots j_n}(\mathbf{x} - \mathbf{x}') \tag{4.23}$$

Since $\mathbf{G}(\mathbf{x}-\mathbf{x}') = O(r^{-1})$ as $r = \|\mathbf{x} - \mathbf{x}'\| \to \infty$, we see that the first three terms of the expression (4.23) decrease as r^{-3}, r^{-4},and r^{-5}, respectively, for sufficiently large values of the separation distance r between the defects.

4.2 ELASTIC INTERACTION BETWEEN DEFECTS

The interaction between the atoms can be obtained from an (approximate) solution of the Schrödinger equation [72] describing electrons, or from a potential energy function determined in some empirical way (for example, MD simulations [73])~~, but they are computationally expensive~~. Most often, it is sufficient to treat the interactions between atoms in terms of the analysis of elastic interactions. However, so far, all KMC computer simulations for microstructure evolution under irradiation have not considered the influence of the internal and applied stress fields on defect motion (for example [74, 57, 26, 75]). We propose here a KMC simulation, where the elastic interactions between SIA/vacancy clusters themselves, SIA and vacancy clusters, and SIA/vacancy clusters and dislocations are explicitly accounted for.

Recently, a new computational method has been developed [76, 77] for accurate evaluation of the elastic field of dislocation aggregates in complex 3-D geometry. The method extends the capabilities of 2-D estimates of elastic field variables in realistic material geometry, and enables calculations of displacements, strain, stress, interaction and self-energies, and finally, the work associated with rotation and translation of defect clusters. In the following sections, the numerical method developed by Ghoniem [76] and Ghoniem and Sun [77] to examine the mechanisms of interaction between small defect clusters and slip dislocation loops is introduced, followed by the calculation needed to develop an specific elastic interaction energies between defects for use in this thesis.

For the specific case of parametric dislocation loop representation, the elastic field tensors (strain ε_{ij} and stress σ_{ij}) of a dislocation loop are given by line integrals over the dislocation loop line vector as follows [78]

$$\begin{aligned}\varepsilon_{ij} &= \frac{1}{8\pi}\oint\limits_C \left[-\frac{1}{2}(\epsilon_{jkl}b_iR_{,l}+\epsilon_{ikl}b_jR_{,l}-\epsilon_{ikl}b_lR_{,j}-\epsilon_{jkl}b_lR_{,i})_{,pp}\right.\\ &\qquad \left.+\frac{1}{1-\nu}\epsilon_{kmn}b_nR_{,mij}\right]dl_k \end{aligned} \tag{4.24}$$

where $R = \|\mathbf{R}\| = \|\mathbf{x}-\hat{\mathbf{x}}\|$.

Since the linear stress-strain relationship is $\sigma_{ij} = 2\mu\varepsilon_{ij} + \lambda\varepsilon_{rr}\delta_{ij}$, the stress tensor is also obtained as a line integral, of the general form

$$\sigma_{ij} = \frac{\mu b_n}{4\pi}\oint\limits_C \left[\frac{1}{2}R_{,mpp}(\epsilon_{jmn}dl_{i'}+\epsilon_{imn}dl_{j'})+\frac{m}{m-1}\epsilon_{kmn}(R_{,ijm}-\delta_{ij}R_{,ppm})dl_{k'}\right] \tag{4.25}$$

where μ and λ are the Lamé constants ($\mu =$ shear modulus, and $\lambda/2(\lambda+\mu) = \nu =$ Poisson's ratio), b_n are the components of Burgers vector, $R_{,ijk}$ are derivatives of the radius vector norm between a loop point at $\hat{\mathbf{x}}$ and a field point $\mathbf{x}$, $dl_{i'}$ are differential line elements along the dislocation line vector, and ϵ_{ijk} is the permutation tensor. Ghoniem [76] developed explicit forms for the integrals of general parametric dislocation loops. An efficient numerical integration scheme has also been developed for calculations of the stress field, as a fast summation by Ghoniem and Sun [77]. Their results read

$$\begin{aligned} \sigma_{ij} &= \frac{\mu}{4\pi} \sum_{\gamma=1}^{N_{\text{loop}}} \sum_{\beta=1}^{N_{\text{s}}} \sum_{\alpha=1}^{Q_{\max}} b_n w_\alpha \left[\frac{1}{2} R_{,mpp} (\epsilon_{jmn} \hat{x}_{i,u} + \epsilon_{imn} \hat{x}_{j,u}) \right. \\ &\left. + \frac{1}{1-\nu} \epsilon_{kmn} (R_{,ijm} - \delta_{ij} R_{,ppm}) \hat{x}_{k,u} \right] \end{aligned} \tag{4.26}$$

where N_{loop}, N_{s}, and $Q_{\max}$ are the total number of loops, segments, and Gaussian quadrature, respectively. w_α is the quadrature weight, and $\hat{x}_{j,u}$ are parametric derivatives of the Cartesian components of the vector $\hat{\mathbf{x}}$, which describes the loop geometry. The interaction energy of two dislocation loops over the volume V of the material is expressed by

$$E_I = \int_V \sigma_{ij}^{(1)} \varepsilon_{ij}^{(2)} dV \tag{4.27}$$

in which $\sigma_{ij}^{(1)}$ is the stress arising from the first dislocation and $\varepsilon_{ij}^{(2)}$ the strain originating in the other. For the present study, if the second loop (defect cluster) is assumed to be infinitesimal, the interaction energy can be simplified to [50]

$$E_I = \delta A^{(2)} n_i^{(2)} \sigma_{ij}^{(1)} b_j^{(2)} \tag{4.28}$$

where $n_i^{(2)}$ is the unit normal vector to the defect cluster habit plane of area $\delta A^{(2)}$. By substituting Eqn. 4.26 into Eqn. 4.28 with $N_{\text{loop}} = 1$, we can readily compute the interaction energy of the cluster, designated with the superscript (2), and the slip loop, of Burgers vector $b_n^{(1)}$, as

$$\begin{aligned} E_I &= \frac{\mu \delta A^{(2)} n_i^{(2)} b_j^{(2)}}{4\pi} \sum_{\beta=1}^{N_\mathrm{s}} \sum_{\alpha=1}^{Q_\mathrm{max}} b_n^{(1)} w_\alpha \left[\frac{1}{2} R_{,mpp} (\epsilon_{jmn} \hat{x}_{i,u} + \epsilon_{imn} \hat{x}_{j,u}) \right. \\ & \left. + \frac{1}{1-\nu} \epsilon_{kmn} (R_{,ijm} - \delta_{ij} R_{,ppm}) \hat{x}_{k,u} \right] \end{aligned} \tag{4.29}$$

In the above equation, we assume that the stress tensor of the grown-in (slip) dislocation loop is constant over the cross-section of a small point-defect cluster. In case we treat one single vacancy or interstitial atom as a center of dilatation, the interaction energy simplifies to

$$E_I = -\frac{4}{9} \pi r_0^3 \varepsilon_{ii}^{(2)} \sigma_{jj}^{(1)} \tag{4.30}$$

where $\varepsilon_{ii}^{(2)}$ is the dilatation and r_0 is the effective radius of a point defect. The above equation does not reveal dependence of the interaction energy surface on the orientation of the cluster Burgers vector, unlike Eqn. 4.29.

Kroupa [50] obtained the formulae for the displacement and stress field around an infinitesimal dislocation loop by extending the derivation used by Eshelby [79]. The stress tensor σ_{ij} is

$$\begin{aligned} \sigma_{ij} &= \left\{ -\frac{k_0 \mu}{4\pi(1-\nu)R^3} \left[\frac{3(1-2\nu)}{R^2} b_k \rho_k n_l \rho_l + (4\nu - 1) b_k n_k \right] \delta_{ij} \right. \\ & + (1-2\nu)(b_i n_j + n_i b_j) + \frac{3\nu}{R^2} \left[b_k \rho_k (n_i \rho_j + \rho_i n_j) + n_k \rho_k (b_i \rho_j + \rho_i b_j) \right] \\ & \left. + \left[\frac{3(1-2\nu)}{R^2} b_k n_k - \frac{15}{R^4} b_k \rho_k n_l \rho_l \right] \rho_i \rho_j \right\} \delta A \end{aligned} \tag{4.31}$$

where $\rho_i = x_i - \hat{x}_i$ is the radius vector between the loop center at point $\hat{\mathbf{x}}$ and a field point at $\mathbf{x}$. $\mathbf{n}$ is the the unit normal vector to the defect cluster habit plane of area δA, and $\mathbf{b}$ Burgers vector. By applying Eqn. 4.28, the elastic interaction energy between two infinitesimal loops can also be obtained.

4.3 REPRESENTATION OF NANO-DEFECTS BY FORCE DIPOLES

4.3.0.2 Representation of nano-defects by force dipoles

Point defects are lattice imperfections having all dimension~~s~~ of the order of one or more atomic spacing. The point defect may be a vacant site~~s~~ in the atomic lattice, called a vacancy, a foreign atom replacing one atom of the lattice, called a substitutional atoms, or a atom situated between the normal sites of the lattice, called an interstitial atom. Sometimes, two or more point defects can build characteristic arrangements which are thermodynamically stable to form a point defect cluster. Our interest will be particularly focus on these nano-scalling point defect clusters. The collection of point defects produces viscous effects at a macroscopic scale, which are of great importance for many processes taking place in crystals. Moreover, the interaction of a nano-defect with other crystal defects is mostly of elastic nature. We will ~~try to~~ develop here elastic models of nano-defects and methods for calculating the elastic interaction of a defect with other defects.

Firstly, let us consider now in detail the physical significance of the partial derivatives of first order of the Green's function $\mathbf{G}(\mathbf{x})$. We can obviously write

$$G_{ij,k}(\mathbf{x}) = \lim_{h \to 0} \frac{1}{h} \left\{ G_{ij}(\mathbf{x}) - G_{ij}(\mathbf{x} - h\mathbf{e}_k) \right\} \tag{4.32}$$

Consequently, the elastic state associated ~~to~~ with the displacement field

$$u_i(\mathbf{x}) = G_{ij,k}(\mathbf{x}) \tag{4.33}$$

is the limiting value as $h \to 0$ of a sum of two elastic states: the first corresponds unit to ~~the~~ a unit concentrated force ~~$\mathbf{e}_j/h$~~ acting at the origin; the second corresponds to a concentrated load ~~$-\mathbf{e}_j/h$~~ acting at the point with position vector he$_k$. A straightforward calculation shows that the resultant of the stress vectors acting on any

e_k is a position vector, not force ??

is along the vector

?

sphere Σ_η with radius η and center at the origin is zero, while their resulting couple ~~equals~~ $-\mathbf{e}_k \times \mathbf{e}_j$. Following the terminology introduced by Love, we say that the elastic field corresponding to the displacement (4.33) is produced by a unit double force, which is statically equivalent to a directed concentrated couple or to $\mathbf{0}$ according as $j \neq k$ or $j = k$. In the latter case we say that the singularity at the origin is a unit double force without moment. The elastic state corresponding to the displacement field

$$u_i(\mathbf{x}) = G_{ij,j}(\mathbf{x}) \tag{4.34}$$

which is produced by three mutually orthogonal unit double forces without moment acting at the origin, is called a center of compression, whereas the elastic state corresponding to the opposite of (4.34) is called a center of dilatation. It has been shown that the effects of a vacancy or an interstitial atom can be approximated by a spherical compression center of dilatation center.

In view of formula (4.33), we propose here that a nano-defect of arbitrary geometric shape can be described by a collection of double forces. Specifically, we have

$$u_i(\mathbf{x}) = G_{ij,k}(\mathbf{x} - \mathbf{x}')f_{kj}(\mathbf{x}') \tag{4.35}$$

where f_{jk} is a second order tensor of which the three diagonal components represents three mutually orthogonal force dipoles without moment, and the rest non-diagonal components are force dipoles with moment along $\mathbf{e}_j \times \mathbf{e}_k$. It should be noted that the resultant force and couple of these components consisting f_{jk} should be equal to zero. The condition of zero resultant force can be achieved in terms of the definition of force dipole. Then, the condition of zero net force couple implies that the tensor f_{jk} must be a symmetric tensor, i.e.

that

$$f_{kj}(\mathbf{x}') = f^T_{kj}(\mathbf{x}') \tag{4.36}$$

Suppose that we have already ~~got~~ obtained the displacement of each and every lattice atom somehow, say by Molecular Dynamics simulation or experiments. We then can use the least squares method to determine the point force dipolar system, i.e. f_{jk}, which are unknown and exerted on the center of the defect to characterize the elastic field of the defect. If the real displacement field is denoted by $\tilde{u}(\mathbf{x})$, we define the error function

$$\Pi = \sum_{m=1}^{N} \|\mathbf{u}(\mathbf{x}) - \tilde{\mathbf{u}}(\mathbf{x})\|^2 = \sum_{m=1}^{N} [\mathbf{u}(\mathbf{x}) - \tilde{\mathbf{u}}(\mathbf{x})]\,[\mathbf{u}(\mathbf{x}) - \tilde{\mathbf{u}}(\mathbf{x})] \tag{4.37}$$

where N is the number of points whose displacements are already known and we used to calculated the error. According to the method of least squares, the best fitting value of f_{jk} has the property that

$$\Pi = \text{aminimum}, \tag{4.38}$$

i.e.

$$\frac{\partial \Pi}{\partial f_{jk}} = 0 \tag{4.39}$$

By solving these six equations we would be able to define a force dipole tensor that can approximately describe the elastic field induced by the existence of the defect.

As far as the interaction energy between two nano-defects is concerned, it can be readily shown that

$$\Phi_{\text{int}} = -\mathbf{f} \cdot \text{grad}\tilde{\mathbf{u}}(\mathbf{x}) = -f_{ij}\tilde{u}_{j,i}(\mathbf{x}) \tag{4.40}$$

where f_{ij} is the force dipole used to represent the nano-defect at $\mathbf{x}$, and $\tilde{\mathbf{u}}(\mathbf{x})$ is the displacement field induced by the defect at $\mathbf{x}'$, which can also be described by a force dipole tensor $\tilde{\mathbf{f}}$. By substituting the expression (4.35) of the displacement field produced by one of the defects into (4.40), it results

$$\Phi_{\text{int}} = -f_{ij}\tilde{f}_{lk}G_{jk,li}(\mathbf{x} - \mathbf{x}') \tag{4.41}$$

4.4 APPLICATIONS

For simplicity, in the following we will choose the geometric center of the nano-defect as origin, i.e., $\mathbf{x}' = \mathbf{0}$.

4.4.1 VACANCY

$$G_{ij} = \frac{1}{16\pi\mu(1-\nu)r}\left[\delta_{ij}(3-4\nu) + \frac{x_i x_j}{r^2}\right] \tag{4.42}$$

$$G_{ij,k} = \frac{1}{16\pi\mu(1-\nu)r^3}\left[-(3-4\nu)\delta_{ij}x_k + \delta_{ik}x_j + x_i\delta_{jk} - \frac{3x_i x_j x_k}{r^2}\right] \tag{4.43}$$

$$\begin{aligned} u_i &= G_{ij,k} f_{kj} \\ &= \frac{1}{16\pi\mu(1-\nu)r^3}\left[-(3-4\nu)f_{ik}x_k + f_{ij}x_j + x_i f_{jj} - \frac{3x_i x_j x_k}{r^2} f_{kj}\right] \end{aligned} \tag{4.44}$$

At $r = r_0$, the displacement field $\tilde{\mathbf{u}}$ is known as

$$\tilde{u}_r(r_0) = Cr^{-2}, \quad \tilde{u}_\phi = \tilde{u}_\theta = 0 \tag{4.45}$$

where C is an arbitrary constant. Substituting (4.44) and (4.45) into (4.39) yields the equations designed to determine the values of f_{ij}. Actually, the derived equations are not completely mutually independent, and some other relations have to be introduced to help with solving equations. Due to the spherical symmetry of the deformation, only the components of dipolar forces whose indices occur in pairs of equal numbers are non-zero, i.e. $f_{12} = f_{13} = f_{23} = 0$. By solving
the equations, we obtain

$$f_{11} = f_{22} = f_{33} = 8\frac{(\nu-1)C\pi\mu}{1-2\nu} = -4\pi C(\lambda + 2\mu) \tag{4.46}$$

The field (4.46) represents three mutually orthogonal force dipoles without moment, having equal intensities, and acting at the ~~centre~~ center of the point defect, and such distribution of concentrated loads is called a spherical dilatation ~~centre~~ center. The values in (4.46) are exactly the same as the solutions given by the elastic theory with the assumption of point defect as a rigid spherical inclusion.

4.4.2 INFINITESIMAL PRISMATIC DISLOCATION LOOP

Let us assume the loop is at the origin of the coordinate system on the x_1x_2 plane ($n_1 = n_2 = 0$, $n_3 = 1$) and suppose that the displacement field is given by Kroupa's formula. Namely, the displacements of a pure prismatic infinitesimal dislocation loop with an area δA, $b_1 = b_2 = 0$, $b_3 = b$ are as follows:

$$\begin{aligned} \tilde{u}_1 &= \frac{K}{6}\frac{x_1}{r^3}\left[-(1-2\nu) + \frac{3x_3^2}{r^2}\right] \\ \tilde{u}_2 &= \frac{K}{6}\frac{x_2}{r^3}\left[-(1-2\nu) + \frac{3x_3^2}{r^2}\right] \\ \tilde{u}_3 &= \frac{K}{6}\frac{x_3}{r^3}\left[1-2\nu + \frac{3x_3^2}{r^2}\right] \end{aligned} \tag{4.47}$$

where

$$r = \sqrt{x_1^2 + x_2^2 + x_3^2} \tag{4.48}$$

$$K = -\frac{3b_3}{4\pi(1-\nu)}\delta A \tag{4.49}$$

The displacements at $(x_1, 0, 0)$, $(0, x_2, 0)$, and $(0, 0, x_3)$ are

$$\begin{aligned} \tilde{u}_1^{(1)} &= -\frac{K}{6}\frac{1}{x_1^2}(1-2\nu),\ \tilde{u}_2^{(1)} = \tilde{u}_3^{(1)} = 0, \\ \tilde{u}_2^{(2)} &= -\frac{K}{6}\frac{1}{x_2^2}(1-2\nu),\ \tilde{u}_1^{(2)} = \tilde{u}_3^{(2)} = 0, \\ \tilde{u}_3^{(3)} &= \frac{K}{3}\frac{1}{x_3^2}(2-\nu),\ \tilde{u}_1^{(3)} = \tilde{u}_2^{(3)} = 0, \end{aligned} \tag{4.50}$$

respectively, However, the displacements at these three points given by (4.44) are

$$u_1^{(1)} = \frac{1}{16\pi\mu(1-\nu)x_1^2}\left[-4(1-\nu)f_{11} + f_{22} + f_{33}\right],\ u_2^{(1)} = -\frac{(1-2\nu)f_{12}}{8\pi\mu(1-\nu)x_1^2},$$

$$
\begin{aligned}
u_3^{(1)} &= -\frac{(1-2\nu)f_{13}}{8\pi\mu(1-\nu)x_1^2} \\
u_1^{(2)} &= -\frac{(1-2\nu)f_{12}}{8\pi\mu(1-\nu)x_2^2},\quad u_2^{(2)} = \frac{1}{16\pi\mu(1-\nu)x_2^2}\left[-4(1-\nu)f_{22}+f_{11}+f_{33}\right], \\
u_3^{(2)} &= -\frac{(1-2\nu)f_{23}}{8\pi\mu(1-\nu)x_2^2} \\
u_1^{(3)} &= -\frac{(1-2\nu)f_{13}}{8\pi\mu(1-\nu)x_3^2},\quad u_2^{(3)} = -\frac{(1-2\nu)f_{23}}{8\pi\mu(1-\nu)x_3^2}, \\
u_3^{(3)} &= \frac{1}{16\pi\mu(1-\nu)x_3^2}\left[-4(1-\nu)f_{33}+f_{11}+f_{22}\right]
\end{aligned}
\tag{4.51}
$$

Substituting (4.50) and (4.51) into (4.37) results

$$
\Pi = \sum_{m=1}^{3}\sum_{i=1}^{3}\left[u_i^{(m)} - \tilde{u}_i^{(m)}\right]^2 \tag{4.52}
$$

By solving the equations given by (4.39) we obtain

$$
f_{12} = f_{13} = f_{23} = 0,\quad f_{11} = f_{22} = -\lambda b_3 \delta A,\quad f_{33} = -(\lambda + 2\mu) b_3 \tag{4.53}
$$

It can be shown that (4.53) are exactly the same as those given by Kroupa. It implies that the displacement field produced by force dipoles (4.53), as well as the strain and stress field will be the same as the results derived by Kroupa.

Although this may be an obvious result, it illustrates the method for applications where the defect geometry cannot be simply represented as a sphere (vacancy) or a disk (SIA cluster).

CHAPTER 5

DEVELOPMENT OF NEW COMPUTATIONAL MODELS FOR RADIATION DAMAGE ACCUMULATION AND SEGREGATION

5.1 INTRODUCTION

Under cascade-producing irradiation, defect production and subsequent defect accumulation are strongly influenced by features of the initial cascade damage event. The temporal and spatial inhomogeneities of cascade damage, as well as details of damage that manifest themselves on the atomic scale, make it necessary to develop atomic-scale models as the basis for understanding the effects of cascade production on microstructure evolution and mechanical property changes in irradiated materials. The ability to correlate and extrapolate irradiation test data on fusion materials hinges on understanding radiation damage at this scale, as well as understanding its influence on behavior at the macroscopic scale.

Advances in atomistic descriptions of cascade events by molecular dynamics (MD) simulations in the past decade, coupled with experimental information, have resulted in the identification of cluster formation directly in cascades, and the subsequent behavior of those clusters, as key elements affecting the evolution of the microstructure. Stochastic annealing simulation provides a bridge between the atomistic and macroscopic scales that enables the direct effects of cascade production on the microstructure to be investigated. The work reported ~~on~~ here is the next step beyond the application of stochastic annealing simulations to the local short-term annealing stage of individual cascades, which has been reported elsewhere [57, 58, 80]. We ~~present~~ here ~~on~~ the simulation of the kinetics of damage accumulation under low dose~~s~~ of cascade-producing irradiation in iron at room temperature.

investigate Spatially Heterogeneous

5.2 A KINETIC MONTE CARLO APPROACH TO RADIATION DAMAGE EVOLUTION ~~WITH ELASTIC INTERACTION CONSIDERATION~~

the

The jump frequency (or the probability per unit time) for a possible jump of ~~a~~ an SIA cluster, i, to take place is given by Equation 3.1. We first tabulate the rate at which an event (i) will take place anywhere in the system, r_i. The probability of selecting an event is equal to the rate at which the event occurs relative to the sum of all possible event rates. Once an event is selected, the system is changed correspondingly, and the list of events that can occur at the next KMC step is updated. Therefore, at each KMC step, one event denoted by m is randomly selected from all possible M events. The reciprocal of an atomic jump frequency is a residence time for a defect cluster that moves by that specific type of jump. Since the jump probabilities of all different types of jumps are independent, the overall probability density for the system to change its state by any type of jump step is just the sum of all possible specific jump probabilities. Therefore, the residence time that would have elapsed for the system in a specific configuration is the reciprocal of the overall jump probability rate $\overset{\tau_R}{\cancel{\Delta t}} = 1/\sum_{i=0}^{M} r_i$, which is independent of the chosen transition. It may also be important to include the appropriate distribution of escape times. For random uncorrelated processes, the distribution of the time elapsing between events is the exponential distribution if the process is a Poisson process. The elapsed time for a particular transition is given by Equation 3.4. The system is then advanced to the final state of the chosen transition and the process is repeated.

All KMC computer simulations for microstructure evolution under irradiation have not yet considered the influence of the internal and applied stress fields on the kinetics of mobile defects, for example in the ALSOME [80] or BIGMAC [26] codes. In most realistic situations, however, interactions between dislocations and point defects play a key role in determining the effects of radiation on mechanical properties. The present KMC method accounts for elastic interactions amongst SIA clusters, nanovoids and dislocations. We explicitly incorporate here the effects of elastic interactions between SIA and vacancy clusters themselves (cluster-cluster type), and between defect clusters and dislocations (dislocation-cluster type). SIA clusters are directly produced on the periphery of neutron collision cascades, and they may contain from a few atoms up to tens of atoms in the near vicinity of the cascade [15, 81]. According to the results of MD simulations [73], the most stable configuration of SIA clusters is a set of $\langle 111 \rangle$ crowdions.

In view of the availability of size-dependent cluster characteristics provided by MD simulations, we simulated $\langle 111 \rangle$ type SIA clusters, consistent with published MD simulations. Such clusters are extremely mobile, and migrate predominantly along highly-packed crystallographic directions, with migration energies of less than 0.1 eV [26, 15]. Small SIA clusters may also spontaneously change their

Burgers vector, and thus have the flexibility to translate along various crystallographic directions if their motion is not obstructed by internal strain fields. Since MD simulations have shown that the majority of SIA clusters have the form of mobile (glissile) perfect dislocation loops, we represent here SIA clusters as small prismatic, rigid and circular dislocation loops. The relationship between radius of the loop (R) and the number of defects (N) is $N = \sqrt{2}\pi R^2/a^2$. We approximate vacancy clusters produced in cascades as small spherical voids, with an effective radius of $r_v = \sqrt[3]{3N\Omega/4\pi}$, where Ω is the atomic volume and N the number of vacancies in the cluster. The total cluster activation energy for migration is then given by:

$$E_i = E_m + \Delta E_{\text{int}} \tag{5.1}$$

where E_m is the activation energy in a perfect crystal, and ΔE_{int} the difference in the interaction energy of a defect cluster placed at two neighboring equivalent positions in the crystal.

The implementation can be demonstrated in detail through ~~a cascade damage~~ the flowchart shown in Fig. 5.1. With the initiation of dislocation distribution, cascade damage rate and matrix temperature as well as the initial calculation and summation of atomic jump rates, the key steps lie in the execution of the thermal diffusion loop and can be described as follows: (1) Select a jump path at random weighting by individual rate; (2) Make the jump; (3) Update and sum up jump rates; (4) Turn ahead simulation clock by n-fold way algorithm; (5) Iterate step 1 through 4 until designated damage dose (in terms of the number of cascades) is implanted. The above seemingly simple procedure may be readily programmed and executed for ideal systems (no interactions involved) without much concern for computation time. For bigger and complex systems, say thousands of atoms with interactions, the step of generating the events table and selecting a jump

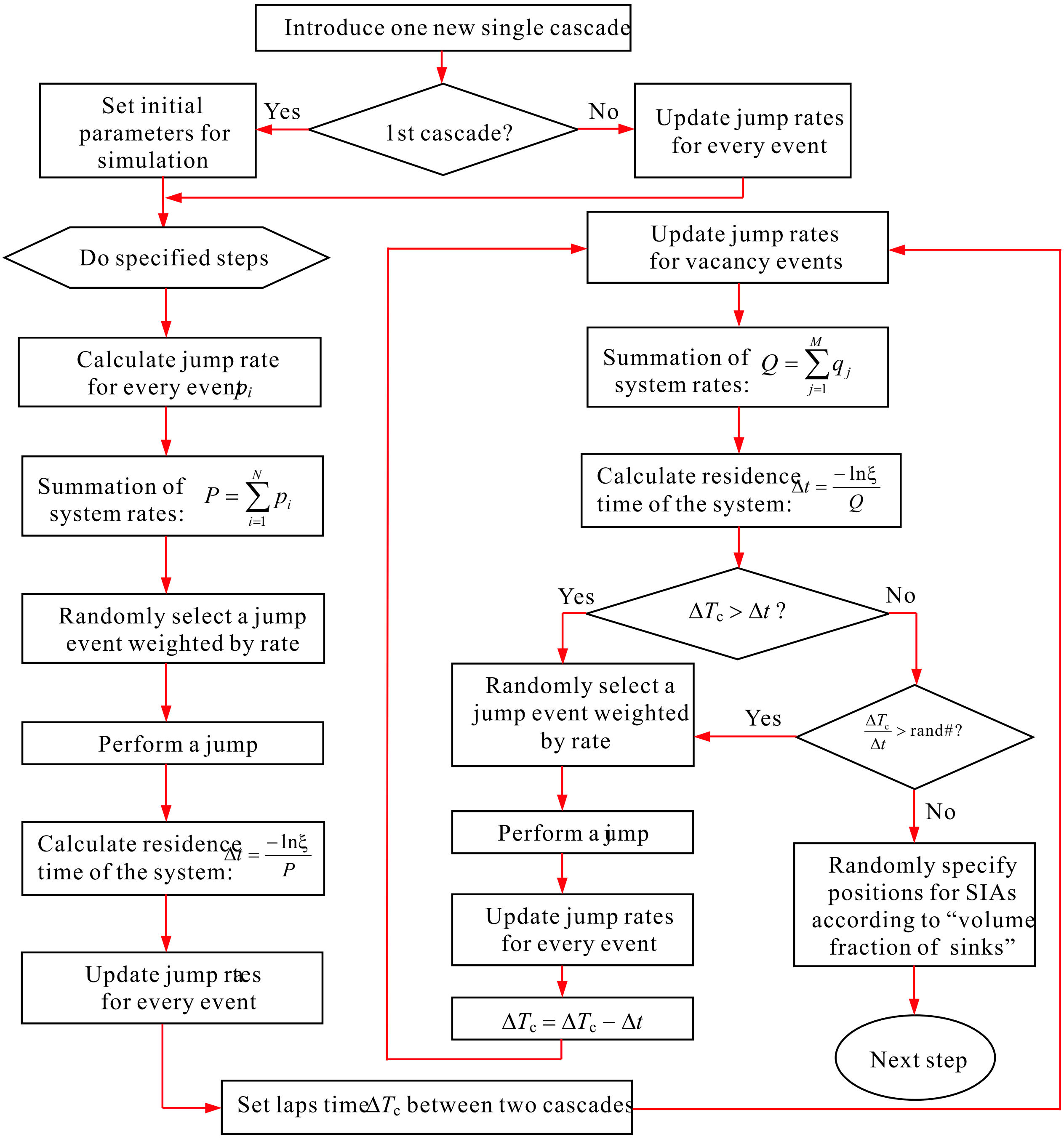

Figure 5.1: Kinetic MC Implementation of the damage evolution of cascade-induced defect clusters.

path from a large number of jump paths can be a daunting task and very careful programming is needed to obtain efficient execution. Otherwise, intrinsically fast MC method (compared to MD) can be unreasonably slow.

5.3 MAIN MODEL FEATURES

The cascade-induced defect distribution process consists of several distinct steps, introduction of defects associated with one high-energy displacement cascade, interaction between defects resulting in instant (intracascade) recombination of defects of opposite types and agglomeration of defects of the same type, diffusion incorporated with interactions between dislocations, impurities and point defects leading to defect annihilation at a sink, trapping of defects by impurities, decoration slip dislocations with defect clusters. To simulate the defect distribution process, all of the process should be incorporated. Although interaction may not be important at a dilute defect density or very large apart distance and can be approximated accordingly using ALSOME [57, 58, 74, 80, 82] or BIGMAC [26, 75] code, in most practical situations the interactions between dislocations and point defects play a key role in determining the effects of radiation on mechanical properties. This interaction effects must therefore be taken into account. The methodology should also address the many diffusional pathways available. It should also connect with the temperature and damage rate these control the available time for microstructure evolution processes before the defect densities reach a dynamic equilibrium state (saturated densities).

In the last section the main idea of KMC scheme has been described. We present here a computer simulation method which explicitly incorporates the effects of the elastic interactions between SIA and vacancy clusters themselves (cluster-cluster type), and between defect clusters and dislocations (dislocation-cluster type). SIA clusters are directly produced on the periphery of neutron collision cascades, and they may contain from a few atoms up to tens of atoms in the near vicinity of the cascade [83]. Such clusters are extremely mobile, and migrate predominantly along highly-packed crystallographic directions, with migration energies of less than 0.1 eV [83, 26]. Small SIA clusters may also spontaneously change their Burgers vector, and thus have the flexibility to translate along various crystallographic directions if their motion is not obstructed by internal strain fields. Since MD simulations have shown that the majority of SIA clusters have the form of mobile (glissile) perfect dislocation loops, in this work, we represent SIA clusters as small prismatic, rigid and circular dislocation loops. As for vacancies, small spherical voids are employed to approximate single vacancies and vacancy clusters. The effective radius of void has been defined as

$$r_v = \sqrt[3]{\frac{3N\Omega}{4\pi}} \tag{5.2}$$

where Ω is the atomic volume and N the number of defects in the cluster. The temperature dependence of the jump frequency of defect clusters diffusion has been given as 3.1. In our KMC simulation, the elastic interaction is incorporated. The influence of other defects and the external stress on one SIA or vacancy cluster is given by the stress field σ_{ij}. By applying the infinitesimal dislocation loop approximation for SIA clusters , the work necessary to form the loop characterized by normal n, Burgers vector b and area δA in the stress field σ_{ij} is SIA cluster interaction energy E_{int}, and is given by Eqn. 4.28. Similarly, we have vacancy cluster interaction energy shown as Eqn. 4.30 where it need to be noted that,

$$\varepsilon_{jj} = \frac{q}{K} = \frac{G\delta V}{\pi a_0^3 K} \tag{5.3}$$

where $3K = 3\lambda + 2G$ called the volume modulus.

The total cluster activation energy is then given by:

$$\tilde{E}_m = E_m + \Delta E_{\text{int}} \tag{5.4}$$

where E_m is the activation energy in a perfect crystal structure and can be obtained by either experiments or MD simulations, and ΔE_{int} the difference in the interaction energy of an defect cluster placed at two neighboring equivalent position in the crystal. This includes the effects of forces and moments on the virtual loop or microvoid motion.

5.3.1 Displacement Cascade Simulations

In this section, we study the evolution of cascade-induced defect clusters in BCC Fe at 300 K using KMC simulations. The input data necessary for these simulations, namely defect migration energies and the initial defect configurations produced by displacement cascades are all obtained by MD simulations. Based on intensive MD simulations, Osetsky *et al.* [73] developed a generalized size dependence of cluster jump frequency to describe the one-dimensional diffusional transport behavior of SIA clusters

$$\omega^n = \omega_0 n^{-S} \exp\left(-\frac{\langle E_m \rangle}{k_B T}\right) \tag{5.5}$$

where $\langle E_m \rangle$ is the averaged effective activation energy, n the number of SIAs in the cluster, and ω_0 is a new, size-independent, pre-exponential factor. The value of $\langle E_m \rangle$ is estimated from the MD simulations as 0.023 ± 0.003 eV for $\frac{1}{2}\langle 111 \rangle$ clusters in BCC Fe. By fitting to the simulation results of various cases, the values $\omega_0 = 6.1 \times 10^{12}$ s^{-1}, $S = 0.66$ for Fe describe the MD data very well and are used in our KMC simulations. There are also a large number of vacancies produced in displacement cascade. The vacancies are allowed to execute random 3-D diffusion jumps with a probability proportional to their diffusivity. The temperature dependence of the defect diffusivity is written as [75]

$$D = D_0 \exp(-\frac{E_m}{k_B T}) \tag{5.6}$$

where D is the defect diffusivity, D_0 the pre-exponential factor, E_m the migration energy of vacancy. The migration rates are defined as

$$r = \frac{6D}{\delta^2} \tag{5.7}$$

where δ is the jump distance and equal to the magnitude of Burgers vector in our simulations. Equation 5.7 has a similar form to Equation 3.1, and is used in some other KMC simulations (e.g., [26, 75, 84]). The values of the migration energy and prefactors obtained from MD simulations for vacancies are 0.87 eV and 1.15×10^{-2} cm^2/s, respectively[26]. The jump rates of vacancies are almost ~~10∼12~~ 10 − 12 orders of magnitude larger than that of SIAs in room temperature. Therefore, vacancies can be treated as immobile when we consider the microstructure evolution during the first few nanoseconds in a cascade. By now, cascades of primary-knock-on-atom (PKA) energy, E_{PKA}, up to 100 keV have been simulated in BCC metals over a wide temperature range[85, 15]. We present here the KMC simulations using the initial defect configurations produced by a cascade of 100 keV PKAs [85]. Figure 5.2 is a typical defect configuration resulting from a 100 keV cascade. The size of the KMC computation box is 1 μm^3. The starting defect microstructure is introduced at a random position of the KMC simulation box according to the spatial configuration obtained by the MD simulations of the corresponding cascade. Then, the system runs for a certain time period at a given temperature (T = 100 K), and a fixed boundary condition is employed (defects that are able to reach the edge of the KMC simulation box are counted to escape away). An MD study of the interactions between glissile interstitial clusters and small dislocation loops in α-Fe and Cu has been carried out by Osetsky *et al.*[86]. As a result of the inter-cluster interactions both glissile and sessile clusters can be obtained and this depends on the metal, reaction type and size of the clusters. In our simulations, when two big clusters (> 37 SIAs) of differently oriented Burgers vectors approach ~~to~~ in each other, they keep their own orientations and the complex formed becomes sessile. Otherwise, one cluster changes its Burgers vector to be parallel to the other, so that a bigger glissile cluster is formed.

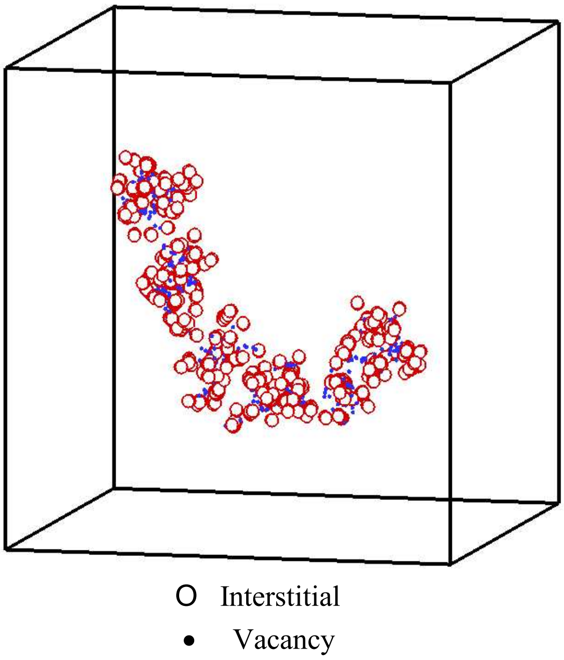

Figure 5.2: Primary damage state at 17 ps for a 100 KeV cascade: (◯) interstitials; (•) vacancies.

~50 nd ~50

Our simulations show that a large portion of the interstitials and vacancies are lost in a very short time (∼50 ps) by recombination. This is consistent with the results of MD modeling in which an extensive amount of recombination of SIAs and vacancies occurs during the cooling stage of HEDCs. Figure 5.3 shows a close view of the microstructure at $t = 94$ ps. It can be seen that some SIAs has coalescence into bigger clusters. The result is supported by MD simulations

??

in which one of the most significant findings is the occurrence of intracascade clustering. Most of the recombination and clustering take place within 10 ns. Most of the glissile interstitials and interstitial clusters escape away from the cascade center within around 60 ns. The value of freely migrating defects(FMDs) production efficiency η obtained by our KMC simulation is $\eta \approx 0.1$ (i.e. 10%). The cases of incorporating with internal dislocations are also studied. Since the density of glissile SIAs is rather low (˜10^{18} m^{-3}), no visible dislocation decorations have been observed.

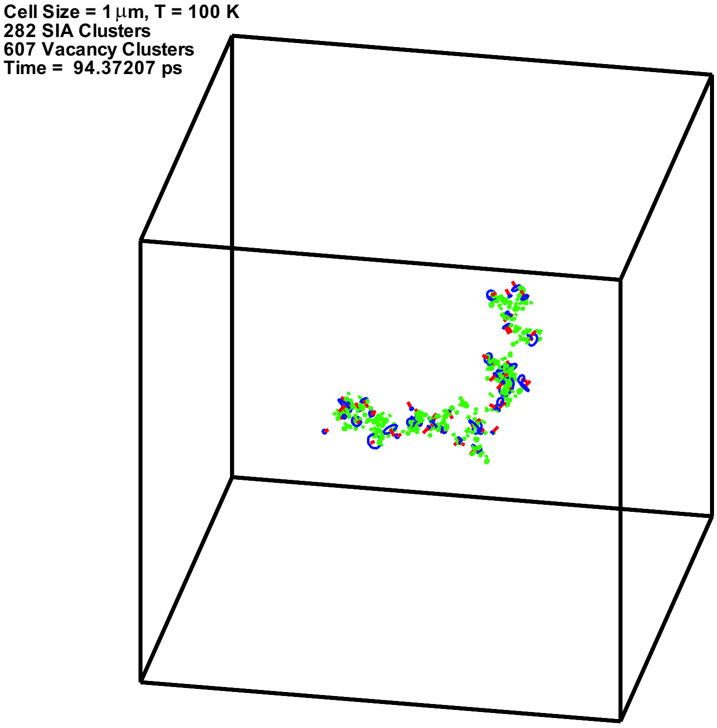

Figure 5.3: A close view of the structure of one single cascade at $t = 94$ ps. Small circular loops represent SIA clusters, and solid points represent vacancies.

5.3.2 DISLOCATION DECORATION

Due to the significance of the effects of glissile SIA clusters on damage evolution, we first establish the dynamics of their motion in the field of grown-in dislocations. The value of the migration energy, diffusion pre-factors, and other input parameters for SIA diffusion used in this work are listed in Table 1. A computational cell of $400a \times 400a \times 400a$ ($a = 0.2867$ nm is the lattice constant) is used with periodic boundary conditions. The ratio of the activation energy for Burgers vector rotation to the 1-D migration energy is set to be eight. A slip dislocation loop lying on the (101) plane, with Burgers vector $\mathbf{b} = a/2[\bar{1}11]$ is introduced into the simulation box. The dislocation loop consists of two curved segments and two straight super-jog segments that are normal to the loop's Burgers vector. A number of SIA clusters with the same size, R, were initially randomly distributed in the simulation box, and their initial jump directions were also randomly specified. The initial SIA cluster density was varied in the range $5 \times 10^{22} - 2 \times 10^{23}$ m^{-3}. When a cluster approaches the dislocation loop within a very short distance, it oscillates back and forth due to its strong interaction with the dislocation. To improve the computational efficiency of such ‘ fast ’ dynamics, we used an ‘adiabatic approximation’ by freezing trajectories of SIA clusters if a prescribed displacement is too small (e.g. less than 1 nm) over an extended period of time (e.g. greater than 10^4 time steps). Once a cluster is stopped, all events related to it are removed from the event table. When two SIA clusters approach one another within one atomic distance, they coalesce and make a larger cluster.

Table 1

Parameters used in the present simulations. Results for E_m and ω_0 are from [73] and [84], respectively.

E_m (eV)	a (Å)	R (a)	T (K)	ω_0 (s^{-1})	G (GPa)	ν
0.02	2.867	3.0	300.0	2.5×10^{13}	81.8	0.29

One of the most striking features in the evolution of dislocation microstructure under cascade damage conditions is most dislocations are observed to be heavily decorated by small, immobilized interstitial clusters [12]. Figure 5.4 shows a TEM micrograph of pure iron irradiated with fission neutrons at about 70 °C. Grown-in (slip) dislocations are clearly decorated with small defect clusters, and the formation of loop rafts is significant. To determine the influence of the elastic field of dislocations on the motion of SIA clusters, cluster-cluster interactions were first excluded. As can be seen in Figure 5.5, the overall mobility and spatial distribution of SIA clusters were significantly changed as a result of dislocation-cluster interactions. After 0.4 ns, the majority of initially glissile clusters were attracted to the slip dislocation loop (near the edge components), and became virtually immobile. In effect, these clusters re-oriented themselves by rotation of their Burgers vectors to respond to the elastic field of dislocations. Thus, their migration was forced towards the source of the internal stress field, rather than being random. The high concentration of SIA clusters results in an extremely inhomogeneous spatial distribution, as can be seen in Figure 5.5. For the same initial configuration as shown in Figure 5.5(a) we also carried out KMC simulations without involving any interaction between SIA clusters and the slip dislocation loop. Figure 5.6 shows the final structure after running the same number of time steps as in Figure 5.5. Even with introducing a standoff distance (taken as 1.5 nm) along the slip dislocation loop, there is no sign of development of dislocation decoration.

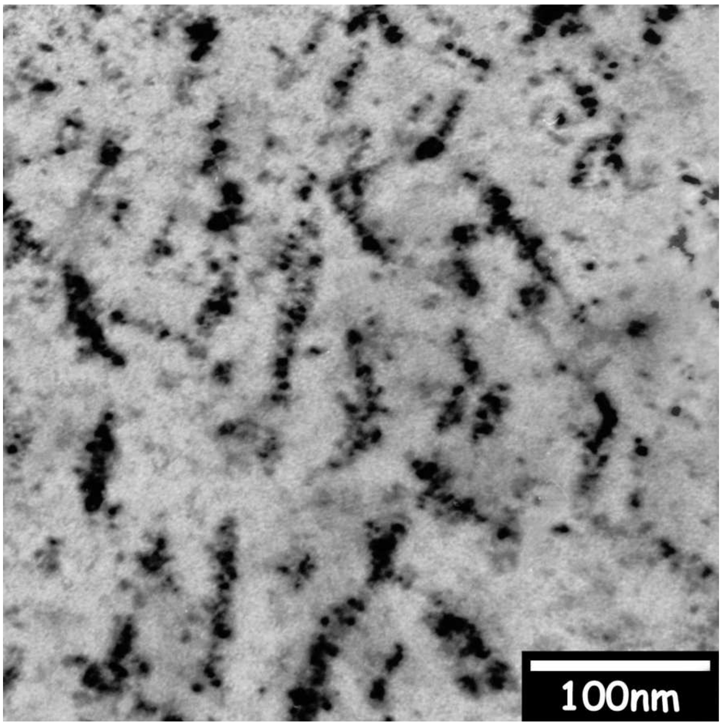

Figure 5.4: TEM micrograph of pure Fe irradiated with fission neutrons at 70 ^{O}C to a displacement dose level of 0.72 dpa.

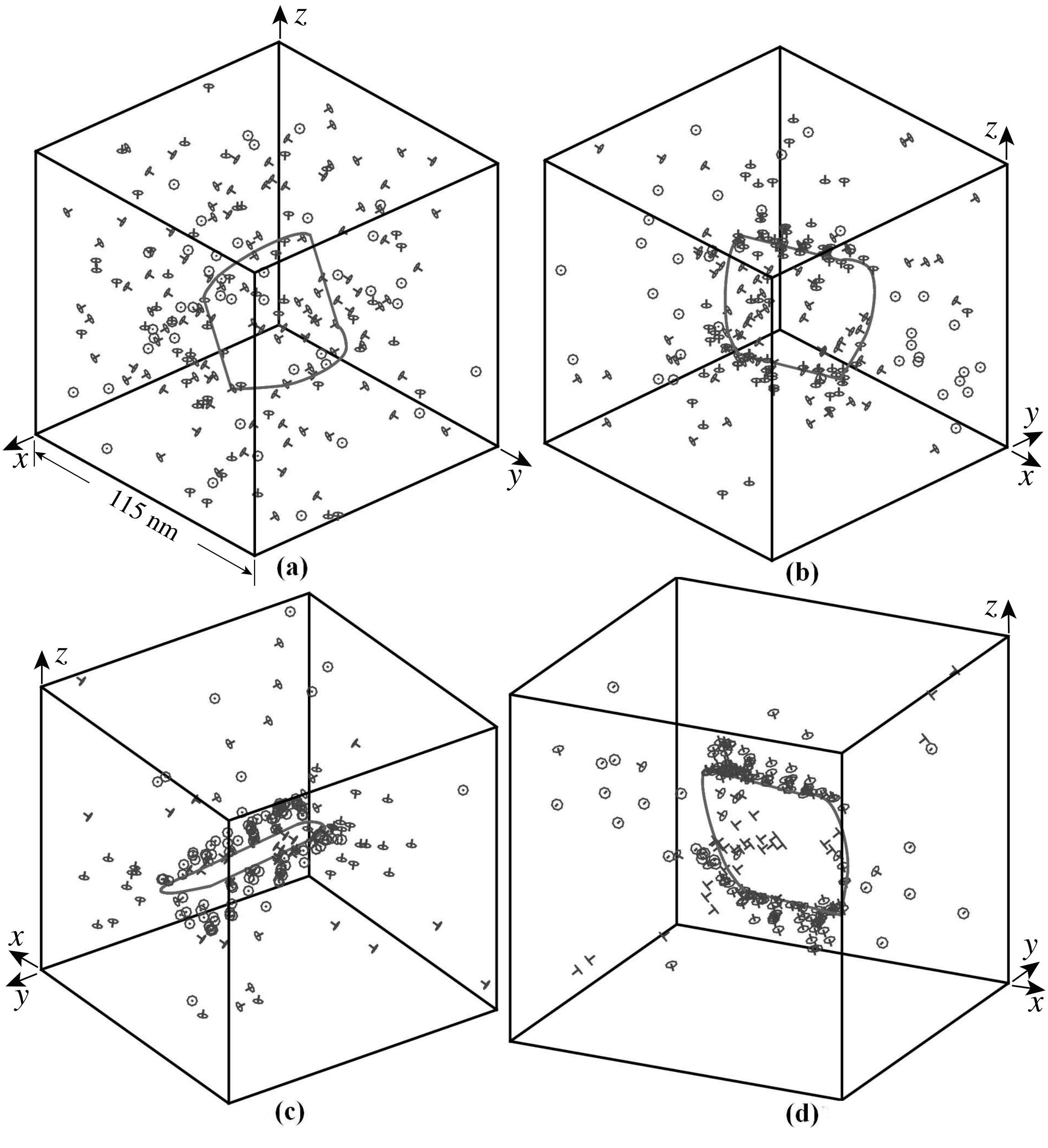

Figure 5.5: KMC simulation results of 200 SIA clusters in the stress field of a 3-D dislocation loop. Burgers vector of the slip dislocation is along [$\bar{1}$ 1 1] direction and the temperature is 300 K. SIA clusters are clearly observed to accumulate along the edge components of the loop. (a) 0 ns; (b) 0.1 ns; (3) 0.3 ns; (d) 0.4 ns.

The comparison between Figures 5.5 (d) and 5.6 reveals that the elastic interaction significantly changes the kinetics of SIA clusters and thereby the microstructure evolution. SIA clusters end up near the core of grown-in dislocations, orienting their Burgers vector parallel to the grown-in dislocation. They form a cluster atmosphere around the grown-in dislocation, similar to the Cottrell impurity atmosphere in BCC metals [30]. The present simulations show clearly how SIA clusters are attracted to dislocations, eventually decorating them, in good qualitative agreement with experimental observations.

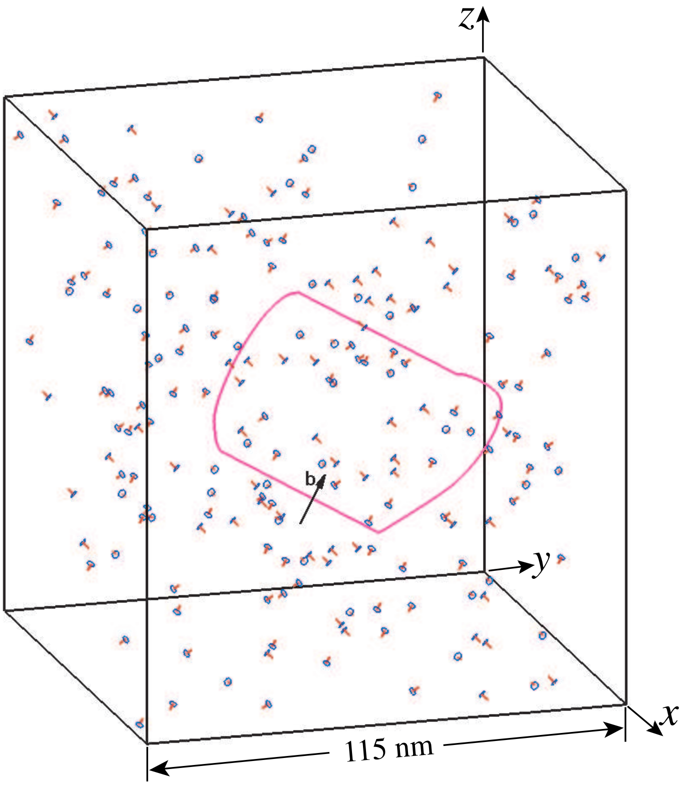

Figure 5.6: KMC simulation results of 200 SIA clusters with no interaction between SIA clusters and the 3-D dislocation loop. Burgers vector of the slip dislocation is along $[\bar{1}\ 1\ 1]$ direction and the temperature is 300 K. Dislocation decoration is not observed.

5.3.3 PINNING AND SMALL RAFTS OF SMALL INTERSTITIAL LOOPS

To investigate the influence of cluster-cluster interactions on their motion, the grown-in dislocation was removed, and the elastic interaction between clusters included in a new KMC simulation. Mutual elastic interactions in between clusters was found to affect their distribution and motion drastically. Because of mutual interaction, two clusters that are oriented along non-parallel crystallographic orientations will either coalesce forming a larger one, or rotate and pin one another at a short distance and move jointly in the same direction. Once two clusters are pinned together, they have less chance to change their orientation, and therefore their motion becomes almost pure one-dimensional. As this process proceeds, some additional clusters may be trapped into this pinned structure by changing their Burgers vectors. This self-organizing mechanism eventually results in the occurrence of SIA $rafts$, which consist of small dislocation loops with the same direction of motion. This feature has been experimentally observed for some time [30].

It has to be noted that when the defect is big enough to behave as a perfect dislocation loop it may not follow the mechanisms mentioned above. Instead, dislocation loops may follow the rule of summation of Burgers vectors and form sessile $\langle 100\rangle$ loops. The formation and growth of $\langle 100\rangle$ interstitial loops in bcc iron have been confirmed by both experiments and MD simulations [**?**]. However, the mechanism for the formation of $\langle 100\rangle$ loops through interactions between $1/2\langle 111\rangle$ loops seems more feasible at high temperature and high irradiation dose. Considering the conditions for our simulations, namely low damage doses and room temperature, the present investigation is focused on $\langle 111\rangle$ interstitial loops. The formation of $\langle 100\rangle$ loops through the direct interaction of $1/2\langle 111\rangle$

loops, as well as the effects of $\langle 100 \rangle$ loops have been excluded.

A simulation of cluster motion integrating the influence of the internal stress field created by grown-in dislocations, as well as the clusters themselves was also performed. Figure 5.7 shows a typical defect evolution time sequence for 200 SIA clusters at 300 K. The effects of internal dislocation fields, aided by cluster mutual elastic interactions, rendered most of the clusters virtually immobile in the vicinity of the slip dislocation. Continuation of the decoration process results in the initiation of a 'dislocation wall'. Similar simulations were performed for a smaller cluster density (50 SIA clusters), and also at a higher temperature (600 K). The results indicate that the SIA cluster density seems to have a greater influence on the transient time for decoration than temperature. At high temperatures, the kinetics of dislocation decorations is faster as a result of increased cluster jump rates. The simulations also show that the $rafting$ structure occurs more readily at lower temperatures.

It should be noted that we excluded absorption reactions between grown-in dislocations and SIA clusters, since our major concern in the present work is the segregation and agglomeration of defect clusters, as supported by direct experimental observations. Except for a direct encounter between a glissile loop and a dislocation, absorption of a loop by the dislocation requires a change in the direction of motion of the loop, either by a thermally activated Burgers vector change or by self-climb. Using MD simulations, Rodney and Martin investigated the mechanisms of the absorption of small interstitial loops by an edge dislocation in fcc nickel [87, 88]. It was shown that small interstitial clusters participating in absorption reactions represent rather weak dispersed barriers and do not have an impact on the yield drop phenomenon observed experimentally. It was also shown that small interstitial loops may find their stable positions a few lattice planes

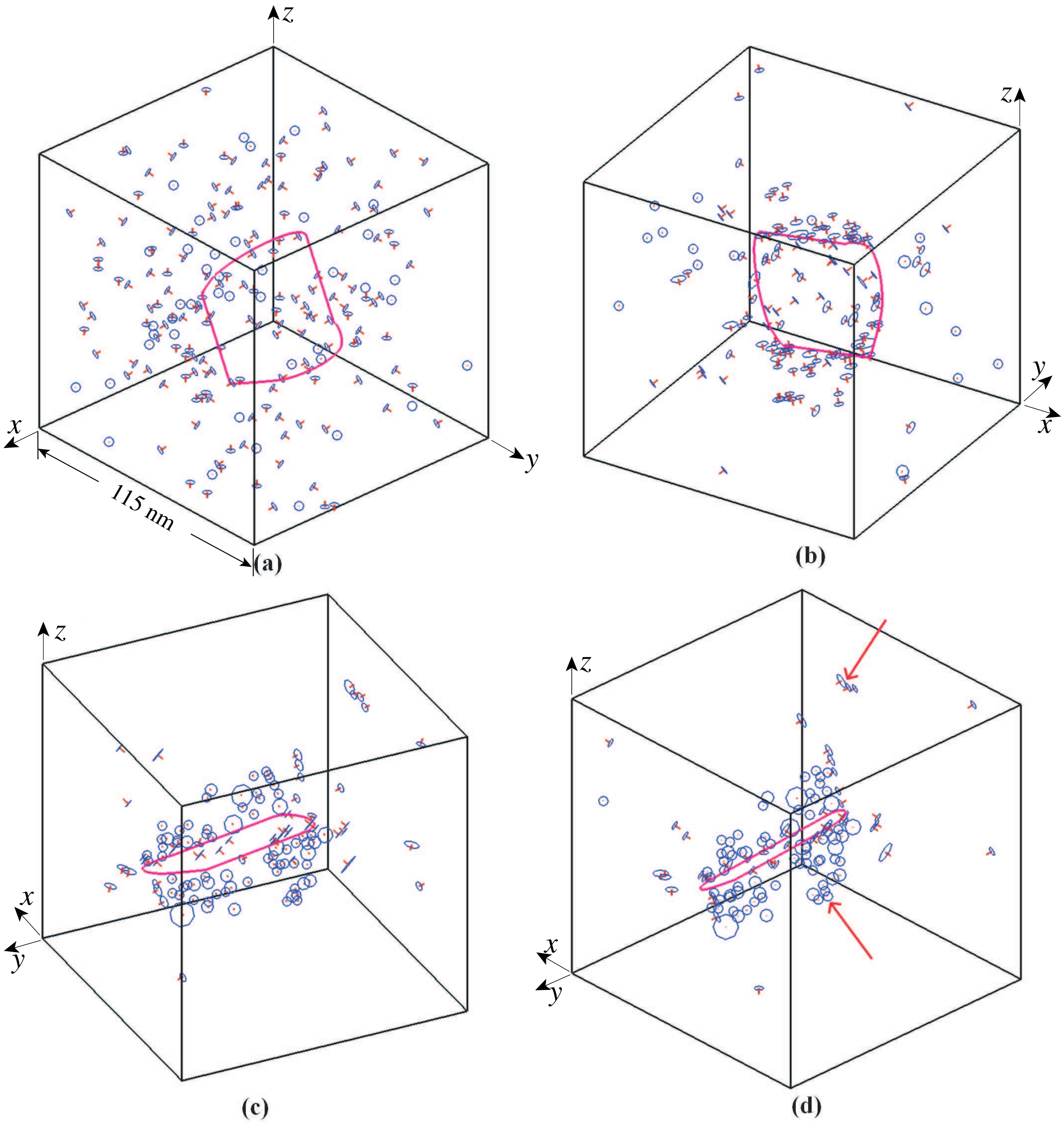

Figure 5.7: KMC simulation of 200 SIA clusters in the stress field of a 3-D dislocation loop. Burgers vector of the slip dislocation is along $[\bar{1}\ 1\ 1]$ direction and the temperature is 300 K. Dislocation decoration and SIA cluster rafts are clearly observed, as indicated by the arrows. (a) 0 ns; (b) 0.4 ns; (3) 0.7 ns; (d) 1.0 ns.

away from the dislocation glide plane dislocation [87]. Decoration of dislocations with small clusters may require that a single trapped loop is immobilized by other loops before it is detrapped from or absorbed by the dislocation [30]. This is shown in Figures 5.5 and 5.7, where the build-up of SIA cluster concentrations in the neighborhood of the dislocation is clearly shown. The exclusion of absorption in our simulations may affect the quantitative distribution of smaller interstitial clusters. However, as the decoration and loop raft formation processes proceed, the probability of interstitial clusters approaching dislocation cores decreases due to the screening effects of existing loops. The exclusion of absorption of interstitial loops by grown-in dislocation would not qualitatively affect the results of the present simulations.

All these three types of interactions have been studied for cases of 50 SIA clusters and 600 K as well to account for the variations of cluster densities and temperatures. A comparison of the evolution time is given in Table 5.1. It can be seen that SIA cluster density seems to have greater influence on reaction time than temperature. Under higher temperature conditions it may took less time for the occurrence of remarkable dislocation decoration phenomenon than in lower temperature. The high temperature increases the thermal activities of clusters, which makes clusters have more chance to approach to reaction range of internal dislocations. The simulations also show that the $rafting$ structure can be more easily to appear in lower temperature and higher cluster density cases.

Table 5.1: Evolution time for Running 800,000 KMC Steps (in ns).

Number of SIA Clusters	D-C Interactions		D-C-C Interactions	
	300 K	600 K	300 K	600 K
50	1.95	1.28	3.29	3.14
200	0.416	0.237	1.04	0.79

The Range of Validity of the Elastic

5.4 ~~VALIDITY OF ELASTIC APPROXIMATION- MD SIMULATION VS ELASTICITY CALCULATION~~

Representation of Defects

The most significant feature of current KMC method, which makes it different from other existing KMC simulations, is that elastic interactions between defects are integrated. Therefore, it is imperative to examine the validity of the treatment of the interactions between dislocations and clusters by elasticity theory, especially at close ranges. Specifically, ~~it is appreciated~~ we need to determine whether or not the dislocation-cluster interaction can be described accurately within the framework of the isotropic continuum theory of dislocations using the infinitesimal loop approximation, or ~~on~~ to what ~~extend~~ extent the interaction can be calculated with enough accuracy by elasticity. The present investigation intends to perform comparative studies for the interaction energy between a perfect SIA cluster and an edge dislocation in bcc iron by atomistic simulations and isotropic elasticity theory. We studied the interaction between dislocations and SIA clusters having the same Burgers vector, as formed by a decoration microstructure in bcc iron.

Molecular statics was used to study the dislocation-cluster interaction energy at a temperature of zero Kelvin in bcc structure. The simulation box was oriented along $[1\bar{1}0]$, $[11\bar{2}]$ and $[111]$ directions, and contained about 1.3 million atoms. The size along the Burgers vector, $\mathbf{b}$, was $185|\mathbf{b}|$ and approximately 12 nm along the dislocation line. Periodic boundary conditions ~~was~~ were applied along the dislocation line, and boundaries along the other two directions were set to be rigid. The atoms in rigid boundaries were displaced according to the elastic solution for the dislocation. An isolated dislocation was first introduced into the simulation box and relaxed. An SIA cluster consisting of 37 SIAs (of effective loop radii 0.75 nm) and with the same Burgers vector as that of the dislocation was then created right at a certain distance, $\mathbf{r}$, along $[1\bar{1}0]$ below the dislocation slip plane, and the simulation box was relaxed again. The dislocation-cluster interaction energy was calculated using the energies of a previously-relaxed isolated dislocation and that of a cluster. The interatomic potential developed by Ackland et al.[89] for α-Fe is employed.

The interaction energies obtained in the computer simulation was compared with the results evaluated by the infinitesimal loop approximation, which is given by

$$E_{\mathrm{INT}}^{\mathrm{I}} = -\frac{\mu b^2 A}{2\pi(1-\nu)}\frac{1}{r} \tag{5.8}$$

where A is the loop area and r is the distance between the cluster center and dislocation line.

Simulation results for the interaction energy of a 37-SIA cluster with an edge dislocation in bcc Fe as a function ~~of the~~ distance r is shown in Figure 5.8. The estimation of the same energy by the infinitesimal loop approximation is also shown. It can be concluded that the agreement between the simulation results and the ones estimated by ~~the~~ isotropic elasticity is quite satisfactory at distance $r > 5a_0$. At shorter distance, however, the results given by the analytical solution overestimate the interaction energy of the dislocation and cluster, which implies that short-range effects cannot be treated within the framework of isotropic elasticity.

divide by 37

Is there an effect of Temp?

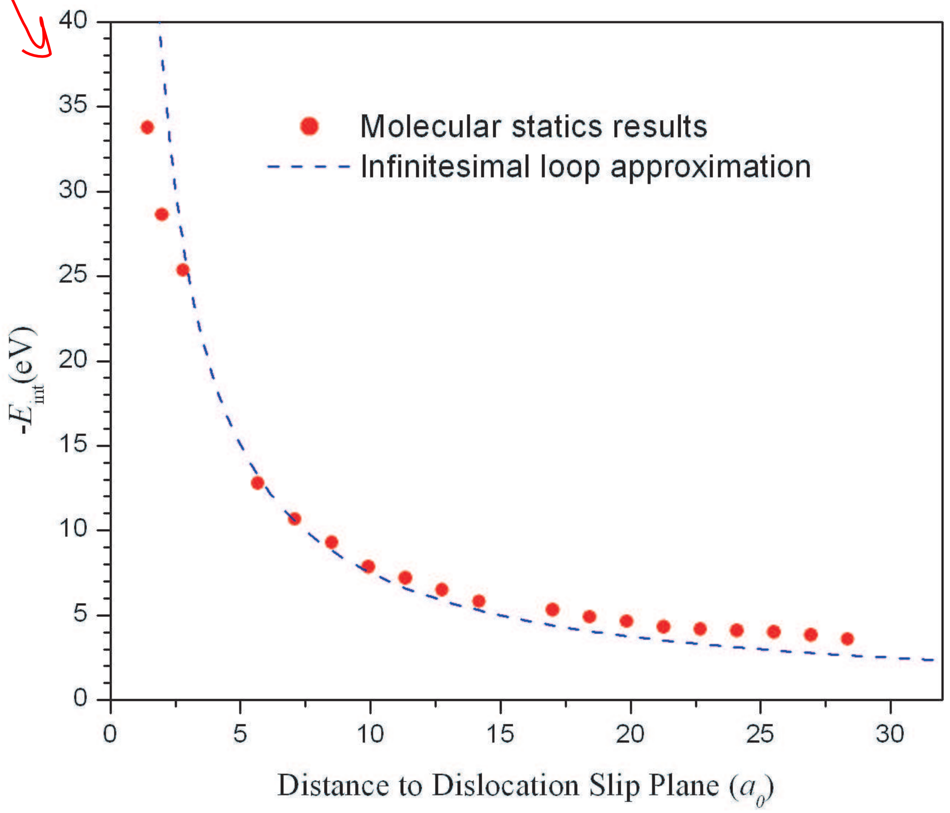

Figure 5.8: Interaction energy between $\frac{1}{2}$ [111] edge dislocation and 37-SIA prismatic cluster in bcc Fe as a function of distance along $[1\bar{1}0]$ direction. Simulation results are compared with the interaction energy evaluated by infinitesimal loop approximation.

per SIA

CHAPTER 6

KINETIC MONTE CARLO SIMULATION OF RADIATION DAMAGE EVOLUTION IN α-IRON

6.1 INPUT PARAMETERS TO KINETIC MONTE CARLO SIMULATIONS

Fitting MD-generated data for several metals, Bacon et al.[15] showed that the number of Frenkel pairs (N_F) is given by: $N_F = A(E_{PKA})^m$, where A and m are constants, and E_{PKA} is the energy of the Primary Knock On Atom. On the other hand, the number of displaced atoms can be written as: $N_F = PN_t$, where P is the displacement dose (dpa), and N_t the total number of atoms in the system. Therefore, the displacement dose level corresponding to one cascade can be readily calculated as:

$$P = \frac{N_F}{N_t} = \frac{A(E_{PKA})^m}{N_t} \tag{6.1}$$

With the relationship between the cascade energy and damage dose, we can determine the number and frequency of cascades required for producing a desired dose at a predetermined dose rate.

Point defect statistics for clusters generated by 40 KeV cascades in α-Fe (e.g. number, size distribution, and mobility) were taken from the MD simulations of

Bacon, Gao and Osetsky. [15] Soneda and Diaz de la Rubia [26] have shown that two thirds of the defects that escape from the parent cascade region are in the form of small SIA clusters, which migrate in one dimension. Therefore, monodefects as well as relatively smaller clusters were ignored in the present simulations. Room temperature neutron irradiation of iron was simulated with a flux of 40 KeV cascades containing interstitial clusters of size ≥ 4 atoms.

It has been shown by MD simulations [90] that small loops consisting of four, five and six atoms transform spontaneously from the faulted into the highly glissile unfaulted configuration. In addition, the change in the Burgers vector of a cluster consisting of four SIAs has been observed to occur in these studies. From the lifetime of one configuration, a value of 0.4 eV is estimated for the energy barrier against this transformation [90]. The height of the barrier for orientation change is expected to increase significantly with increasing cluster size. MD studies show that small, strongly bounded interstitial clusters (two to about five-SIA clusters) exhibit long-range, three-dimensional (3D) diffusion, which occurs by reorientation of constituent $\langle 111 \rangle$ dumbbells from one $\langle 111 \rangle$ to another. [84] As the cluster size increases, thermally-activated reorientation from one Burgers vector to another becomes increasingly more difficult to achieve, no 3-D motion is observed even at very high temperatures. Osetsky et al. [73] developed a generalized size dependence of cluster jump frequency to describe the one-dimensional diffusional transport behavior of SIA clusters

$$\omega^n = \omega_0 n^{-S} \exp\left(-\frac{\langle E_m \rangle}{k_B T}\right) \tag{6.2}$$

where $\langle E_m \rangle$ is the averaged effective activation energy, n the number of SIAs in the cluster, and ω_0 is a new, size-independent, pre-exponential factor. The value of $\langle E_m \rangle$ was found not depending on size and close to that of the individual crowdion. It is estimated for clusters containing up to 91 SIAs in iron that

$\langle E_m \rangle = 0.023 \pm 0.003$ eV for $\frac{1}{2}\langle 111 \rangle$ clusters in bcc iron. By fitting to the simulation results of various cases, the values $\omega_0 = 6.1 \times 10^{12}$ s^{-1}, $S = 0.66$ for Fe describe the MD data very well, and were used in our KMC simulations.

Soneda and Diaz de la Rubia [26] studied the direction change frequency of 2-SIA and 3-SIA clusters in α-Fe using MD simulations and obtained the activation energies of 0.09 eV and 0.27 eV for 2-SIA and 3-SIA clusters, respectively. Gao et al. [91] investigated possible transition states of interstitials and small interstitial clusters in SiC and α-Fe using the *dimer method.* The activation energies of directional change were found to be 0.163, 0.133 and 0.342 eV for 1-, 2-, and 3-SIA clusters, respectively. In our work, we assume that the relationship between the activation energy of directional change for a interstitial cluster and the size of the cluster is linear, and is equal to 0.05 eV per interstitial atom. In fact, MD simulations have shown that the motion of small SIA clusters and loops is the result of the motion of individual crowdions, [15, 73] and the reorientation may occur in a one-by-one fashion. [86] The value of 0.05 eV/atom is probably an underestimation for the energy barrier for direction change of a small cluster, say size less than four, but for larger clusters, it reflects the preferential 1-D motion of large interstitial clusters. Figure 6.1 show the trajectories of the centers of mass of a 6-SIA cluster for diffusion at 300 K with respect to different energy barriers for directional change. MD simulations revealed that defect structure of a cascade is characterized by a vacancy-rich core surrounded by a shell of SIA clusters. We represent this vacancy-rich core region as an immobile spherical recombination center. The size of a recombination center or nano-void is given by an equivalent diameter. The number of vacancies in the core of a cascade is assumed to follow a Gaussian distribution with mean value of 100 and a standard deviation of 8 vacancies.

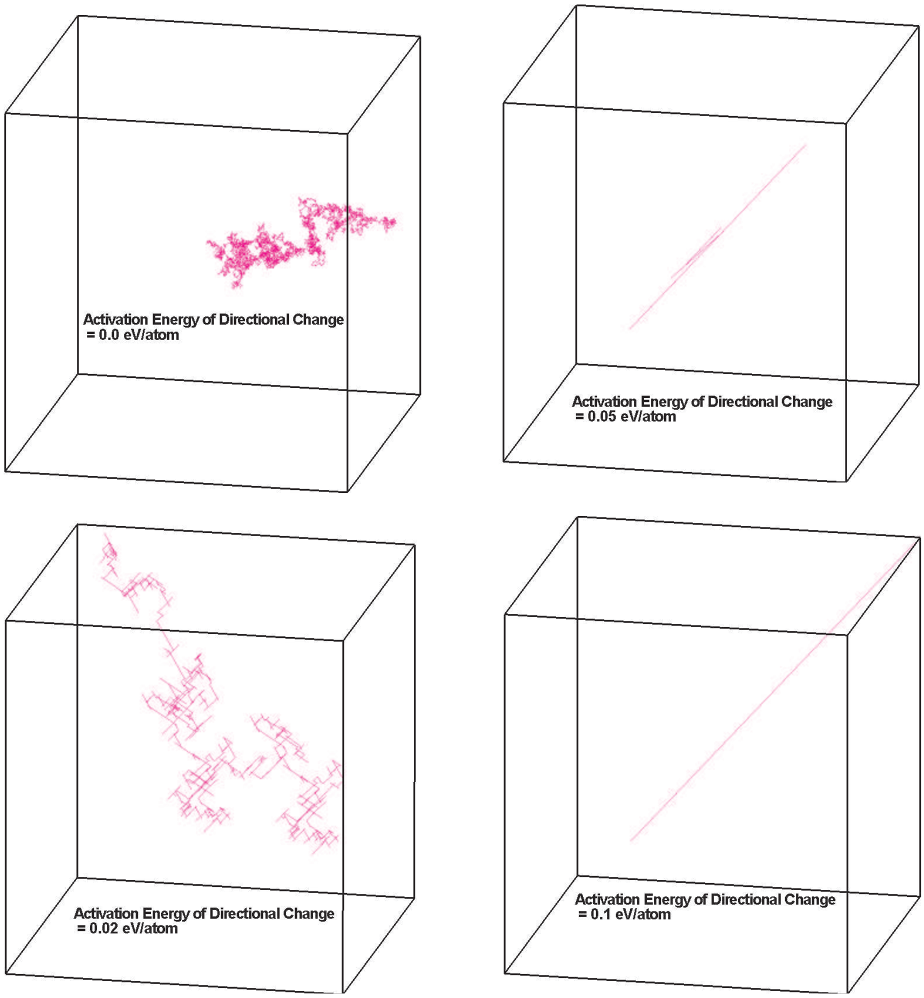

Figure 6.1: Centre-of-mass trajectories of a 6-SIA cluster migration for 10000 consecutive steps.

6.2 DOSE DEPENDENCE OF DEFECT DENSITY

Doses up to 5.21×10^{-3} dpa were simulated at a displacement damage rate of 5×10^{-8} dpa/s, and damage accumulation was studied as a function of dose. Figure 6.2 shows the interstitial cluster density as a function of dose, with and without recombination between SIA clusters and nano-voids. In addition, SIA clusters containing more than 100 interstitial atoms (diameter > 2.5 nm) are counted as 'visible' defects. The corresponding cluster density is calculated and compared with experimental data for bcc Fe irradiated at $\simeq 70$ °C in the HFIR reactor to displacement dose levels in the range of 10^{-4} to 0.72 dpa [9], and for pure iron irradiated in the DR-3 reactor at Risø National Laboratory at 320 K as shown in Figure 6.3. At low dose (dpa $< 10^{-4}$ dpa), the cluster density increases almost linearly with the dose. The increase in cluster density then slows down when the dose level is higher than 10^{-4} dpa. The cluster density approaches a saturated value and does not change much beyond a dose level of 3.5×10^{-3}.

At the beginning of irradiation, cluster densities of both interstitials and vacancies are rather low, and the chance that one interstitial cluster can get close enough to another interstitial or vacancy cluster is rather small as well. Because of the 1-D motion of SIA clusters, the recombination cross section with vacancy clusters produced in the cascade core and the agglomeration cross section with other interstitial clusters are small. Theoretically, there are only two mechanisms by which an SIA cluster could change its direction of motion: either thermal activation or interaction with other defects. The effect of thermal activation can be ruled out here because our simulations are carried out at low temperature (i.e. room temperature). At low damage dose levels, the large distance between clusters renders the interaction between them weak and can hardly affect their migration, thus the density of clusters increases linearly with dose.

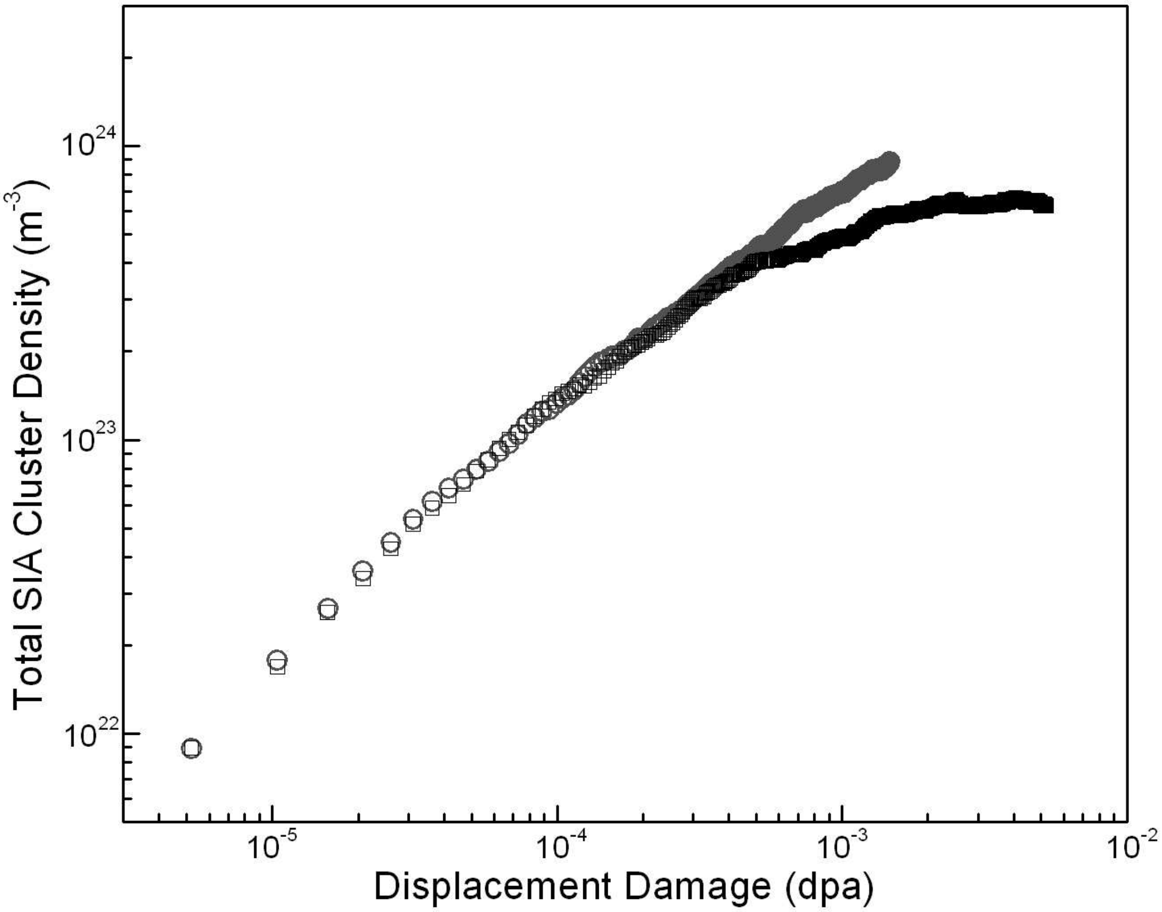

Figure 6.2: Dose dependence of the total SIA cluster density in bcc Fe: -○-, no recombination; -□- with recombination.

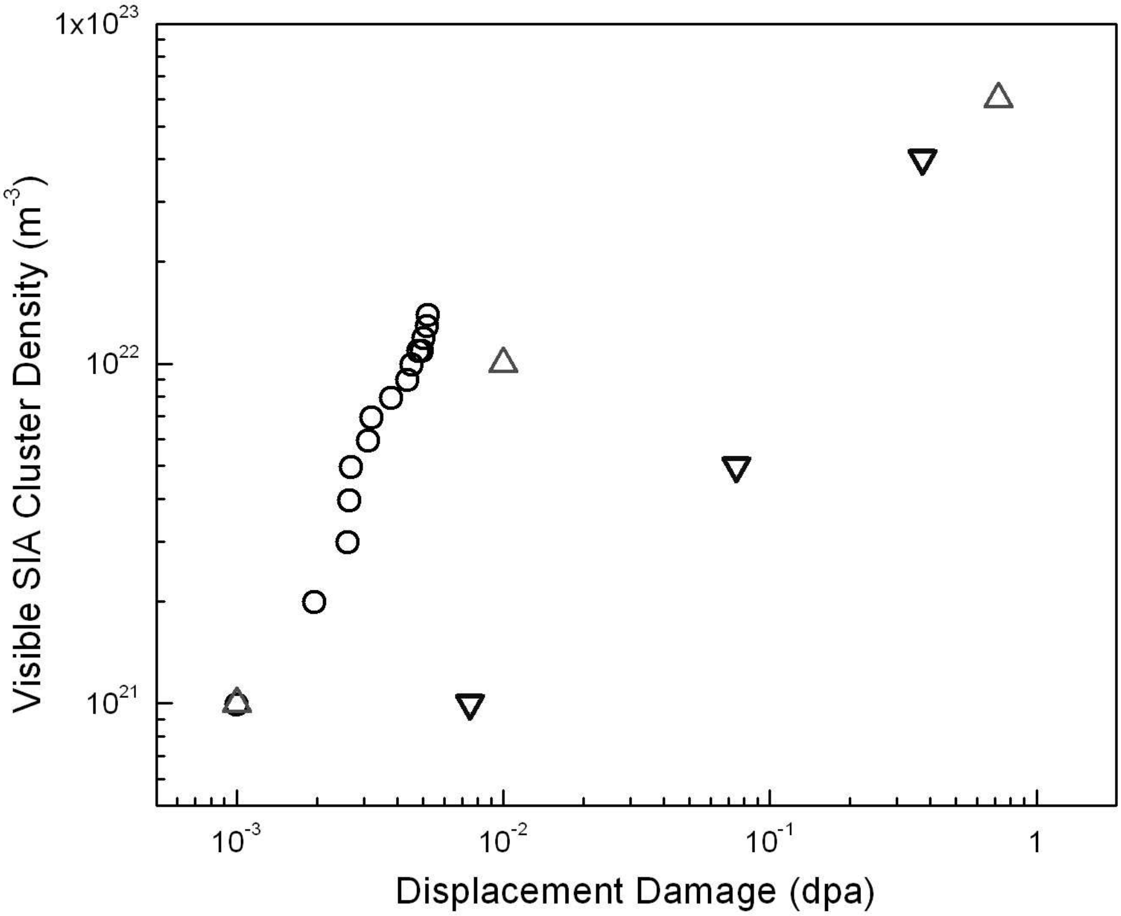

Figure 6.3: Dose dependence of the total visible SIA cluster density in bcc Fe: -○-, KMC simulation results; -△- experimental results of Eldrup *et al*. (2002); -▽- experimental results of Singh *et al*. (1999).

When the damage builds up to an appreciable level, on the order of 10^{-4} dpa, the simulation box becomes crowded with defects. The probability of mutual interaction between clusters becomes appreciable, leading to more pronounced recombination and agglomeration events. Consequently, these non-linear reactions slow down the increase in the density of SIA clusters. At higher accumulated damage levels, on the order of 3.5×10^{-3} dpa in the present case, the number of SIA clusters that recombine or coalesce reaches dynamic equilibrium with the number of clusters produced by fresh cascades. Then, SIA cluster density in the simulation box reaches a saturation level.

It is found that the presence of nano-voids has a significant effect on the evolution dynamics of SIA clusters. As we can see in Figure 6.2, at a dose level lower than 5×10^{-4} dpa, the difference between SIA cluster densities, with and without nano-voids, is not large. However, when nano-voids are included in the simulation, the surviving SIA cluster density deviates from the case when nano-voids are not included. For example, the density of surviving SIA clusters is less by a factor of 2 at 1.5×10^{-3} dpa, when nano-voids are included.

Although the density of SIA clusters reaches steady state after 3.5×10^{-3} dpa, SIA cluster sizes continue to grow, and the density of visible clusters increases as well. In order to compare the results from our simulations with experimentally measured cluster densities, it is necessary to assume a minimum size that can be resolved in experiments. A value between 1.5 and 2 nm in diameter is quoted in the literature as the minimum size resolved by TEM [92]. In the present simulations, we assume that SIA clusters containing more than 100 atoms are visible. It is shown in Figure 6.3 that the density of visible SIA clusters obtained in the simulations presented here is larger than the experimental measurement at high dose levels. The high mobility of SIA clusters allows them to be absorbed on other sinks, such as grain boundaries or free surfaces. Hence we can consider the agreement with the experimental conditions on the cluster density [9] as qualitative.

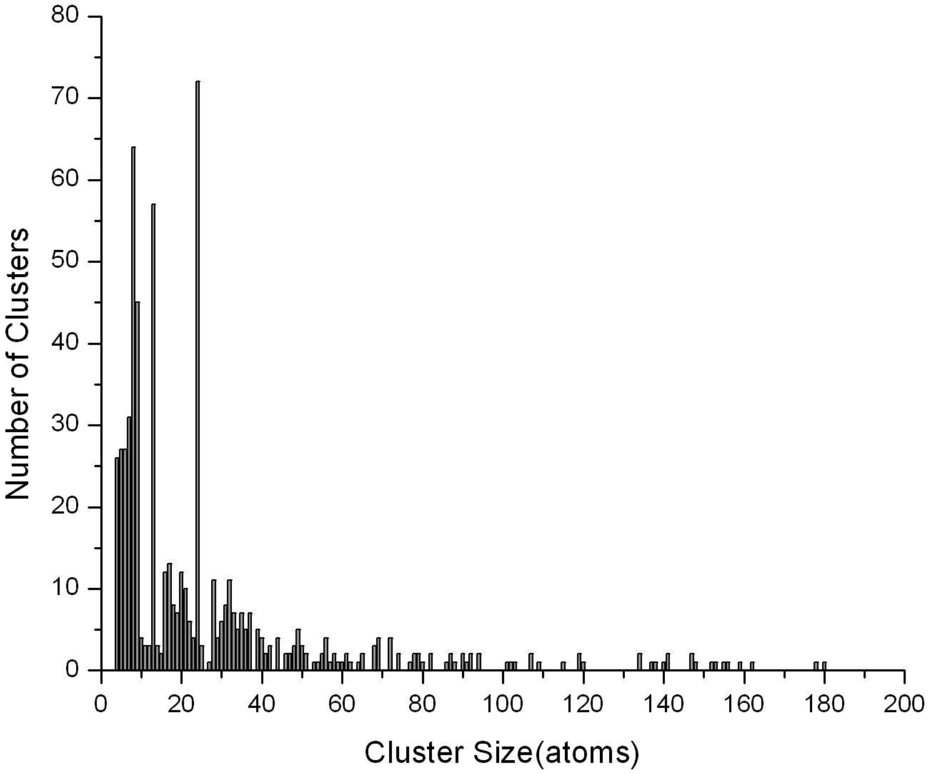

Figure 6.4: Size distribution of SIA clusters at a dose level of 5.21×10^{-3} dpa.

The size distribution of SIA clusters at a dose of 5.2×10^{-3} dpa is shown in Figure 6.4. More than half of the total interstitial clusters consist of more than 30 defects, though small clusters consisting of less than 10 SIAs still have the largest concentration. It can be expected that the size distribution will continue to shift to larger sizes as damage accumulates. It is found here that mobile SIA cluster can be immobilized, either by getting trapped near a dislocation or by getting locked with another large cluster ($>$ 37 SIAs) of a different Burgers vector.

6.3 CHARACTERISTICS OF DECORATION AND RAFT FORMATION

The dislocation decoration process builds up quickly with dose, and at 3×10^{-4} dpa, grown-in dislocations attract SIA clusters. At higher doses, dislocation decoration becomes very significant, as can be seen in Figure 6.5. When an extremely mobile 1-D migrating interstitial cluster passes through the neighborhood of a pre-existing dislocation, it will feel the influence of its strain field. As long as the defect-dislocation interaction is attractive and the distance is small, the cluster cannot escape from the attractive zone by thermally-activated random walk. Once an SIA cluster is trapped into the strain field of a dislocation, it will rotate its Burgers vector to accommodate to the strain field of the dislocation and migrate along the direction of lowest energy barrier

It can be clearly seen in Figure 6.5(b) that the pure edge components of the slip dislocation attract more SIA clusters in its vicinity. Trapped clusters can still serve as sinks for the glissile clusters and increase their size before they rotate their Burgers vectors and finally get absorbed by dislocations. With the accumulation of clusters along the dislocation line, a repulsive force field is then gradually built up against further cluster trapping. Figure 6.6(a) shows contours of the interaction energy between an interstitial defect cluster of Burgers vector $a/2[\bar{1}\ 1\ 1]$ and an edge dislocation on the $(\bar{1}\ \bar{2}\ 1)$-plane in bcc iron; and Figure 6.6(b) shows contours of the interaction energy between an interstitial defect cluster of Burgers vector $a/2[\bar{1}\ 1\ 1]$ and a pre-existing same-type cluster and an edge dislocation on the $(\bar{1}\ \bar{2}\ 1)$-plane.

When the attractive stress field of the dislocation is fully compensated for by existing clusters, the SIA content in the primary trapping region achieves

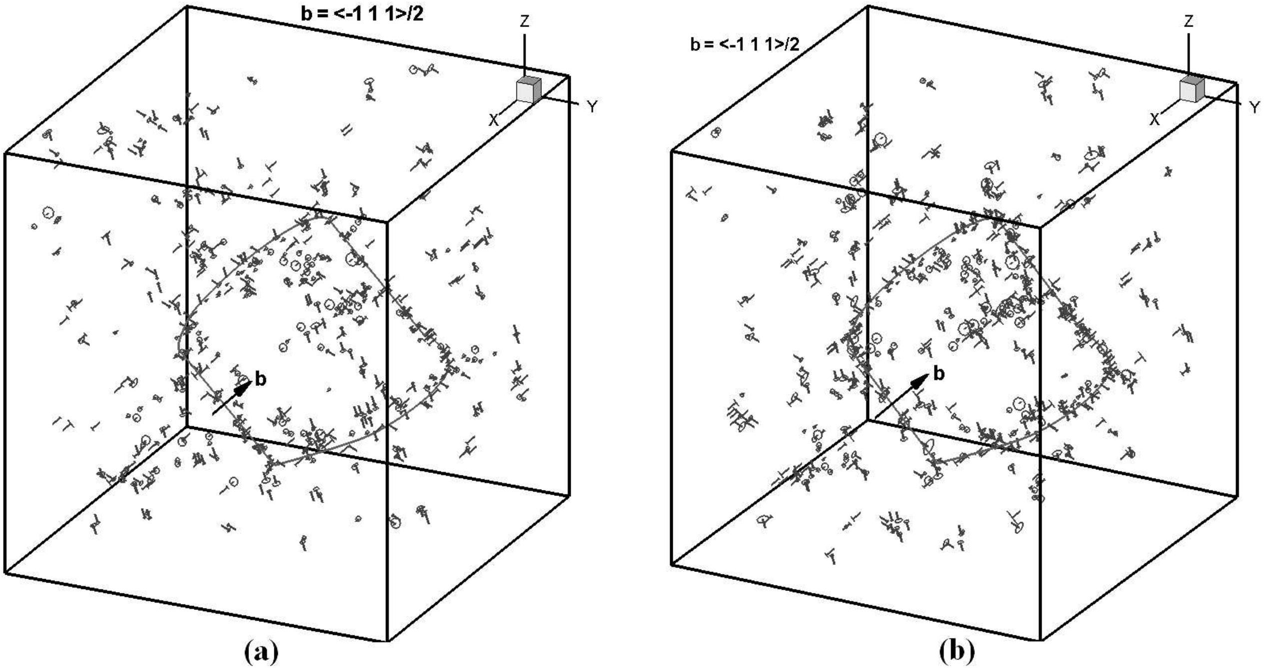

Figure 6.5: Spatial distribution of SIA clusters in bcc Fe at 300 K, (a) 1.3×10^{-3} dpa, (b) 5.2×10^{-3}.

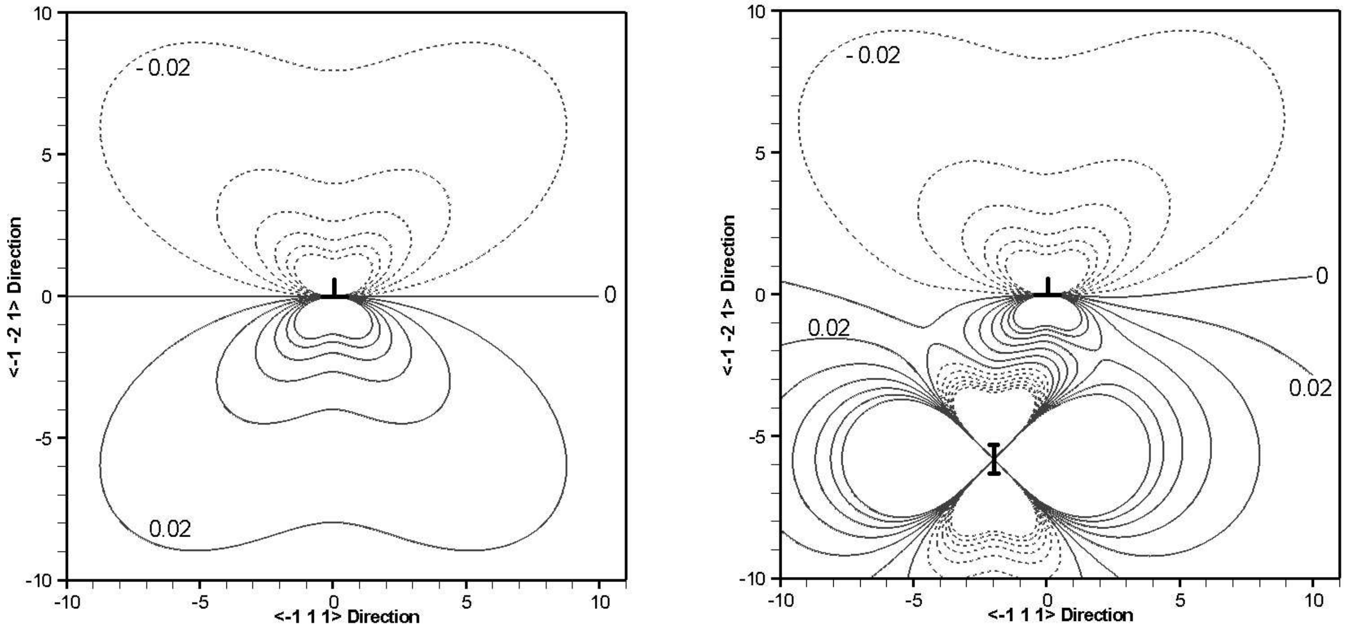

(a) **(b)**

Figure 6.6: (a) Local iso-energy contours for the interaction energy of a SIA cluster of Burgers vector $a/2[\bar{1}\ 1\ 1]$ with an edge dislocation on the $(\bar{1}\ \bar{2}\ 1)$ -plane in bcc iron; (b) local iso-energy contours of the interaction energy of an interstitial defect clusters of Burgers vector $a/2[\bar{1}\ 1\ 1]$ with a pre-existing same type cluster and an edge dislocation on the $(\bar{1}\ \bar{2}\ 1)$ -plane. Contours are plotted at 0.02 (in $\mu\delta A/(1-\nu)$, where μ is the shear modulus and δA is the surface area of the SIA cluster) increment. The length on the axes is in units of lattice constant, a.

saturation and the decoration process stops. Although dislocation decoration saturates at a low dose, the primary region of cluster trapping shifts the stress field of the dislocation, and cluster trapping occurs only ahead of the existing dislocation/loop structure, where the interaction remains attractive [30]. For increasing dose, cluster trapping continues away from the dislocation and results in dislocation wall formation. As seen in Figure 5.7(d), our simulations have already shown the extension of cluster trapping and the formation of dislocation wall.

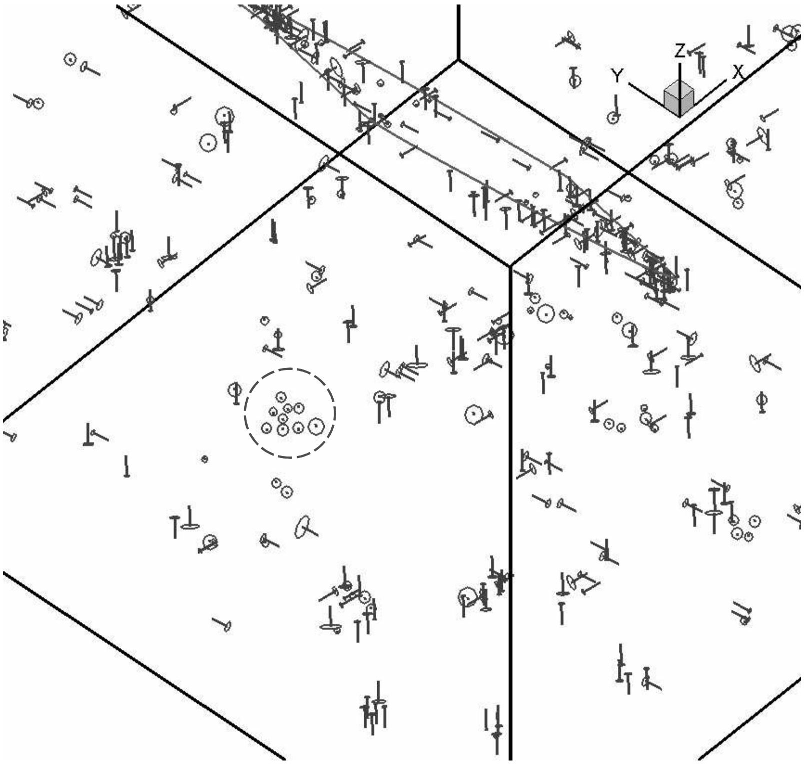

Figure 6.7: A close-up view of the configuration of a raft of interstitial clusters formed at a dose level of 1.8×10^{-3} dpa. The raft is enclosed in a dotted circle.

In addition to dislocation decoration, another major striking feature of microstructure evolution is the formation of dislocation loop rafts. Figure 6.7 shows a configuration of SIA cluster raft formed at a dose level of 1.8×10^{-3} dpa. The Burgers vectors of the clusters making up the raft are all parallel to one another, which is in agreement with experimental observations [30]. If the interaction between two close SIA clusters is attractive and strong enough to overcome the energy barrier for directional change, they adjust their relative positions and orientations. This scenario is similar to the pinning of clusters, which has been demonstrated in the previous section.

To shed light on the nature of cluster-cluster self-trapping, we consider the forces between two identical clusters. In Figure 6.8 a prismatic dislocation loop is fixed at the origin, and another identical one is moved along its slip direction. The glide force on the moving loop is plotted as a function of its relative position. It is shown that 5 equilibrium positions (zero force) exist between the two parallel clusters. However, only three of them are stable, at a relative angle of $\pm 30.5^{\mathrm{O}}$ or 90^{O}. When multiple clusters interact, this simple picture is somewhat disturbed. Nevertheless, extended stable cluster complexes form by this self-trapping mechanism. Figure 6.9 shows the force field along the slip direction of an existing raft obtained in our simulations. Two additional clusters that will join the raft in the following time step are also shown in dotted lines. It can be seen that raft formation is 'autocatalytic', since a raft nucleus is stable, but keeps expanding through the association of other clusters on its periphery. As the number of clusters within a raft increases, the mobility of the raft as a whole decreases. The decrease in the mobility of individual clusters can be attributed to mutual elastic interactions between clusters that are members of a raft.

why is this different from the value given on page 11 ?

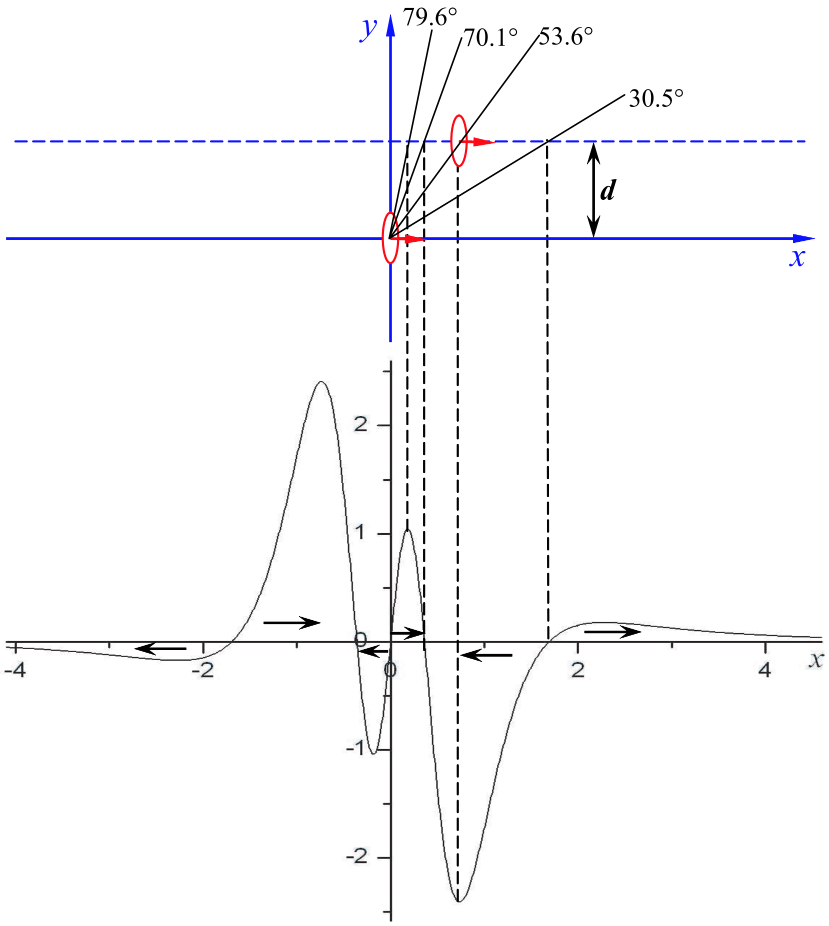

Figure 6.8: The glide force between two prismatic dislocation loops with parallel Burgers vectors as a function of their relative positions. The force is scaled by $\mu b_1 b_2 A_1 A_2 / 4\pi(1-\nu)d^4$, where b_i and A_i $(i = 1, 2)$ are the Burgers vectors and surface areas of the two loops, respectively.

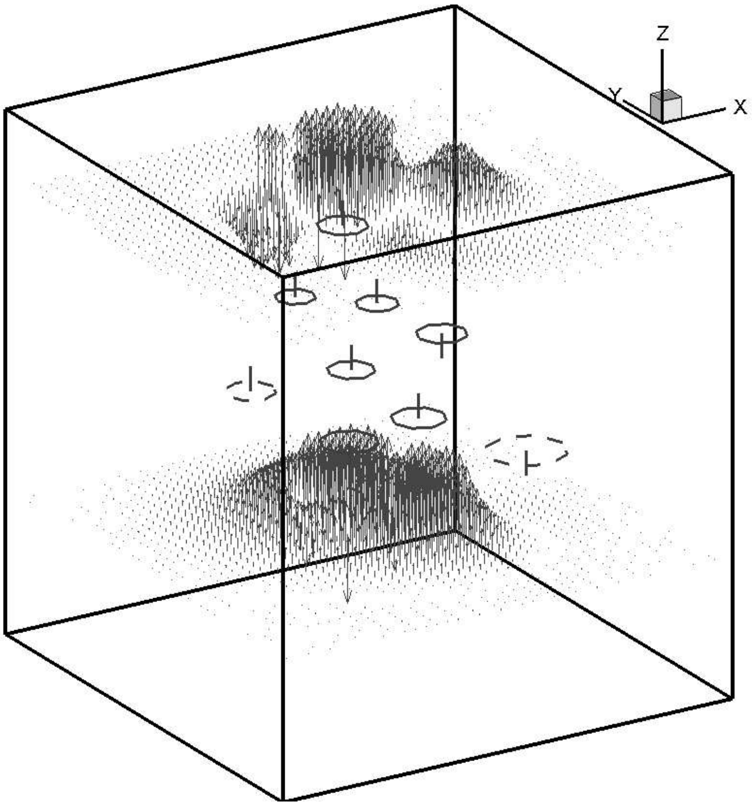

Figure 6.9: Force field distribution along the glide direction of an existing raft of SIA clusters (in solid lines). Two new SIA clusters (in dashed line) which will join the raft are also shown.

6.4 GENERAL CONDITIONS FOR DECORATION AND RAFT FORMATION

Trinkaus et al. [30] have shown that a grown-in dislocation would have a large drainage area for accumulating one-dimensionally migrating glissile loops in its neighborhood. Our simulations also demonstrate that even at a fairly low dose of 1.3×10^{-3} dpa, clear dislocation decoration is observed. The energy barrier for directional change is a critical parameter in controlling when, how and to what extent dislocation decoration and raft formation occur. The maximum range for the elastic interaction that is strong enough to overcome the barrier and thereby leads to a Burgers vector change is strongly dependent on this parameter. In other words, the interaction between defects and the microstructure contributes to dislocation decoration and the formation of rafts in terms of changing the diffusivity and the characteristics of mixed 1D/3D migration. Brimhall and Mastel [27] proposed that loops move through the lattice by a combination of prismatic glide and self-climb to form rafts. Our present simulations, however, suggest that raft formation could be achieved just by prismatic glide and rotation of glissile SIA clusters. A necessary condition for pronounced formation of rafts is that the group of clusters within a raft is large enough to trap a single glissile cluster in the strain field formed by the group and prevent it from further Burgers vector rotation. Our simulations indicate that small rafts containing two or three clusters are still mobile; more specifically, these small patches still perform 1-D migration, although at reduced mobility. With the size of a patch increasing, the overall mobility decreases, and a raft consisting of more than five clusters is literally immobile. Due to thermal activation or interaction with other defects, a SIA cluster trapped in the outer region of a raft may break away and detrap from the raft.

CHAPTER 7

EFFECTS OF NEUTRON IRRADIATION ON DYNAMIC PROPERTIES OF EDGE DISLOCATIONS

7.1 INTRODUCTION

Plastic deformation in crystalline metals is known as a collective consequence of the motion of a large number of dislocations. An enormous amount of investigations concerned with dislocation mechanics have been performed from both atomistic and continuum perspectives. However, modeling the behavior of large numbers of dislocations is a computationally intensive task. Only relatively recently have computational models of the collective behavior of discrete dislocations been developed. Large-scale Dislocation dynamics (DD) simulations, in which the individual dislocations are described as straight or curved segments of line defects in an elastic solid, have been successfully used to study characteristic plastic deformations, such as dislocation pattern formation and work-hardening relations in macroscopically homogeneously deformed solids [93, 94, 95].

It is well established that a large number of point defects and point defect clusters are created in high-energy displacement cascades in metals exposed to irradiation by high-energy neutrons [22, 15]. Atomistic simulations have shown that small SIA clusters can form perfect loops and perform fast thermally-activated one-dimensional motion in a variety of bcc, fcc and hcp metals [96, 84, 97]. The motion and interaction of SIA clusters can lead to the formation of rafts of small dislocation loops and decoration of dislocations by loops [30, 98]. Analytical calculations as well as KMC simulations have supported this conclusion. Based on experimentally observed microstructure, the analytical CISH model [30, 12] provides a rational explanation for the observed phenomena in post-irradiation deformation experiments, namely, irradiation hardening and the occurrence of yield drop. However, the materials tested in the post-irradiated state respond to conditions that are fundamentally different from those that are likely to be experienced by the materials subjected simultaneously to ~~an~~ a flux of neutrons and stresses in a real reactor environment. Under these conditions, freshly generated mobile dislocations are likely to interact with both glissile and sessile SIA clusters, as well as vacancies produced continuously by cascades and it is therefore relevant to investigate the influence of these interactions on dislocation motion. In fact, in-reactor tensile tests have been carried out recently on both pure copper and copper alloy in a fission reactor and results on the mechanical response and concurrent microstructure evolution are now available [99]. In addition, atomistic simulations of both α-iron and copper are performed to investigate interactions between a gliding edge dislocation and decoration formed by a row of SIA loops [100]. It is shown that SIA loops lying within a few nanometers of the dislocation slip plane can be dragged at very high speed.

Large-scale three-dimensional DD simulations have been used to investigate the relation between the irradiation field and mechanical behavior including irradiation hardening and post-yield deformation[101]. The KMC simulations described in previous chapters can provide valuable information on the spatial and size distribution of defect clusters produced in displacement cascades. The microstructure predicted by KMC simulation can then be used to serve as input to

DD simulation to investigate radiation effect on plastic deformation in a more realistic way.

The main objective of this chapter is to study fundamental aspects of dynamics of dislocation interaction with radiation-induced defect clusters, specifically with both glissile and sessile SIA clusters in dislocation decorations, as well as distributed nano-voids that resemble vacancy-rich cascade core regions. The investigation of the behavior of single gliding dislocations under irradiation can characterize the effects of interaction with various microstructures and provide guidance to ongoing large-scale simulations. In Section 7.2, the method used in the context is described, which is a modified version of the parametric dislocation dynamics method developed by Ghoniem et al.[102], with considering inertial effects (i.e. the kinetic energy of moving dislocations). To describe the drag influence of SIA clusters on a gliding dislocation for the configurations generated by KMC simulations, a model developed by Rong et al.[103] is incorporated into the current simulation scheme in Section 7.3. The phenomenon of radiation-induced increase in the yield stress is then discussed from two perspectives, specifically for glide resistance to dislocation motion due to distributed vacancy clusters in Section 7.4.1 and the pinning effect of SIA clusters to decorated dislocations in Section 7.4, respectively. Finally, the dislocation glide affected by interaction of dislocations with various obstacles to their glide is investigated in Section 7.5.

7.2 PARAMETRIC DISLOCATION DYNAMICS

Dislocations are line singularities in solid materials. A new parametric method of dislocation dynamics has recently been developed and applied to study three-dimensional problems of deformation in material deformation[77, 102, 104, 95]. The basic idea of parametric dislocation dynamics method is to represent dislocation line with a reduced set of degrees of freedom (DOF) and solve the corresponding equations of motion (EOM) of the DOF. By far, the discretization of dislocation line into cubic spline curves has been proved to be satisfactory on both computational efficiency and accuracy for most applications.

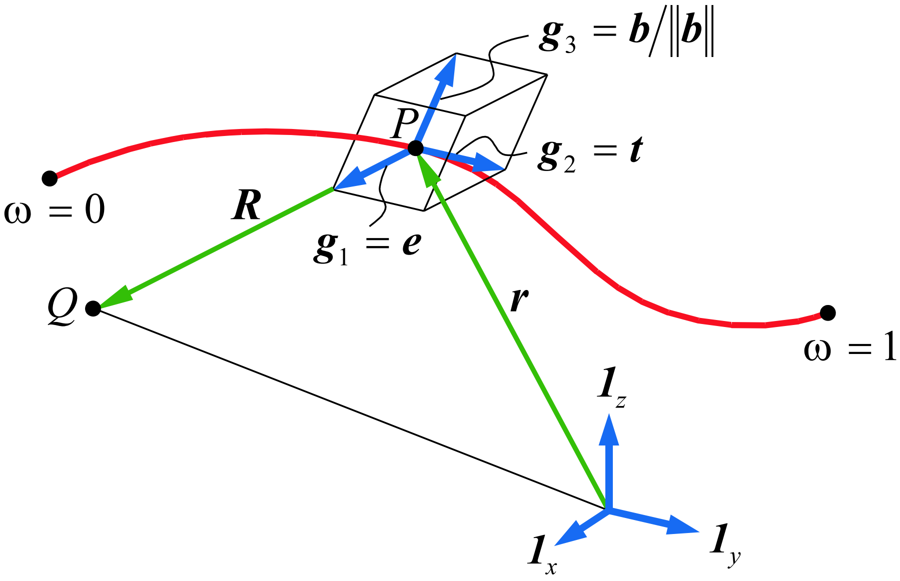

Figure 7.1: Parametric representation of a general curved dislocation segment, with relevant vector defined (after [104]).

As shown in Figure 7.1, a general vector form of the dislocation line equation for segment j can be expressed as

$$\mathbf{r}^{(j)}(\omega) = \sum_{i=0}^{4} C_i(\omega)\mathbf{Q}_i \tag{7.1}$$

where $\mathbf{r}$ is the position vector of a point on dislocation segment, $C_i(\omega)$ are cubic spline shape functions dependent on a parameter ω $(0 \le \omega \le 1)$, and $\mathbf{Q}_i$ are a set of generalized coordinates of the two dislocation end nodes. Specifically, $C_i(\omega)$ are given by

$$C_1(\omega) = 2\omega^3 - 3\omega^2 + 1$$

$$\begin{aligned} C_2(\omega) &= -2\omega^3 + 3\omega^2 \\ C_3(\omega) &= \omega^3 - 2\omega^2 + \omega \\ C_4(\omega) &= \omega^3 - \omega^2 \end{aligned} \tag{7.2}$$

and $\mathbf{Q}_i$ are:

$$\begin{aligned} \mathbf{Q}_1 = \mathbf{P}^{(j)}(0), \qquad \mathbf{Q}_2 &= \mathbf{P}^{(j)}(1), \\ \mathbf{Q}_3 = \mathbf{T}^{(j)}(0), \qquad \mathbf{Q}_4 &= \mathbf{T}^{(j)}(1) \end{aligned} \tag{7.3}$$

where $\mathbf{P}^{(j)}(i)$ and $\mathbf{T}^{(j)}(i)$ $(i = 1, 2)$ are the position and tangent vectors of the beginning and ending node of segment j, respectively.

7.2.1 THE EQUATION OF MOTION

Under most dynamic conditions, dislocations move so slowly that the dynamic stresses and displacements are approximated quite accurately by the static solutions. Therefore, in existing DD methodology the dynamic term has been ignored for the sake of computational simplicity. However, dynamic effects are thought to be important in some specific scenarios, for example, in the study of dislocations being suddenly released from cluster atmospheres under high applied stresses. Here, by reinstating the kinetic energy which was ignored in the derivation based on thermodynamics by Ghoniem et al.[102], we present a modified variational form for the equations of motion (EOM) for dislocation loops. Following Ghoniem et al.[102], consider a body in thermodynamic equilibrium, of volume Ω, and its boundary $\mathcal{S}$, containing a dislocation loop in an initial position (1), as shown in Figure 7.2. By the prescribed external mechanical forces, as well as thermodynamic internal forces, the dislocation loop will experience transition from the initial state to a new on designated as (2). According to the first law of thermodynamics, the following condition of energy conservation must be met

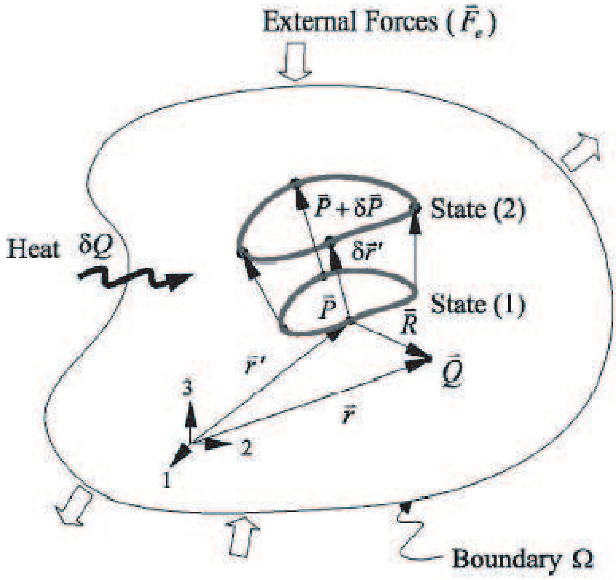

Figure 7.2: Representation of dislocation loop motion in an infinitesimal transition, illustrating thermodynamic variables (after [102]).

during this transition of states,

$$dU^t + \delta E^t = \delta Q^t + \delta C^t + \delta W^t \tag{7.4}$$

where dU^t is the change in internal energy, δE^t the change in kinetic energy, δQ^t the change in heat energy, δC^t the change in chemical energy by atomic diffusion, and δW^t the change in its mechanical energy. The kinetic energy associated with a moving dislocation is due to the fact that there is motion of material about a dislocation. By analogy with the problem of the vibration of a string, we can define an 'effective mass', m, per unit length of dislocation line. The dislocation line vector is denoted by $\mathbf{s} = \mathbf{t}|\mathbf{s}|$, where $\mathbf{t}$ is a unit tangent vector. The total kinetic energy associated with a moving dislocation is then written as an integration along the dislocation line Γ

$$E = \oint_{\Gamma} \frac{1}{2} m\dot{\mathbf{r}} \cdot \dot{\mathbf{r}} |d\mathbf{s}| \tag{7.5}$$

(see references ?? for a discussion of the "effective" mass concept) where $\mathbf{r}$ is the displacement vector of core atoms of the dislocation loop.

Consider an infinitesimal variation in the position of a dislocation loop in a time interval δt. During loop motion from state (1) to state (2) in Figure 7.2, the variation in kinetic energy over this period of time can be shown as

$$\begin{aligned}\delta E^t &= \frac{d}{dt}\left[\oint_\Gamma \frac{1}{2} m\dot{\mathbf{r}}\cdot\dot{\mathbf{r}}|d\mathbf{s}|\right]\delta t \\ &= \oint_\Gamma m\dot{\mathbf{r}}\cdot\ddot{\mathbf{r}}\delta t|d\mathbf{s}| \\ &= \oint_\Gamma m\ddot{\mathbf{r}}\cdot\delta\mathbf{r}|d\mathbf{s}|\end{aligned}$$

The variation in kinetic energy during time interval δt reads

$$\delta E^t = \oint_\Gamma m\ddot{\mathbf{r}}\cdot\delta\mathbf{r}|d\mathbf{s}|dt \tag{7.6}$$

Following the treatments in Ref. [102] with including the kinetic energy term, it can be shown that during the transition the total Gibbs energy change over δt, δG^t, is given by

$$\delta G^t = -\oint_\Gamma \left(\mathbf{f}^t - m\ddot{\mathbf{r}}\right)\cdot\delta\mathbf{r}|d\mathbf{s}| \leq 0 \tag{7.7}$$

where $\mathbf{f}^t = \mathbf{f}_s + \mathbf{f}_O + \mathbf{f}_{\mathrm{PK}}$ is the total force. Here the following generalized thermodynamic forces is defined similar to Ghoniem et al.[102]: $\mathbf{f}_{\mathrm{PK}} \equiv$ the *Peach-Koehler force* per unit length, $\mathbf{f}_S \equiv$ the *self-force* per unit length, and $\mathbf{f}_O \equiv$ the totial *osmotic force*[105] for point defect γ per unit length, where $\gamma = (-1)$ for vacancies and $(+1)$ for interstitials.

In compact tensor form, Equation 7.8 can be written as

$$\delta G^t = -\oint_\Gamma \left(f_k^t - m\ddot{r}_k\right)\delta r_k|d\mathbf{s}| \leq 0 \tag{7.8}$$

On the other hand, we can denote $B_{\alpha k}$ as a diagonal resistivity (inverse mobility) matrix with respect to the drift velocity $\mathbf{V}$, and follow the same procedure by Ghoniem et al.[102] to obtain the following equivalent form of Gibbs energy variation:

$$\delta G^t = -\oint_\Gamma B_{\alpha k} V_\alpha \delta r_k |d\mathbf{s}| dt \leq 0 \tag{7.9}$$

The resistivity matrix can have three independent components (two for glide and one for climb), depending on the crystal structure and temperature. It is expressed as

$$B_{\alpha k} = \begin{bmatrix} B_1 & 0 & 0 \\ 0 & B_2 & 0 \\ 0 & 0 & B_3 \end{bmatrix} \tag{7.10}$$

Combining Equation 7.8 with Equation 7.9, we have

$$\oint_\Gamma \left(f_k^t - m\ddot{r}_k - B_{\alpha k} V_\alpha \right) \delta r_k |d\mathbf{s}| dt \leq 0 \tag{7.11}$$

The magnitude of the virtual displacement $\delta \overset{r}{\cancel{d}}_k$ and the the time interval $[t_1, t_2]$ are not specified, and hence ban be arbitrary. This implies that Equation 7.11 represents force balance on every atom of the dislocation core, where the acting force component f_k^t is balanced by the combination of viscous dissipation in the crystal via the term $B_{\alpha k} V_\alpha$ and inertial force $m\ddot{r}_k$. However, it is the integral EOM that has more sense in practical applications from the perspective of reducing the independent DOF that describe loop motion.

Now we can take the general procedure of PDD method, and divide the dislocation loop into N_s curved segments. The line integral in Equation 7.11 can be written as a sum over each parametric segment j, i.e.,

$$\sum_{j=1}^{N_s} \int_j \delta r_i \left(f_i^t - m\ddot{r}_i - B_{ik} V_k \right) |d\mathbf{s}| = 0 \tag{7.12}$$

In each segment j, we can choose a set of generalized coordinates q_m at the two ends, thus allowing parametrization of the form:

$$r_i(\omega) = \sum_{i=0}^{N_{DF}} C_{im}(\omega) q_m \tag{7.13}$$

where $C_{im}(\omega)$ are shape functions, dependent on the parameter ω ($0 \leq \omega \leq 1$), and N_{DF} is the number of total generalized coordinates at two ends of the loop segment. The arc length differential for segment j is given by

$$|d\mathbf{s}| = (r_{l,u} r_{l,u})_{\frac{1}{2}}\, d\omega = \left(\sum_{p,s=1}^{N_{DF}} q_p C_{lp,\omega} C_{ls,\omega} q_s \right)^{\frac{1}{2}} d\omega \tag{7.14}$$

Substituting all these to the integral form of the governing EOM 7.12, we obtain:

$$\begin{aligned} \sum_{j=1}^{N_s} \int_0^1 \sum_{m=1}^{N_{DF}} \delta q_m C_{im}(\omega) \left[f_i^t - B_{ik} \sum_{n=1}^{N_{DF}} C_{kn} q_{n,t} - m \sum_{j=1}^{N_{DF}} C_{ij} q_{j,tt} \right] & \\ \times \left(\sum_{p,s=1}^{N_{DF}} q_p C_{lp,\omega} C_{ls,\omega} q_s \right)^{\frac{1}{2}} d\omega = 0. & \end{aligned} \tag{7.15}$$

Let,

$$f_m = \int_0^1 f_i^t C_{im}(\omega) \left(\sum_{p,s=1}^{N_{DF}} q_p C_{lp,\omega} C_{ls,\omega} q_s \right)^{\frac{1}{2}} d\omega, \tag{7.16}$$

$$\gamma_{mn} = \int_0^1 C_{im}(\omega) B_{ik} C_{kn}(\omega) \left(\sum_{p,s=1}^{N_{DF}} q_p C_{lp,\omega} C_{ls,\omega} q_s \right)^{\frac{1}{2}} d\omega, \tag{7.17}$$

and

$$\eta_{mn} = \int_0^1 C_{im}(\omega) m C_{in}(\omega) \left(\sum_{p,s=1}^{N_{DF}} q_p C_{lp,\omega} C_{ls,\omega} q_s \right)^{\frac{1}{2}} d\omega. \tag{7.18}$$

For the entire dislocation loop, we map all local DOFs $q_i^{(j)}$ of each segment j onto a set of global coordinates, shuch that the global coordinates are equal to the local coordinates at each beginning node of the segment:

$$\left\{ q_1^{(1)}, q_2^{(1)}, q_3^{(1)}, \ldots, q_1^{(2)}, q_2^{(2)}, q_3^{(2)}, \ldots \right\} = \{Q_1, Q_2, Q_3, \ldots, Q_{N_{tot}}\}^{\mathrm{T}} \tag{7.19}$$

Following a similar procedure to the FEM, we assemble the EOM for all contiguous segments in global matrices and vectors, as:

$$[\mathcal{F}_k] = \sum_{j=1}^{N_s} [f_m]^{(j)}, \quad [\Gamma_{kl}] = \sum_{j=1}^{N_s} [\gamma_{mn}]^{(j)}, \quad [\mathcal{M}_k] = \sum_{j=1}^{N_s} [\eta_{mn}]^{(j)} \tag{7.20}$$

then, from Equation 7.15 we can get

$$\sum_{j=1}^{N_{tot}} \mathcal{M}_{kl} Q_{l,tt} + \sum_{j=1}^{N_{tot}} \Gamma_{kl} Q_{l,t} = \mathcal{F}_k \tag{7.21}$$

Equation 7.21 represents a set of time-dependent second-order ordinary differential equations (ODEs), which describe the motion of ensemble of dislocation loops as an evolutionary dynamic system. Comparing it with the EOM used in already-existing PDD[102], the main difference is that inertial effect is included in this modified version. The velocity of an edge dislocation under suddenly applied uniaxial tensile stress $\sigma_{11} = 2$ GPa is shown in Figure 7.3, including the result

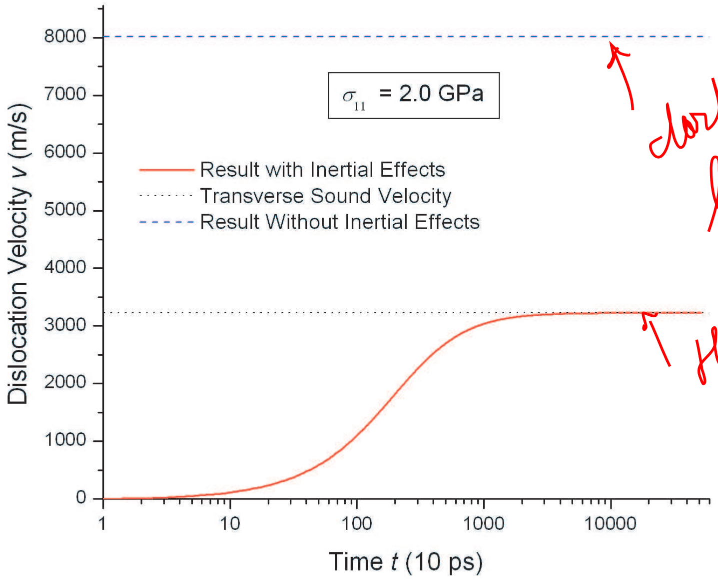

darker line

thicker

Figure 7.3: Velocity of an edge dislocation as a function of time under a suddenly applied uniaxial tensile stress $\sigma_1 = 2$ GPa.

with considering inertial effect as well as that without. The current EOM enables the dislocation velocity to increase gradually from zero to a saturate value, and the transverse sound velocity is the upper limit; while by the old EOM[102] the velocity can abruptly jump to an unrealistic high value of more than 8000 m/s without experiencing a course of increasing.

Observing the EOM 7.21, it can be seen that there are two material properties that control the motion of dislocation: one is the mass matrix $[\mathcal{M}_{kl}]$ of a dislocation in connection with the kinetic energy it carries while moving at constant velocity; and the other is the resistivity matrix $[\Gamma_{kl}]$ in connection with the dissipation of energy while a dislocation moves at its steady-state velocity under an essentially constant driving forces. A dynamic interaction between mass forces and resistant forces comes into play when the driving forces varies abruptly: for example, when the applied stress is suddenly dropped, or when the dislocation is suddenly exposed to an increased or decreased glide resistance by, say, running into an isolated barrier or being released from a pinning position. In principle, the kinetic energy must then be dissipated before the dislocation comes to rest. Under certain circumstances, inertial effects may assistant a dislocation to overcome an obstacle: when the mass is large, the resistance is small, and the change in net driving force is rapid.

Such inertial effects have, in the existing DD studies, been largely neglected: dislocation have been considered to be *overdamped*[106], i.e. moving at their resistivity-limited velocity, at all times. However, dislocation elements in real materials experience rapidly changing driving forces, especially when interacting with various obstacles, and the possibility of inertial effects must be taken into account.

7.2.2 THE MASS OF DISLOCATIONS

We have already defined m as the effective mass per unit length of the dislocation in Section 7.2.1. By analogy with the formula for kinetic energy in mechanics, we can calculate the value of m in terms of the kinetic energy of a straight dislocation segment moving at uniform velocity. For a screw dislocation, it has been shown that the sum of the kinetic energy E_k and the potential energy E_e of a unit length of dislocation moving at a constant velocity v is given by[107, 108]

$$E = E_k + E_e = E_s/(1 - v^2/C_t^2)^{\frac{1}{2}} \tag{7.22}$$

where E_s is the self-energy per unit length of screw dislocation at rest, and C_t is the transverse sound velocity and its value is obtained from $C_t \equiv \sqrt{\frac{\mu}{\rho}}$ in terms of the shear modulus μ and the mass density of the materials ρ. The theory of dislocation motion in isotropic media at uniform velocity concludes that dislocation motion is quite analogous to the motion of particles in special relativity theory[108]. The energy of the dislocation becomes infinite as the velocity of transverse sound waves is approached. This sound speed, therefore, sets an upper limit for the speed of an ordinary dislocation.

At velocities small compared to the velocity of sound, i.e. $v/C_t \ll 1$, Equation 7.22 is expanded as

$$E = E_s \left(1 + \frac{1}{2}\frac{v^2}{C_t^2} + \cdots\right) \approx E_s + \frac{1}{2}E_s\frac{v^2}{C_t^2} \tag{7.23}$$

It indicates that at low velocities the elastic energy of a screw dislocation is not changed and the kinetic energy is given by $\frac{1}{2}E_s\frac{v^2}{C_t^2}$. Since the latter term has the same velocity dependence as the energy of a moving mass, it is natural to derive an expression for the mass m_{SCREW} in terms of E_s and C_r at a low velocity:

$$m_{\text{SCREW}} = \frac{E_s}{C_t^2} \tag{7.24}$$

Rewriting Equation 7.24 as

$$E_s = m_{\mathrm{SCREW}} C_t^2 \tag{7.25}$$

it is Einstein's equation relating energy with rest mass, except that here C_t is the velocity of sound instead of light. At high velocities Equation 7.22 can be written as

$$E = m_{\mathrm{SCREW}} C_t^2 / (1 - v^2/C_t^2)^{\frac{1}{2}} = m^{\star}_{\mathrm{SCREW}} C_t^2 \tag{7.26}$$

where $m^{\star}_{\mathrm{SCREW}} = m_{\mathrm{SCREW}}/(1 - v^2/C_t^2)^{\frac{1}{2}}$ is the effective mass for a screw dislocation moving at high velocities, which includes the relativistic effect of a factor of $1/(1 - v^2/C_t^2)^{\frac{1}{2}}$ by analogy with Einstein's equation for a moving particle.

The energy of a moving edge dislocation cannot be described by Equation 7.23[108], and it is, therefore, impossible to define a rest mass of an edge dislocation in terms of the self-energy of the stationary dislocation. However, it has been shown[108] that at low velocities potential energy does not contain terms in v^2 and the kinetic energy of an edge dislocation is equal to

$$E_k = \frac{1}{2} E_s (v^2/C_t^2) \left[1 + C_t^4/C_\lambda^4\right] \tag{7.27}$$

where $C_\lambda = \sqrt{(\lambda + 2\mu)/\rho}$ is the longitudinal sound velocity. The effective mass m_{EDGE} of a slow moving edge dislocation would be

$$m_{\mathrm{EDGE}} = \frac{E_s}{C_t^2} \left(1 + C_t^4/C_\lambda^4\right) = m_{\mathrm{SCREW}} \left(1 + C_t^4/C_\lambda^4\right) \tag{7.28}$$

At high velocities the kinetic energy of the moving edge dislocation is[108]

$$E_k = E_s \left[\frac{1}{2(1 - v^2/C_t^2)^{\frac{3}{2}}} - \frac{7}{2(1 - v^2/C_t^2)^{\frac{1}{2}}} \right] = E_s \frac{7v^2/C_t^2 - 6}{2(1 - v^2/C_t^2)^{\frac{3}{2}}} \tag{7.29}$$

The energy approaches infinity as $(1 - v^2/C_t^2)^{-\frac{3}{2}}$ rather than $(1 - v^2/C_t^2)^{-\frac{1}{2}}$ as in the case of screw dislocations. Although the definition of the dislocation mass based on the equation analogous to Einstein's equation cannot be applied to the case of moving edge dislocation, it is still plausible to define a dislocation mass in terms of kinetic energy as follows due to the dominance of $(1 - v^2/C_t^2)^{\frac{3}{2}}$.

$$m^{\star}_{\text{EDGE}} = \frac{E_s}{C_t^2}\frac{1}{(1 - v^2/C_t^2)^{\frac{3}{2}}} = m_{\text{SCREW}}\frac{1}{(1 - v^2/C_t^2)^{\frac{3}{2}}} \tag{7.30}$$

At low velocities, the mass for screw dislocations and that for edge ones are very similar, since the transverse speed of sound C_t is usually about half the longitudinal speed of sound C_λ. Therefore, we can use Equation 7.24 for the mass of both kinds of dislocations. The general dislocation is neither pure screw nor pure edge in character but is made up of a linear combination of both. The energy of a moving dislocation of mixed character is simply the sum of the energy of its edge component and of its screw component, and so is its mass. We can thus use Equation 7.24 for any dislocations moving at low velocities. At high velocities the behavior of a dislcation of mixed type will be approximately the same as that of a pure edge dislocation, because the energy of the edge component approaches infinity as $(1 - v^2/C_t^2)^{-\frac{3}{2}}$ while the screw component approaches infinity much more slowly as $(1 - v^2/C_t^2)^{-\frac{1}{2}}$. By a similar argument, the mass of a dislocation of mixed character should be approximately the same as that of a pure edge dislocation.

In Section 7.2.1, we have Equation 7.18 as the mass matrix of a dislocation segment, which has the same form as the so-called consistent-mass matrix used in finite element. In practice, a special form of mass matrix called 'lumped' matrices are often employed due to their general economy and because they lead to some especially attractive time-integration schemes. The simplest way to construct lumped-mass matrices is to assume that the element's mass is concentrated at nodal points, and by doing that the mass matrices obtained are diagonal ones. In our applications, we shall employ lumped-mass matrix.

a

For cubic spline shape functions given in Equation 7.2, the lumped-mass matrix can be readily shown to be

$$[\mathcal{M}]^e = \frac{W}{2}\begin{bmatrix} 1 & 0 & 0 & 0 & 0 & 0 & 0 & 0 \\ 0 & 1 & 0 & 0 & 0 & 0 & 0 & 0 \\ 0 & 0 & 0 & 0 & 0 & 0 & 0 & 0 \\ 0 & 0 & 0 & 0 & 0 & 0 & 0 & 0 \\ 0 & 0 & 0 & 0 & 1 & 0 & 0 & 0 \\ 0 & 0 & 0 & 0 & 0 & 1 & 0 & 0 \\ 0 & 0 & 0 & 0 & 0 & 0 & 0 & 0 \\ 0 & 0 & 0 & 0 & 0 & 0 & 0 & 0 \end{bmatrix} \tag{7.31}$$

where $W = ml$ is the total mass of the dislocation element with a length of l.

7.3 THE DRAG COEFFICIENT OF an INTERSTITIAL LOOP DRAGGED BY A GLIDING DISLOCATION

Computer simulations and experiments have shown that, highly mobile interstitial clusters that are directly produced in displacement cascades move one-dimensionally with a very low activation energy of the order of 0.02 eV, and can approach to decorate grow-in dislocations due to long-range interaction between them. If the applied stress is high enough, the dislocations may be released from this 'atmospheres' of small interstitial loops that decorate them. Due to the mutual interaction between them, the newly released dislocations may be able to make the interstitial loops glide with them. This scenario was first put out by Makin[44], who calculated the long-range elastic interaction between a dislocation and loop and proposed that loops lying close to the glide plane of a dislocation with the same Burgers vector, **b**, may be dragged along by it. Rodney and

Marin[88, 109] were the first that reported loop drag effects in MD simulations of small interstitial loops captured by a dissociated dislocation in Ni. Recently, Rong et al.[103] have shown by MD simulations in bcc iron and fcc copper that interstitial loops lying within a few nanometers of the dislocation slip plane can be dragged at very high speed. The drag coefficient, B, associated with this process has been determined as a function of metal, temperature, as well as loop size and spacing. A model for loop drag, based on the diffusivity of interstitial loops, has been developed[103] and is briefly reviewed in the following. At steady state

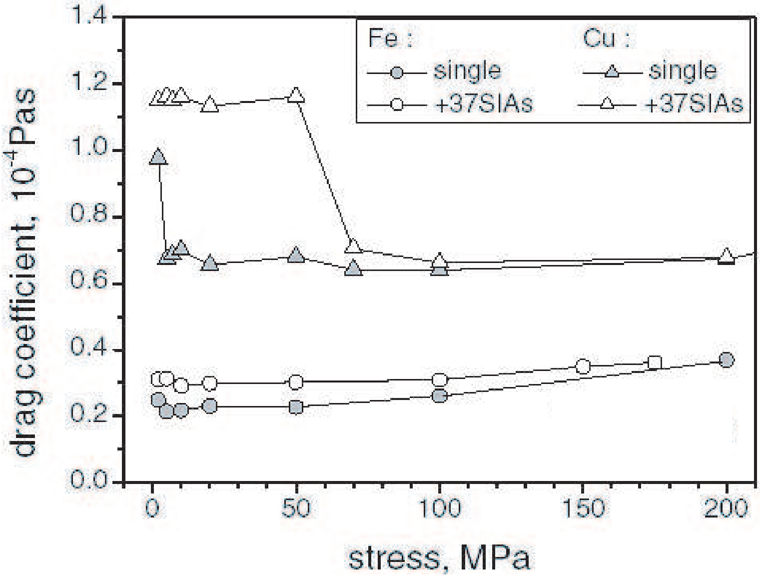

Figure 7.4: Drag coefficient versus applied resolved shear stress for single (grey symbols) and decorated (open symbols) dislocations in Fe (circle) and Cu (triangles) simulated at 300 K[103].

under a constant driving force $b\tau$, a dislocation moves with a constant velocity. Then, by assuming its velocity is sufficiently smaller than that of sound, say, less than approximately half of the transverse sound speed, and omitting relativistic effects, the total drag coefficient per unit length is defined as

$$B = \frac{\tau b}{v}. \tag{7.32}$$

In crystals with a ~~peierls~~ Peierls potential, the drag coefficient may depend on v. But in close-packed crystals without an appreciable lattice friction, experiments indicate that a dislocation moving through an obstacle free crystal experiences a linear-viscous drag[106]. The values of B for iron and copper have been evaluated utilizing the results of MD simulations[103], and are presented in Figure 7.4.

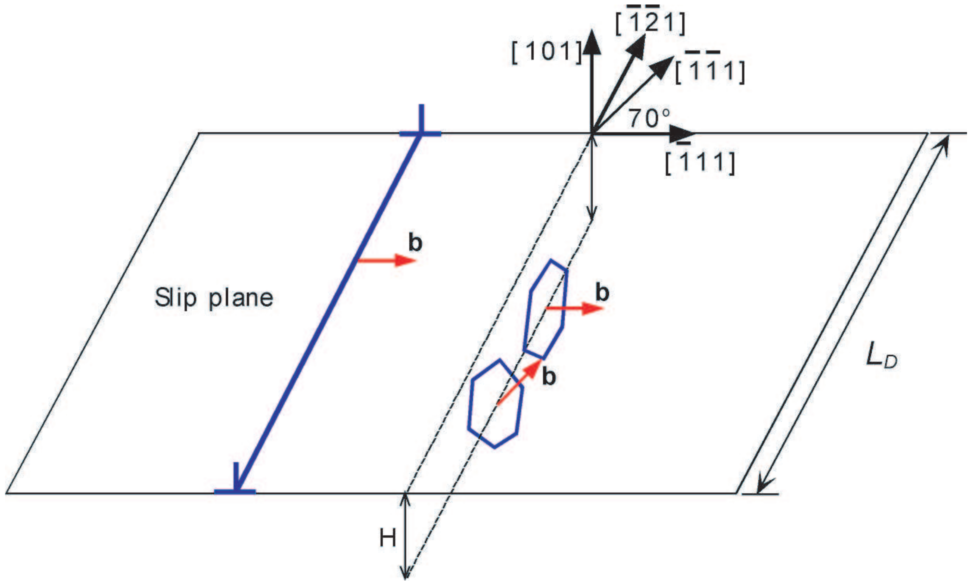

Figure 7.5: Schematic illustration of the investigated system.

When a row of loops is dragged by the gliding dislocation line with the same Burger vector **b**, as shown in Figure 7.5, the force per unit length needed to maintain the velocity v may be written

$$\tau b = (\tau_{\text{disl}} + \tau_{\text{loop}})b = (B_{\text{disl}} + B_{\text{loop}})v, \tag{7.33}$$

where terms corresponding to the dislocation line on its own and those due to loop drag are distinguished by subscript ‘disl’ and ‘loop’, respectively. The mobility of a loop is often defined as

$$m_{\text{loop}} = \frac{v}{F_{\text{L}}} = \frac{v}{\tau_{\text{loop}} b L_D} = \frac{1}{B_{\text{loop}} L_D} \tag{7.34}$$

where F_{L} is the force exerted by the dislocation line on the loop in the direction of loop glide, and L_D is the inter-loop spacing along the dislocation line. By the Einstein mobility relation, the mobility of a diffusing loop can also be given by

$$m_{\text{loop}} = \frac{D}{kT} \tag{7.35}$$

where D is the diffusivity and k is the Boltzmann constant. For one-dimensional diffusion, particularly, D may be written in terms of jump frequency, ω^n, of a loop of n interstitials (Equation 6.2), as[110]

$$D = \frac{1}{2} f b^2 \omega^n \tag{7.36}$$

where f is the correlation factor. Hence

$$B_{\text{loop}} = \frac{1}{m_{\text{loop}} L_D} = \frac{kT}{D L_D} = \frac{2kT}{f b^2 \omega^n L_D} \tag{7.37}$$

f indicates a preference for a jump to be in the same direction as the previous one and its value decreases as temperature and size increases. According to MD simulations, values that ~~varies~~ vary from 3 to 5 are reasonable choices for loops created in our KMC simulations for iron at room temperature. Equation 7.37 was first proposed by Rong et al.[103] to estimate the drag coefficient for a dislocation gliding with a row of dragged loops in decoration.

A loop can be dragged along with the moving dislocation if the force required does not exceed the maximum, F_{max}, exerted on the loop by the dislocation. This maximum force can be evaluated in terms of isotropic elasticity theory and the infinitesimal loop approximation, similar to what has been implemented in the KMC simulations. Therefore, the maximum velocity, v_{max}, at which one might expect the dislocation to break away from the 'atmospheres' of small loops, can be estimated as follows

$$v_{\max} = \frac{F_{\max}}{m_{\text{loop}}} = \frac{F_{\max}}{B_{\text{loop}} L_D} \tag{7.38}$$

For loops whose ~~b~~Burgers vector is parallel to the glide plane of the dislocation but not the same as the glide direction of the dislocation, for example, $[\bar{1}\bar{1}1]$ direction shown in Figure 7.5, they can still be dragged, but in a direction at an angle ~~*theta*~~ θ to the glide direction of the dislocation, and result in a substantial reduction in dislocation velocity at a given stress. Their contribution to B is much greater than that of loops with the same glide direction as that of the dislocation. Theoretically, in order to be dragged by the dislocation moving with velocity v, the loop speed along its glide cylinder has to be $v/\cos\theta$. In addition, the component of the driving force F_{L} in the glide direction of the dislocation is $F_{\text{L}}\cos\theta$ in the glide direction of the loop. Thus, F_{L} for a given v has to be three times larger than for a loop with the same size and distance to the dislocation glide plane but with the same glide direction as the dislocation[103].

For the configuration shown in Figure 7.6, which is extracted from the result of previous KMC simulations for bcc Fe irradiated to a dose level of 5.2×10^{-3} dpa at 300 K(Figure 6.5(b)), values of B_{loop} predicted by Equation 7.37, as well as estimates of $v_{\max}$ obtained from Equation 7.38 for an edge dislocation to break away from decorating loops are presented in Table 7.1. $v_{\max}$ that is higher than the transverse sound velocity in bcc iron implies that the loop will be dragged with the dislocation all the way and never be dumped.

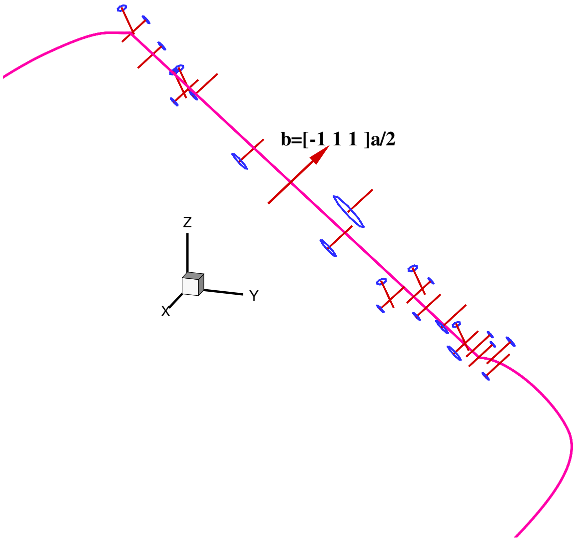

Figure 7.6: Spatial distribution obtained by KMC simulations for SIA loops that can be dragged by the edge component of the dislocation loop in bcc Fe irradiated to a dose of 5.2×10^{-3} dpa at 300 K.

7.4 IRRADIATION-INDUCED INCREASE IN THE YIELD STRESS

The initiation of the plastic flow, commonly referred to as yielding, takes place when a significant number of grow-in dislocations are set free (i.e., unlocked) to move and act as dislocation sources. The multiplication and movement of these free dislocations and the resulting dislocation-dislocation interactions leads to work hardening as plastic deformation continuous. In unirradiated metals, the ‘clean’ and ‘atmosphere’-free dislocations will start operating as Frank-Read sources[111] when the applied stress is sufficient to overcome the restoring forces on the dislocations due to their line tension. In irradiated materials, the presence of irradiation-induced defects alters the plastic deformation behavior significantly and the corresponding phenomena have been extensively studied since the 1950s.

It is well recognized that the defects produced by neutron irradiation must interact with the dislocations to produce the change in the mechanical properties of metals and alloys. Two types of interaction are involved. Some of the radiation induced SIA clusters that are produced directly in high energy displacement cascade may approach to the grown-in ~~grow~~-in dislocations (dislocation sources) by thermally activated 1-D transport, be trapped in the strain field of the dislocations and decorate them. These SIA clusters may form a Cottrell atmosphere, and act as barriers to the generation of dislocations (source hardening). In addition to this type of interaction, the radiation induced defects may act as distributed barriers to impede the motion of the dislocation after it has been released from decoration clusters (friction hardening). In the first part of this section, the effect of distributed defects on dislocation motion will be investigated; and the influence of decoration clusters will be studied in the second part.

7.4.1 THE PLANE GLIDE RESISTANCE (FRIEDEL STATISTICS) DUE TO V~~ACANCIES~~ Vacancy Clusters

A ~~An~~ vacancy-rich zone will be created in the center of a displacement spike, as mentioned in Section 1.1. In FCC metals, ~~T~~hese zones are expected to collapse into vacancy loops or stacking fault tetrahedra (SFTs) during the cooling down phase of the cascades. Although production of large compact planar or three-dimensional vacancy clusters directly in displacement cascades have not been observed through MD simulations in bcc metals, very loose complexes of vacancies in second and higher order neighbor shells have been reported[54, 112]. The possibility that these closely correlated vacancies might collapse into clusters over somewhat longer times has been investigated using MC simulations. The expectation of vacancy clustering was confirmed in the MC simulations, where many of the isolated vacancies had

In BCC metals, vacancy-rich zones tend to form nano-voids.

clustered within 70 μs [113]. Once dislocation sources are unlocked from their decoration atmosphere, they will then multiply and interact with the defect clusters randomly distributed in the matrix of the crystal. Vacancy clusters in the form of voids are much stronger obstacles to dislocation motion than precipitates and interstitials[114]. In this regards, the contribution of vacancies would be our main consideration for strengthening mechanism in terms of internal friction. We investigate here the interaction between moving dislocations and nano-voids as a possible mechanism of radiation hardening immediately beyond the yield point.

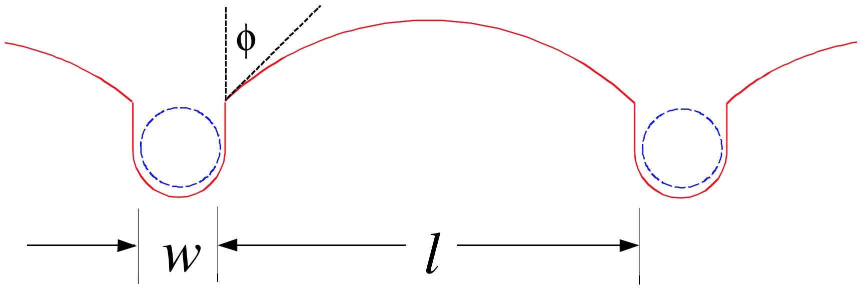

Figure 7.7: Schematic of shape of dislocation line near the Orowan-type obstacles.

We follow Friedel[48] (see also Kocks et al.[106]) in taking into account the plane resistance due to a random distribution of point-like obstacles that interact with a dislocation. The asymptotic maximum plane resistance is found by assuming steady-state propagation of quasi-straight dislocation lines. This means that the area swept by the dislocation after release at one obstacle must, on ~~in the~~ average, be equal to the average area per particle. The average center-to-center void spacing $(l + w)$, as shown in Figure 7.7, is usually given geometrically in terms of the volume fraction. In the preceding KMC simulations, vacancy clusters are approximated as spherical nano-voids. For uniform spheres of radius r, distributed randomly in three dimensions and taking up a volume fraction c, one has

$$(l+w)^2 = r^2\frac{2\pi}{3c} \tag{7.39}$$

The average diameter of the circles formed by intersection of these spheres with the slip plane of the dislocation is

$$w = \frac{\pi}{2}r \tag{7.40}$$

The plane resistance in terms of the resolved shear stress encountered by individual dislocations that move long distances through a random dispersion of obstacles is related to the relative strength f of the individual obstacles and their spacing l by the Friedel relation[106]:

$$\tau_c = f^{3/2}\frac{b}{w}\mu\sqrt{c} \tag{7.41}$$

In principle, f is determined by the angle between adjacent dislocation segments at the point where the dislocation breaks free of the obstacle[106]. As shown in Figure 7.7, if the critical angle is ϕ, $f \equiv \cos\phi$. The value of f is limited by the possibility of 'Orowan looping' for impenetrable obstacles that are hard enough that the dislocation is unable to cut through them and can only pass through the field of obstacles by the bowing of dislocation segments around them. A dipole is drawn out by the two dislocation arms surrounding a single obstacles. The limiting effective resistance force of an impenetrable obstacle is the energy to draw out the respective dipole[106]:

$$\begin{aligned} F_{\text{SCREW-DIPOLE}} &= \frac{\mu b^2}{2\pi}\ln\frac{w}{r_0} \\ F_{\text{EDGE-DIPOLE}} &= \frac{\mu b^2}{2\pi(1-\nu)}\ln\frac{w}{r_0} \end{aligned} \tag{7.42}$$

where r_0 is the effective dislocation core radius and we have used $r_0 = b$ for metals. The value of f thus fulfills the condition

$$f \le f_{\max} = \frac{F_{\text{DIPOLE}}}{2E} \tag{7.43}$$

where E is the self-energy per unit length of a dislocation, or line energy. For order-of-magnitude estimates, ~~it is often to~~ we often take $E_{\text{SCREW}} = 2\mu b^2$ for a screw dislocation in isotropic materials. For an edge dislocation, we have the following ~~simply~~ simple relationship:

$$E_{\text{EDGE}} = \frac{1}{1-\nu} E_{\text{SCREW}} \tag{7.44}$$

In fact, most obstacles are not as strong as Orowan impenetrable obstacles and may be partially cut or sheared by the dislocation as it bows out. This reduces the amount of energy required for a dislocation to glide through the field of obstacles, and correspondingly results in a lower f. For nano-voids, we choose the value of f to be $\sim 0.8 f_{\max}$.

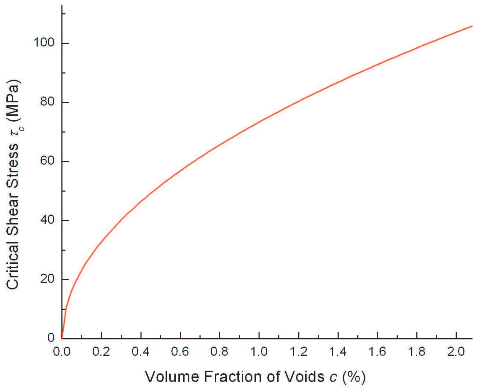

Figure 7.8: The dependence of the plane glide resistance in terms of critical shear stress on the volume fraction of nano-voids for an edge dislocation in neutron irradiated bcc iron.

Figure 7.8 shows the dependence of the plane glide resistance in terms of the critical shear stress on the volume fraction of nano-voids for edge dislocations in neutron irradiated bcc iron. The number of vacancies contained in one single nano-void is specified to be fifteen, in view of MD[112] and MC[113] simulations indicating that small vacancy cluster-complexes are highly mobile and only a small faction (about 10%) of the stable vacancies is distributed within the range of a loose complex of vacancies in correlated neighboring locations that may coalesce~~s~~ to form one relatively large three-dimensional vacancy cluster.

When it comes to comparing ~~compare~~ the critical resolved shear stress value obtained from Equation 7.41 with a measured uniaxial yield strength, a conversion factor, namely the Taylor factor, must be applied. The average value of the Taylor factor is 3.06 for equiaxed bcc and fcc metals[115].

In an effort to interpret the observed increase in the critical shear stress for plastic deformation due to neutron irradiation, two mechanisms were proposed. ~~contributions to the increase of strength of the irradiated material.~~ First ~~On the one hand~~, the original dislocation structure present in the crystal will be pinned down by the defects produced during irradiation. A clear example in neutron-irradiated Mo single crystal is shown in Fig. 8, where dislocations are locked by small clusters with a very small separation. Notice also that there is a distribution of loops in the rest of the crystal matrix, but at a lower density and larger spacing. Trinkaus et al. [16] have recently ~~lately~~ reviewed the conditions for this dislocation decoration and arrived at the conclusion that the direct clustering of SIAs or vacancies in a region near the dislocation cannot be due to three-dimensional diffusion and agglomeration of single SIAs, but rather that the decoration is produced by the accumulation of one-dimensionally migrating glissile loops, that were produced originally in the cascades. MD simulations [14,17,18] have actually demonstrated this one-dimensional motion. The clusters remain in a metastable state near to the dislocation and can only be absorbed by it after a thermally activated [16,19,20] or elastic force field-induced [21] change in Burgers vector direction.

The second contribution is attributed to ~~will come from~~ the unlocked source dislocation that will then multiply and interact with the distribution of defect clusters present in the matrix of the crystal which are separated at a much larger distance; for the crystal taken as an example in the above discussion the mean distance in the matrix $L = (Nd)^{-1/2} \sim 280$ nm, a factor of about one hundred times larger than the value for dislocation locking. It has been shown [3,15] that the hardening by this defect structure is well represented by the dispersed obstacle model [22], where the increase of strength, beyond the upper yield point, compared to the unirradiated state, is given by

$$\Delta\tau = \alpha\mu b(Nd)^{1/2}, \tag{7.45}$$

where α is a factor that accounts for the strength of the obstacle. It was found [3] that in the irradiated Cu single crystals there is a linear relation between the measured values of $\Delta\tau$ and $(Nd)^{1/2}$ with a resultant value of a $\alpha = 0.1 - 0.2$, which describes soft obstacles. It should be pointed out that these measurements were performed in the yield region. Beyond it, as it is further discussed in Section 3.3, the contribution from dislocation-dislocation interaction to the work hardening is the main component of the flow stress. Furthermore, for higher dose levels, where only a yield region at approximate constant stress level (see Fig. 7) is observed, $\Delta\tau$ reflects the resistance to dislocation motion in the channels.

7.4.2 INTERACTION BETWEEN A STRAIGHT EDGE DISLOCATION AND SIA CLUSTER DECORATIONS

It has been shown by both experiments and computer simulations that the Frank-Read sources are decorated by small SIA clusters during neutron irradiation. These clusters are produced directly in the multi-displacement cascades and small SIA clusters are extremely mobile, which have been demonstrated by MD simulations (see the preceding chapters). Using PDD method, Ghoniem et al. investigated the dynamics of a expanding Frank-Read source dislocation interaction with sessile SIA clusters in dislocation decoration[116]. In the present study, the same method is extended to a more realistic case where the spatial and dimensional distribution of clusters that are trapped in the strain field of the dislocation form dislocation decoration are obtained from KMC simulations.

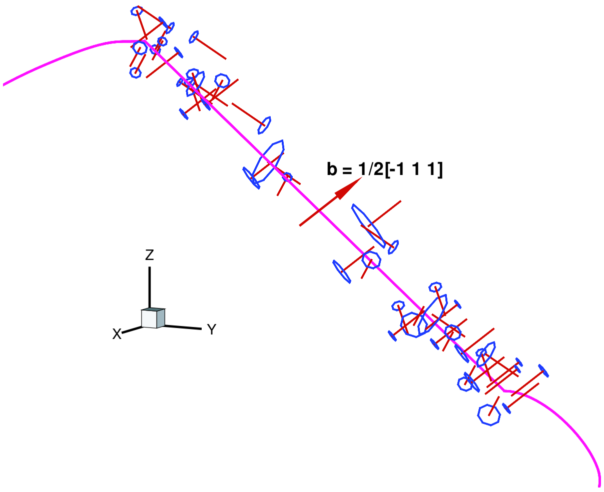

Figure 7.9: Spatial distribution obtained by KMC simulations for SIA loops that are ~~is~~ in the region of decoration of the dislocation loop in bcc iron irradiated to a dose of 5.2×10^{-3} dpa at 300 K.

The configurations obtained by KMC simulations at a variety of dose levels are used as typical distributions of SIA clusters in decorations to consider the interaction between ~~an~~ a moving straight edge dislocation and the full field of multiple decoration clusters. For example, Figure 7.9 shows the spatial distribution of SIA loops in the region of decoration, which is extracted from the result of KMC simulations in Figure 6.5(b). It is noted that a number of the decorating clusters have Burgers vectors different from that of the dislocation in Figure 7.9. This deviation from a perfect dislocation decoration structure is ~~attribute~~ attributed to the event that a virtually immobile complex may be formed when two (or more) clusters of different oriented Burgers vectors join due to the mutual attraction[86]. The immobile complexes can grow further due to the interaction with other SIA clusters. To determine the magnitude of collective resistance of clusters, systematic PDD simulations for the dynamics of interaction between SIA clusters and the dislocation are performed. The clusters are assumed to be perfect prismatic dislocation loops, (the same as what has been adopted in KMC simulations), and their elastic field is calculated ~~by~~ using Kroupa's [50] formulas for infinitesimal loops. The edge dislocation with Burgers vector $\mathbf{b} = \frac{1}{2}[\bar{1}11]$ is gliding on the (101) plane. A Uniaxial tensile stress along the [100] direction ~~of different magnitude are~~ is applied to determine the value of $\sigma_1 1$ required for the dislocation to overcome the barrier. As the edge dislocation moves in the elastic field of SIA clusters, each point on the dislocation line is subject to a resistive (or attractive) force. This means that in order to move further, a higher stress will have to be applied, so that the dislocation could be pulled out of this local environment. It also implies that increase in the yield stress would be expected for the initiation of the plastic flow. When the dislocation is locked ~~in~~ from the distributed clusters, it has to adjust its shape to accommodate ~~to~~ the strain filed of clusters. The particular section of the dislocation in the vicinity of clusters acts like a vibrating string. Figure 7.10 shows a close view of the detailed dynamics of the collective cluster interaction with a moving edge dislocation, where the configuration of cluster is transferred from Figure 7.9. When the applied tensile stress reaches to a critical value, which depends on the specific distribution of clusters at corresponding dose levels, with the assistance of inertial effect as well as self-forces resulting from local curvatures, the dislocation can finally break through the collective cluster field.

The results for the increase in yield stress $\Delta\sigma_{11}$ due to the interaction between dislocation and clusters in decoration are shown in Figure 7.11 as a function of dose level. The estimations of resistance imposed by the distributed vacancy clusneed a better figure

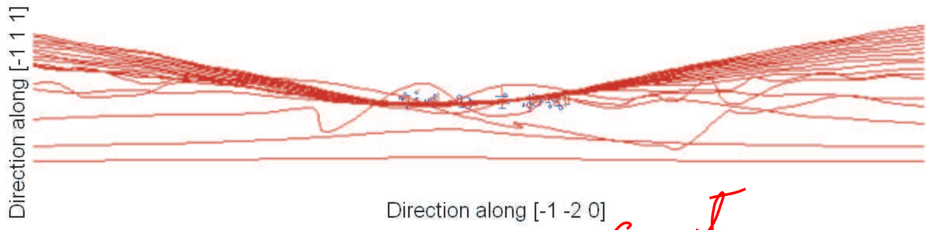

Figure 7.10: Dynamics of an edge dislocation ~~interaction~~ Interacting with a distribution of SIA clusters in bcc iron. The Burgers vector of the dislocation is $\mathbf{b} = \frac{1}{2}[\bar{1}11]$, and the configuration of clusters is produced by KMC simulations, as in Figure 7.9.

ters (approximated as nano-voids) are provided as well. The ~~combining~~ combined effects of both decoration clusters and nano-voids of current calculations are compared with the experimental results for pure iron irradiated and test at 70 °C[9]. At a dose level of 1×10^{-4} dpa, the current result shows a very good match ~~the~~ with experimental ~~datum~~ data. As the radiation dose increases, the contribution from decoration clusters (source hardening) and nano-voids (distributed barriers) both increase. This is consistent with the development of the ~~microstructures~~ microstructure, namely, that the density of nano-voids keeps increasing and the decoration along the dislocation line continuously builds up. The present model predicts a little larger $\Delta\sigma_{11}$ compared with the experimental results at a higher dose level of 5.2×10^{-3}. One possible cause could be attributed to the coarseness of the model that estimates the glide resistance of distributed vacancy clusters. Indeed, the density of vacancy clusters are assumed to be a simple linear function of irradiation dose rate in the current model. This assumption may be rational at very low dose levels. As radiation damage proceeds, There are more and more defects occurring in the unit volume of materials, which means that the interaction and reaction between defects become stronger and more ~~frequently~~ frequent. Annihilation, absorption, and agglomeration of vacancy clusters change the spatial and size distribution of ~~them~~ defects. To obtain an accurate description regarding the distribution of vacancy clusters, detailed dynamic simulations may be preferred to be carried out for the evolution of ~~vacancies~~. vacancy clusters

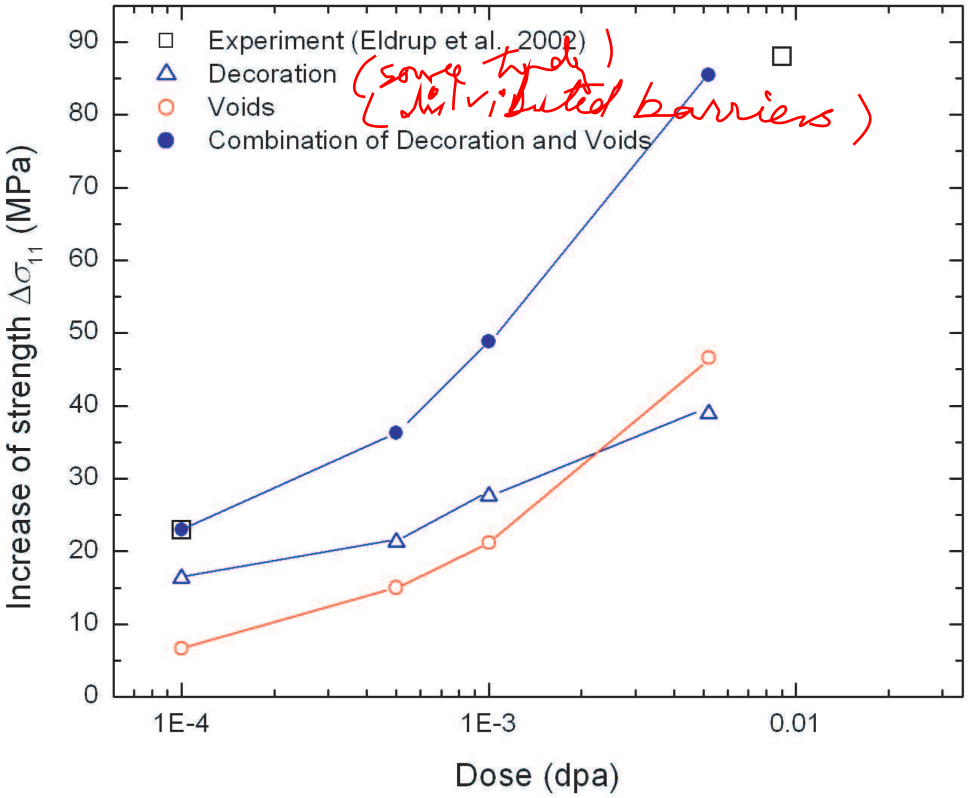

Figure 7.11: Dose dependence of the increase in yield stress due to the interaction with clusters in decoration as well as ~~the~~ distributed vacancy clusters (nano-voids) in bcc iron irradiated at 300 K. Numerical results are compared with the experimental data of pure iron irradiated and tested at 70 °C[9].

It is also noted that the interaction between the dislocation and SIA clusters in decorations contributes more to the increase of yield stress than the glide resistance of nano-voids at low dose levels (< 10^{-3} dpa). At 1×10^{-4} dpa, the interaction between the dislocation and decoration SIA clusters makes up ~~a~~ the major part the increase of yield stress. Its contribution, however, decreases in proportion to that of the distributed nano-voids as the irradiation dose increases. At 5.2×10^{-3} dpa, the increase of yield stress due to ~~the impediment of~~ nano-voids ~~to dislocation motion~~ has exceeded that due to the SIA clusters in decoratio~~n~~s. It implies that at high dose levels, plane glide resistance due to distributed vacancy clusters (distributed barriers) may play a more significant role in modifying the plastic deformation behavior of irradiated materials than the SIA clusters in decoration region (i.e. source hardening).

7.5 VELOCITY OF EDGE DISLOCATIONS IN NEUTRON-IRRADIATED BCC IRON

The Interaction of dislocations with SIA clusters in the decoration region, as well as interstitial clusters dragged by moving dislocations, affects the glide behavior of dislocations dramatically, and thereby alter~~s~~s the microstructure evolution and microscopic~~al~~ plastic deformation behavior of materials. As far as the dynamics of a dislocation is concerned, it is not only the geometric~~al~~ shape that is taken by a dislocation interacting with other defects and microstructures, but also the mobility of dislocation in different scenarios. Of particular interest in this context are the dislocation interaction with SIA clusters, the mobility of clusters and the influence of the dragging effect on dislocation velocity. In this section we present the result of PDD simulations of dislocation velocity, ~~with~~ taking into account interactions between a gliding edge dislocation and decoration formed by small interstitial clusters. The conditions ~~settings~~ for the moving edge dislocation and interstitial clusters in the current simulation are the same as those employed in Section 7.4.2 for the case at a dose of 5.2×10^{-3} dpa, and the drag effect discussed in Section 7.3 is applied as well.

The applied external stress as a function of time is shown in Figure 7.12. Initially, a constant uniaxial tensile stress along [100] of $\sigma_{11} = 30$ MPa is suddenly

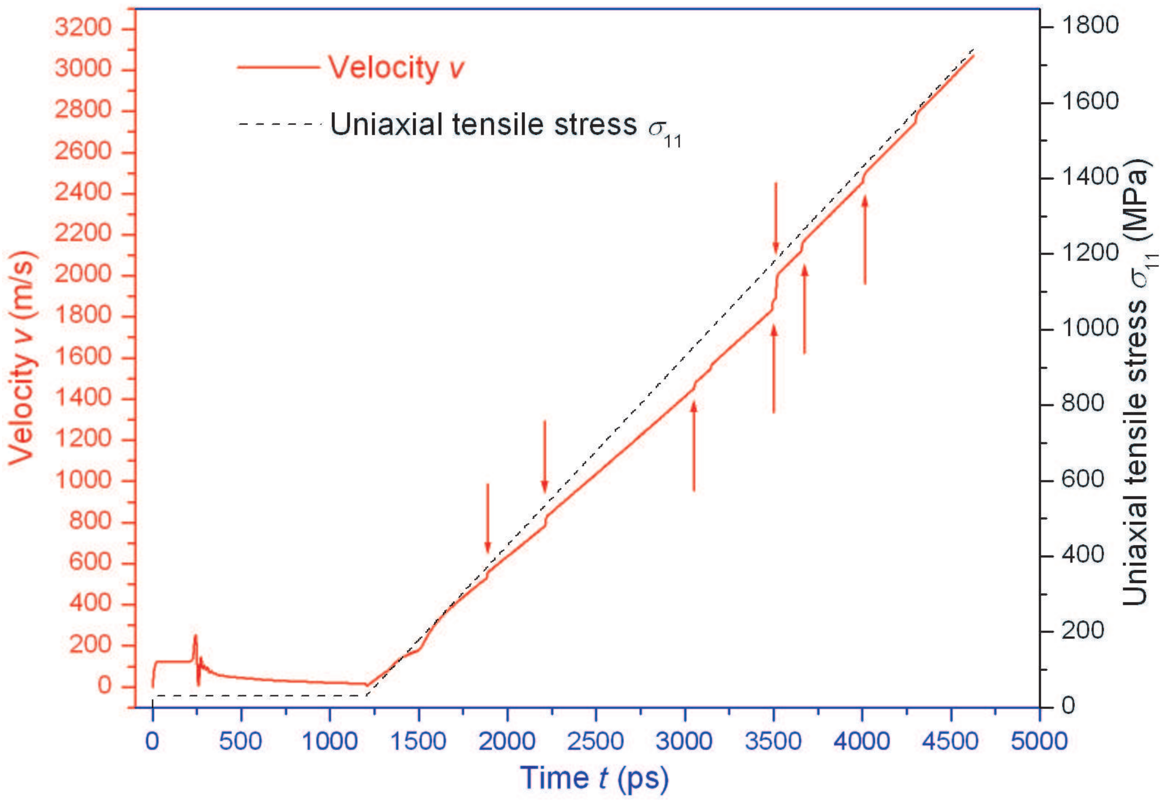

Figure 7.12: Time dependence of dislocation velocity in bcc iron under applied uniaxial tensile stress for an edge dislocation interacting with SIA clusters in decorations~~, penetrating through decoration atmosphere and breaking away from dragged interstitial clusters~~. Vertical arrows indicate velocities at which certain dragged clusters detach~~ed~~ from the moving edge dislocation.

applied and kept for 1.4 nanosecond. The stress σ_{11} is then gradually increased at a constant rate of 0.5MPa/ps. The time dependence of the edge dislocation's velocity is presented in Figure 7.12 as well. As soon as the stress is applied, the velocity of the edge dislocation increases from zero to a stable value of around 120 m/s within 30 ps. The dislocation motion is not affected by the strain field of the interstitial clusters located ahead of its moving path when the distance between them is still rather large. As the dislocation comes closer to the interstitial clusters, the interaction between them keeps increasing and starts affecting the dislocation velocity. The fluctuation on the velocity-time line in Figure 7.12 indicates that the interaction between the edge dislocation and the clusters is quite intensive, and the edge dislocation vibrates back and forth like a string. Once the dislocation line segment is completely submerged into the atmosphere of interstitial clusters, its velocity decreases to nearly zero and remains trapped by the force field of clusters because the applied stress is not high enough to release it from the atmosphere (see Figure 7.11 for the critical value of applied stress). When the applied stress ~~starts being~~ is increased, and then exceeds the critical value required to unlock the dislocation from the cluster atmosphere, The velocity of the edge dislocation begins to grow accordingly. The released dislocation ~~is travelling~~ Travels with some of the clusters in The decoration, whose Burgers vectors are parallel the the glide plane of the dislocation. When the dislocation velocity reaches a certain values $v_{\max}$ presented in Table 7.1, the force exerted on the corresponding interstitial cluster is no longer able to provide the force required to ~~make the cluster be~~ dragged the cluster ~~moving~~ with the dislocation. As a result, the interstitial cluster is then discarded by the moving dislocation. ~~The~~ cap Breakaway of the dislocation from ~~the~~ dragged interstitial clusters results in part of the resistance provided by the dragged clusters to dislocation motion suddenly vanishing and a reduction in the effective drag coefficient, and the dislocation velocity therefore acquires ~~a~~ an abrupt jump. The steps on the velocity-time line marked by vertical arrows in Figure 7.12 clearly show~~s~~ the abrupt increases in dislocation velocity as the dislocation breaks away from the dragged clusters. The changes in slope at different stages in the velocity-time plot indicate ~~reflect the~~ a reduction of the resistance force to dislocation motion due to dragged clusters.

It is worth ~~being pointed out~~ noting that the stress-time line in Figure 7.12 resembles the time dependence of dislocation velocity if the dislocation and the matrix material are perfectly clean, and inertial effects of the moving dislocation ~~is~~ are completely ignored. The results of current simulations present a more accurate and realistic consideration for motion of dislocations in irradiated materials. The dynamic behavior associated with ~~the~~ drastic changes in the dislocation velocity may be important in investigating the microstructure evolution and plastic deformation in irradiated materials.

When the applied stress exceeds the average glide resistance in any slip plane in which there are mobile dislocations, large-scale slip becomes possible. We have split the influence of radiation-induced defects on dislocation motion into two parts, namely that due to nano-voids and that resulting from dislocation decoration, and investigated them respectively. The impediment of distributed nano-voids to the motion of the ~~gliding~~ dislocation is taken into account in terms of the plane glide resistance. The Velocity of an edge dislocation as a function of time under different applied uniaxial tensile stresses σ_{11} larger than the plane glide resistance is presented in Figure 7.13 for bcc Fe irradiated to a dose of 5.2×10^{-3} dpa, provided dislocation interaction with interstitial clusters in the decoration is ignored.

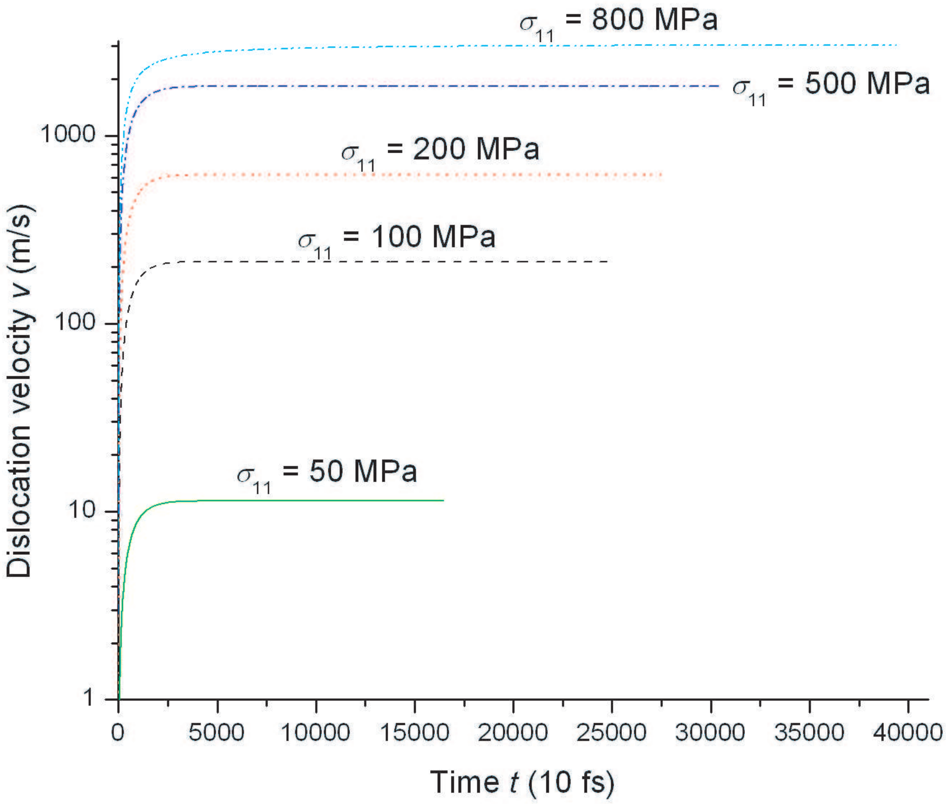

Figure 7.13: Velocity of an edge dislocation as a function of time under different applied uniaxial tensile stresses σ_{11} larger than the plane glide resistance due to randomly distributed nano-voids in bcc Fe irradiated to a dose of 5.2×10^{-3} dpa.

Table 7.1: Values of B_{loop} predicted by Equation 7.37 and v_{max} obtained from Equation 7.38 for an edge dislocation to break away from the dragged loops.

Loop size (number of SIAs)	$\text{B}_{\text{loop}}(\mu\text{Pa}\cdot\text{s})$	$v_{\text{max}}(m/s)$
8	1.048	2120.902
5	0.7867	2744.461
180	7.001	8202.532
10	1.201	7211.216
47	3.086	5934.538
42	2.881	7353.640
9	3.378	1822.291
6	2.638	4581.404
4	0.6866	1547.468
9	1.126	6315.763
5	0.7867	2454.282
7	2.898	34856.379
34	2.533	6284.055
9	1.126	10577.672
9	1.126	3698.463
8	3.144	526.698
9	1.126	3879.120
28	2.250	10737.560
9	3.378	1891.479
9	3.378	782.097
8	1.048	1450.169
13	1.409	1830.918

super sonic ? ?

CHAPTER 8

CONCLUSIONS and Summary of Thesis contributions

Understanding and predicting the mechanical ~~performances~~ behavior of metals and alloys under neutron irradiation conditions require ~~a~~ detailed ~~understanding~~ knowledge of both the materials microstructure as it evolves during irradiation and the connection between the microstructure ~~features~~ and mechanical properties. The motion of fast thermally-activated, one-dimensionally migrating SIA clusters, and their interaction with each other and with dislocations result in a number of interesting microstructure features, and consequently changes in the mechanical behavior. An approach to KMC simulations that incorporates the elastic interaction between various components of the microstructure has been developed. The main purpose of this approach is to investigate the evolution of spatial heterogeneities in the microstructure of irradiated materials. The model evolves atomic configurations by identifying their thermally activated atomic jump events and implements a probabilistic scheme for their subsequent execution. In applying the KMC method to the investigation of radiation-induced microstructure evolution, the likelihood that an SIA cluster migrates from one lattice site to another depends upon its local atomic configuration which can be characterized by an activation energy and a jump attempt frequency. The SIA cluster is approximated as an infinitesimal prismatic dislocation loop and the interaction energy with all other neighboring loops, vacancies and dislocations is calculated. The energy difference between the current position and a tentative one is evaluated and utilized to modify the activation energy of the corresponding jump event. The simulation first deduces the set of jump probabilities for every allowed jump event using precalculated activation energies and then executes jumps according to their relative probabilities. After a jump is executed, time is advanced by a computational time step determined by the residence time of the system, i.e. the reciprocal of the sum of the jump rates for all the allowed jump events of the system. This process is then repeated until the time between designated displacement cascades is exhausted. A new displacement cascade is then introduced and the algorithm iterated. By using this new approach to KMC, the interaction among defect clusters and microstructures that is crucial for studying microstructure evolution and was absent from existing KMC simulations has been integrated. The parallelized KMC enables a realistic simulation of the evolution of radiation-induced damage.

Computer algorithm

The KMC model has been applied to the investigation of point defect segregation and damage accumulation under cascade irradiation in bcc Fe. The following features are in agreement with experimental observations: (1) the overall sessile SIA cluster density, its dose dependence and eventual saturation, (2) the formation of dislocation decoration, (3) the "autocatalytic" formation of SIA cluster rafts, their Burgers vector orientation and lower mobility.

The importance of glissile SIA clusters produced in displacement cascades has been demonstrated to play a decisive role in the irradiation-induced microstructural evolution. The 1-D motion of glissile SIA clusters and the interaction between defects and the dislocation microstructure were shown to be the main cause for the appearance and development of decorations and rafts. At a rather low dose around 1.0×10^{-3} dpa, a large portion of the initially glissile clusters are shown to be trapped around the slip dislocation loop (the majority of them are distributed near the edge component) and become virtually immobile. The high concentration of SIA loops around slip dislocations results in an extremely inhomogeneous spatial distribution. the simulations quantitatively show how SIA clusters are attracted to dislocations to decorate and lock them in place. The present work suggests that raft formation can be achieved by prismatic glide of glissile interstitial clusters and rotation of their Burgers vectors under the influence of internal strain fields (e.g. generated by dislocations).

The parametric dislocation dynamics method was modified by adding an effective mass term to the EOM of dislocation to take into account inertial effects of moving dislocation, and used to investigate~~d~~ the increase in the yield stress due to dislo~~cat~~ions' interaction with interstitial loops in the ~~dislocation~~ decoration region, and with distributed nanoscale voids. The mass of a dislocation is evaluated in terms of the kinetic energy of a dislocation moving at a uniform velocity ~~with~~ in analogy ~~to~~ with its counterpart in mechanics. Observed radiation-induced increases in the yield stress in tensile tests ~~was~~ were investigated from two perspectives: (1) the plane glide resistance due to distributed nano-voids, and (2) dislocation interaction with SIA clusters in the decoration region. The former effect was investigated b~~y~~ using Friedel statistics for a random distribution of point-like obstacles, and the latter was examined by performing parametric dislocation dynamics simulations. The combination of the above two effects was compared with experimental measurements and a reasonably good agreement was shown. The study in this thesis indicates that at low damage dose levels, dislocation interaction with radiation-induced interstitial clusters in the dislocation decoration region is the main mechanism for the increase in yield strength, while at higher dose levels, ~~the~~ impediment ~~to~~ of dislocation motion by randomly distributed obstacles ~~seems to be in ascendant~~ dominates. The influence of radiation-induced defect clusters on dislocation mobility has also been investigated using dislocation dynamics simulations. Future work will focus on ~~the~~ continued improvement of simulation methods and the coupling of the techniques and analysis present in this thesis with large scale computer simulations to predict microstructure evolution in irradiated materials.

References

[1] Douglas S. Billington and James H. Crawford, Jr. *Radiation Damage in Solids.* Princeton University Press, Princeton, New Jersey, 1961.

[2] M. O. Hagler and M. Kristiansen. *An Introduction to Controlled Thermonuclear Fusion.* Lexington Books, Lexington, MA, 1977. p. 16.

[3] T. Kammash. *Fusion Reactor Physics.* Ann Arbor Science, Ann Arbor, MI, 3rd edition, 1977. p. 21 and 351.

[4] W. M. Stacey, Jr. *Fusion Plasma Analysis.* Wiley and Sons, New York, 1981. p. 225.

[5] W. M. Stacey, Jr. *Fusion: An Introduction to the Physics and Technology of Magnetic Confinement Fusion.* Wiley and Sons, New York, 1984. p. 88.

[6] D. J. Rose and M. Clark, Jr. *Plasma and Controlled Fusion.* MIT Press, Cambridge, MA, 1961. p. 228.

[7] L. Spitzer, Jr. *Physics of Fully Ionized Gases.* Interscience, New York, 1956. p. 88.

[8] B. N. Singh, D. J. Edwards, and P. Toft. Effects of neutron irradiation on mechanical properties and microstructures of dispersion and precipitation hardened copper alloys. *J. Nucl. Mater.*, 238(2-3):244–259, 1996.

[9] M. Eldrup, B. N. Singh, S. J. Zinkle, T. S. Byun, and K. Farrell. Dose dependence of defect accumulation in neutron irradiated copper and iron. *J. Nucl. Mater.*, 307-311:912–917, 2002.

[10] A. W. McReynolds, W. Augustiniak, M. McKewon, and D. B. Rosenblatt. Neutron irradiation effects in Cu and Al at 80 °K. *Phys. Rev.*, 98(2):418–425, 1955.

[11] T. H. Blewitt, R. R. Coltman, R. E. Jamison, and J. K. Redman. Radiation hardening of copper single crystals. *J. Nucl. Mater.*, 2(4):277–298, 1960.

[12] B. N. Singh, A. J. E. Foreman, and H. Trinkaus. Radiation hardening revisited: role of intracascade clustering. *J. Nucl. Mater.*, 249(2-3):103–115, 1997.

[13] B.N. Singh, A. Horsewell, and P. Toft. Effects of neutron irradiation on microstructure and mechanical properties of pure iron. *J. Nucl. Mater.*, 271-272:97–101, 1999.

[14] M. Victoria, N. Baluc, C. Bailat, Y. Dai, M. I. Luppo, R. Schaublin, and B. N. Singh. The microstructure and associated tensile properties of irradiated fcc and bcc metals. *J. Nucl. Mater.*, 276:ii4–122, 2000.

[15] D. J. Bacon, F. Gao, and Osetsky Y. N. The primary damage state in FCC, BCC and HCP metals as seen in molecular dynamics simulations. *J. Nucl. Mater.*, 276(2):1–12, 2000.

[16] B. von Guerard, D. Grasse, and J. Peisl. Structure of defect cascades in fast neutron irradiated alumium by diffuse X-ray scattering. *Phys. Rev. Lett.*, 44(4):262–265, 1980.

[17] D. Grasse, B. von Guerard, and J. Peisl. fast neutron irradiation of molybdenum studied by diffuse X-ray scattering. *J. Nucl. Mater.*, 120(2-3):304–308, 1984.

[18] R. Rauch, J. Peisl, A. Schmalzbauer, and G. Wallner. Correlation of interstitials within defect cascades in Al(Zn) and Cu observed by diffuse X-ray scattering. *J. Nucl. Mater.*, 168(1-2):101–108, 1989.

[19] T. Diaz de la Rubia and M.W. Guinan. New mechanism of defect production in metals: a molecular-dynamics study of interstitial-dislocation-loop formation in high-energy displacement cascades. *Phys. Rev. Lett.*, 66(21):2766, 1991.

[20] A. J. E. Foreman, C. A. English, and W. J. Phythian. Molecular dynamics calculations of displacement threshold energies and replacement collision sequences in copper using a many body potential. *Phil. Mag. A*, 66(5):655–669, 1992.

[21] A. J. E. Foreman, C. A. English, and W. J. Phythian. The molecular dynamics simulation of irradiation damage cascades in copper using a many body potential. *Phil. Mag. A*, 66(5):671–695, 1992.

[22] A. F. Calder and D.J. Bacon. A molecular dynamics study of displacement cascades in Alpha-iron. *J. Nucl. Mater.*, 207:25–45, 1993.

[23] W. J. Phythian, R. E. Stoller, A. J. E. Foreman, A. F. Calder, and D. J. Bacon. A comparison of displacement cascades in copper and iron by molecular dynamics and its application to microstructural evolution. *J. Nucl. Mater.*, 223(3):245, 1995.

[24] R. E. Stoller, G. R. Odette, and B. D. Wirth. Primary damage formation in bcc iron. *J. Nucl. Mater.*, 251:49–60, 1997.

[25] Y. N. Osetsky, M. Victoria, A. Serra, S. I. Golubov, and V. Priego. Computer simulation of vacancy and interstitial clusters in bcc and fcc metals. *J. Nucl. Mater.*, 251:34–48, 1997.

[26] N. Soneda and T. Diaz de la Rubia. Defect production, annealing kinetic and damage evolution in α-fe: an atomic-scale computer simulation. *Philos. Mag. A*, 78(5):995–1019, 1998.

[27] J. L. Brimhall and B. Mastel. Neutron irradiated molybdenum-relationship of microstructure to irradiation temperature. *Radiat. Effects*, 3:203–215, 1970.

[28] J.O. Stiegler and E.E. Bloom. Void formation in irradiated nickel 270. *Rad. Eff.*, 8(1-2):33, 1971.

[29] J. Bently, B. L. Eyre, and M. H. Loretto. High temperature neutron irradiation damage in molybdenum. In *Fundamental Aspects of Radiation Damage in Metals*, pages 925–931, Gatlinburg, TN, 1975. US-ERDA Conference 751006.

[30] H. Trinkaus, B. N. Singh, and A. J. E. Foreman. Mechanisms for decoration of dislocations by small dislocation loops under cascade damage conditions. *J. Nucl. Mater.*, 249(2-3):91–102, 1997.

[31] A. J. E. Foreman and J. D. Eshelby. Atomic energy research establishment report. Technical Report R4170, 1962.

[32] R. S. Barnes. The migration of large clusters of point defects in irradiated materials. *J. Phys. Soc. Japan*, 18, Suppl. III:305–311, 1963.

[33] B. L. Eyre, D. M. Maher, and A. F. Bartlett. Neutron irradiation damage in molybdenum part v. mechanisms of vacancy and interstitial loop growth during post-irradiation annealing. *Phil. Mag. A*, 24:767–797, 1971.

[34] V. K. Sikka and J. Moteff. Damage in neutron-irradiated molybdenum : (I). characterization of as-irradiated microstructure. *J. Nucl. Mater.*, 54:325–345, 1974.

[35] J. H. Evans. Void swelling and irradiation-induced void shrinkage in neutron irradiated molybdenum and TZM. *J. Nucl. Mater.*, 88:31–41, 1980.

[36] K. Yamakawa and Y. Shimomura. Defects in fission-neutron irradiated Mo at high temperature in the JOYO reactor. *J. Nucl. Mater.*, 155-157:1211–1216, 1988.

[37] B. N. Singh, J. H. Evans, A. Horsewell, P. Toft, and D. J. Edwards. Microstructure and mechanical-behavior of TZM and Mo-5-percent Re Alloys irradiated with fission neutrons. *J. Nucl. Mater.*, 223(2):95–102, 1995.

[38] B. N. Singh, J. H. Evans, A. Horsewell, P. Toft, and G. V. Muller. Effects of neutron irradiation on microstructure and deformation behaviour of mono- and polycrystalline molybdenum and its alloys. *J. Nucl. Mater.*, 258-263:865–872, 1998.

[39] A. H. Cottrell. *Dislocations and Plastic Flow in Crystals.* Oxford University Press, London, 1953.

[40] M. Kiritani. Point defect processes in the defect structure development from cascade damage. *Mater. Sci. Forum*, 15-18:1023–1045, 1987.

[41] S. Kojima, T. Yoshiie, and M. Kiritani. Defect structure evolution from cascade damage in14 mev neutron irradiated nickel and nickel alloys. *J. Nucl. Mater.*, 155-157:1249–1253, 1988.

[42] Y. Satoh, I. Ishida, T. Yoshiie, and M. Kiritani. Defect structure development in14 mev neutron irradiated copper and copper dilute alloys. *J. Nucl. Mater.*, 155-157:443–448, 1988.

[43] C. H. Woo and B. N. Singh. Production bias due to clustering of point defects in irradiation-induced cascades. *Phil. Mag. A*, 65(4):889–912, 1992.

[44] M. J. Makin. Long-range forces between dislocation loops + dislocations. *Phil. Mag.*, 10:695, 1964.

[45] A. K. Seeger. On the theory of radiation damage and radiation hardening. In *Proceedings of The Second United Nations International Conference on The Peaceful Uses of Atomic Energy*, volume 6, pages 250–273, Geneva, September 1958. United Nations, New York.

[46] E. Orowan. In *Symposium on Internal Stresses in Metals and Alloys*, page 451. Institute of Metals, London, 1948.

[47] P. M. Kelly. Progress report on recent advances in physical metallurgy. iii. the quantitative relationship between microstructure and properties in two-phase alloys. *Int. Metall. Rev.*, 18:31–36, 1973.

[48] J. Friedel. *Dislocations.* Addison-Wesley, Cambridge, MA, 1964.

[49] F. Kroupa and P. B. Hirsch. *Discuss. Faraday Soc.*, 38:49, 1964.

[50] F. Kroupa. Dislocation loops. In B. Gruber, editor, *Theory of Crystal Defects*, pages 275–316, New York, 1966. Academic Press.

[51] S. J. Zinkle and Y. Matsukawa. Observation and analysis of defect cluster production and interactions with dislocations. *J. Nucl. Mater.*, 329-333:88–96, 2004.

[52] J. Huang and N. M. Ghoniem. the dynamics of dislocation intercation with sessile self-interstitial atom (SIA) defect clusters atomospheres. *J. Comp. Mater. Sci.*, 23:225–234, 2002.

[53] T. Diaz de la Rubia. Irradiation-induced defect production in elemental metals and semiconductors: a review of recent molecular dynamics studies. *A. Rev. Mater. Sci.*, 26:613–649, 1996.

[54] Y. N. Osetsky, D. J. Bacon, B. N. Singh, and B. D. Wirth. Atomistic study of the generation, interaction, accumulation and annihilation of cascade-induced defect clusters. *J. Nucl. Mater.*, 307-311:852–861, 2002.

[55] D.G. Doran. Computer simulation of displacement spike annealing. *Rad. Eff.*, 2(4):249, 1970.

[56] J.R. Beeler. *Radiation Effects Computer Experiments*. North-Holland, Amsterdam, 1983.

[57] H.L. Heinisch. Simulating the production of free defects in irradiated metals. *Nucl. Instrum. & Meth. in Phys. Res. B*, 102(1-4):47, 1995.

[58] H.L. Heinisch and B.N. Singh. Stochastic annealing simulation of differential defect production in high energy cascades. *J. Nucl. Mater.*, 232(2-3):206, 1996.

[59] M. Jaraiz, G.H. Gilmer, J.M. Poate, and T.D. de la Rubia. Atomistic calculations of ion implantation in si: Point defect and transient enhanced diffusion phenomena. *Appl. Phys. Lett.*, 68(3):409, 1996.

[60] N. Metropolis, A.W. Rosenbluth, M.N. Rosenbluth, A.H. Teller, and E. Teller. Equation of state calculation by fast computing machines. *J. Chem. Phys.*, 21:1087, 1953.

[61] A. B. Bortz, M. H. Kalos, and J. L. Lebowitz. A new algorithm for monte carlo simulation of ising spin systems. *J. Comput. Phys*, 17(1):10, 1975.

[62] H. Metiu, Y.-T. Lu, and Z. Zhang. Epitaxial-growth and the art of computer-simulations. *Science*, 255(5048):1088, 1992.

[63] A.F. Voter and J.D. Doll. Dynamical corrections to transition state theory for multistate systems: Surface self-diffusion in the rare-event regime. *J. Chem. Phys.*, 82:80, 1985.

[64] Y.-T. Lu, P. Petroff, and H. Metiu. Growth-kinetics simulation of the al-ga self-organization on (100) gaas vicinal surfaces. *Appl. Phys. Lett.*, 57(25):2683, 1990.

[65] H. C. Kang and W. H. Weinberg. Kinetics of precursor-mediated ordering of two-dimensional domains. *Phys. Rev. B*, 38(16B):11543, 1988.

[66] C. C. Battaile and D. J. Srolovitz. A kinetic monte carlo method for the atomic-scale simulation of chemical vapor deposition: application to diamond. *J. Appl. Phys.*, 82(12):6293, 1997.

[67] R. Siems. *Phys. Stat. Sol.*, 30:645, 1968.

[68] R. Bullough and J.R. Hardy. *Phil. Mag.*, 17:833, 1968.

[69] C.S. Hartley and R. Bullough. On the description of crystal defects by point-force arrays. *J. Appl. Phys.*, 48:4557, 1977.

[70] Kröner E. *Phys. kondens. Materie.*, 2:262, 1964.

[71] C. Teodosiu. *Elastic Models of Crystal Defects.* Editura Academiei, Bucuresti; Springer-Verlag, New York, 1982.

[72] P. Ballone, W. Andreoni, R. Car, and M. Parrinello. Equilibrium structures and finite temperature properties of silicon microclusters from ab initio molecular-dynamics calculations. *Phys. Rev. Lett.*, 60(4):271, 1988.

[73] Yu. N. Osetsky, D. J. Bacon, A. Serra, B. N. Singh, and S. I. Golubov. Stability and mobility of defect clusters and dislocation loops in metals. *J. Nucl. Mater.*, 276:65–77, 2000.

[74] H.L. Heinisch, B.N. Singh, and T. Diaz de la Rubia. Calibrating a multimodel approach to defect production in high energy collision cascades. *J. Nucl. Mater.*, 212-215:127, 1994.

[75] M. J. Caturla, N. Soneda, E. Alonso, B. D. Wirth, T. Diaz de la Rubia, and J. M. Perlado. Comparative study of radiation damage accumulation in cu and fe. *J. Nucl. Mater.*, 276:13, 2000.

[76] N. M. Ghoniem. Curved parametric segments for the stress field of 3-d dislocation loops. *Transactions of the ASME, J. Eng. Mater. Tech.*, 121(2):136, 1999.

[77] N. M. Ghoniem and L. Z. Sun. Fast-sum method for the elastic field of three-dimensional dislocation ensembles. *Phys. Rev. B*, 60(1):128, 1999.

[78] N. M. Ghoniem, B. N. Singh, L. Z. Sun, and T. Diaz de la Rubia. Interaction and accumulation of glissile defect clusters near dislocations. *J. Nucl. Mater.*, 276:166–177, 2000.

[79] J.D. Eshelby. The determination of the elastic field of an ellipsoidal inclusion, and related problems. *Proc. Roy. Soc. Lond. A*, 241:376, 1957.

[80] H. L. Heinisch and B. N. Singh. Stochastic annealing simulation of intracascade defect interactions. *J. Nucl. Mater.*, 251:77–85, 1997.

[81] T. Diaz de la Rubia and M. W. Guinan. New mechanism of defect production in metals: a molecular-dynamics study of interstitial-dislocation-loop formation in high-energy displacement cascades. *Phys. Rev. Lett.*, 66(21):2766–69, 1991.

[82] H.L. Heinisch. Computer simulation of high energy displacement cascades. *Radiat. Eff. Def. Solids*, 113:53, 1990.

[83] D.J. Bacon and T. Diaz de la Rubia. Molecular dynamics computer simulations of displacement cascades in metals. *J. Nucl. Mater.*, 216:275, 1994.

[84] N. Soneda and Diaz de la Rubia. Migration kinetics of the self-interstitial atom and its clusters in bcc Fe. *Phil. Mag. A*, 81(2):331–343, 2001.

[85] R. E. Stoller. priviate communication, 2002.

[86] Yu. N. Osetsky, A. Serra, and V. Priego. Interactions between obile dislocation loops in Cu and α-Fe. *J. Nucl. Mater.*, 276:202–212, 2000.

[87] D. Rodney and R. Phillips. Structure and strength of dislocation junctions: an atomic level analysis. *Phys. Rev. Lett.*, 82(8):1704, 1999.

[88] D. Rodney and G. Martin. Dislocation pinning by glissile interstitial loops in a nickel crystal: A molecular-dynamics study. *Phys. Rev. B*, 61(13):8714–8725, 2000.

[89] G. J. Ackland, D. J. Bacon, A. F. Calder, and T. Harry. Computer simulation of point defect properties in dilute fe-cu alloy using a many-body interatomic potential. *Phil. Mag. A*, 75(3):713–732, 1987.

[90] H. Trinkaus, B.N. Singh, and A.J.E. Foreman. Impact of glissile interstitial loop production in cascades on defect accumulation in the transient. *J. Nucl. Mater.*, 206(2-3):200, 1993.

[91] F. Gao, G. Henkelman, W. L. Weber, L. R. Corrales, and H. Jonsson. Finding possible transition states of defects in silicon-carbide and alpha-iron using the dimer method. *Nucl. Instr. and Meth. B*, 202:1–7, 2003.

[92] B. N. Singh and S. J. Zinkle. Defect accumulation in pure fcc metals in the transient regime: a review. *J. Nucl. Mater.*, 206:212–229, 1993.

[93] C. Depres, C. F. Robertson, and M. C. Fivel. Low-strain fatigue in 316l steel surface grains: a three dimensional discrete dislocation dynamics modelling of the early cycles. part-1: Dislocation microstructures and mechanical behaviour. *Phil. Mag. A*, 84(22):2257, 2004.

[94] Hussein M. Zbib and T.D. Rubia. A multiscale model of plasticity: Patterning and localization. *Society of Materials Science of Japan*, A:341, 2001.

[95] Z. Q. Wang, R. J. McCabe, N. M. Ghoniem, R. Lesar, A. Misra, and T. E. Mitchell. Dislocation motion in thin cu foils: Comparison between computer simulation and experiment. *Acta. Materialia*, 52(6):1535–1542, 2004.

[96] Yu.N. Osetsky, A. Serra, B.N. Singh, and S.I. Golubov. Structure and properties of clusters of self-interstitial atoms in fcc copper and bcc iron. *Phil. Mag. A*, 80(9):213, 2000.

[97] N. de Diego, Y. N. Osetsky, and D. J. Bacon. Mobility of interstitial clusters in alpha-zirconium. *Metall. Mater. Trans. A*, 33A(3A):783–789, 2002.

[98] M. Wen, N. M. Ghoniem, and B. N. Singh. Dislocation decoration and raft formation in irradiated materials. *Phil. Mag. A*, 85(22):2561–2580, 2005.

[99] B. N. Singh, D. J. Edwards, S. Tähtinen, P. Moikanen, P. Jacquet, and J. Dekyser. Final report on in-reactor tensile tests on ofhc-copper and cucrzr alloy. Technical Report Risø-R-1481(EN), Risø National Laboratory, Roskilde, Denmark, October 2004.

[100] Y. N. Osetsky, D. J. Bacon, Rong. Z., and B. N. Singh. Dynamic properties of edge dislocations decorated by interstitial loops in α-iron and copper. *Phil. Mag. Letters*, 84(11):745–754, 2004.

[101] T. Diaz de la Rubia, H. M. Zbib, T. A. Khraishi, B. D. Wirth, M. Victoria, and M. J. Caturla. Multiscale modelling of plastic flow localization in irradiated materials. *Nature*, 406(24):871–874, 2000.

[102] N.M. Ghoniem, S.-H. Tong, and L.Z. Sun. Parametric dislocation dynamics: A thermodynamics-based approach to investigations of mesoscopic plastic deformation. *Phys. Rev. B*, 61(2):913, 2000.

[103] Z. Rong, Y. N. Osetsky, and D. J. Bacon. A model for the dynamics of loop drag by a gliding dislocation. *Phil. Mag. A*, 85(14):1473–1493, 2005.

[104] N.M. Ghoniem, J. Huang, and Z. Wang. A new covariant-contravariant vector forms for the elastic field of parametric dislocations in isotropic crystals. *Phil. Mag. Lett.*, 82(2):55, 2002.

[105] J.P. Hirth and J. Lothe. *Theory of Dislocations.* Wiley, New York, 2nd edition, 1982.

[106] U. F. Kocks, A. S. Argon, and M. F. Ashby. *Thermodynamics and Kinetics of Slip*, volume 19 of *Progress in Materials Science.* Pergamon Press Inc., New York, 1st edition, 1975.

[107] F. C. Frank. On the equations of motion of crystal dislocations. *Proc. Phys. Soc. A*, 62:131–134, 1949.

[108] J. Weertman. High velocity dislocations. In P. G. Shewmon and V. F. Zackay, editors, *Response Of Metals To High Velocity Deformation*, volume 9, pages 205–247. Interscience Publishers: New York, 1961.

[109] D. Rodney and G. Martin. Dislocation pinning by small interstitial loops: A molecular dynamics study. *Phys. Rev. Lett.*, 82(16):3272–3275, 1999.

[110] Y. N. Osetsky, D. J. Bacon, A. Serra, S. I. Bachu, and S. I. Golubov. One-dimensional atomic transport by clusters of self-interstitial atoms in iron and copper. *Phil. Mag. A*, 83(1):61–91, 2003.

[111] F. C. Frank and W. T. Read. Multiplication processes for slow moving dislocations. *Phys. Rev.*, 79(4):722–723, 1950.

[112] R. E. Stoller. The role of cascade energy and temperature in primary defect formation in iron. *J. Nucl. Mater.*, 276:22–32, 2000.

[113] B. D. Wirth and G. R. Odette. Kinetic lattice monte carlo simulations of cascade aging in iron and dilute iron-copper alloys. In V. V. Bulatov, T. D. de la Rubia, P. Phillips, E. Kaxiras, and N. M. Ghoniem, editors, *MRS Symposium Proceedings on Multiscale Modeling of Materials*, volume 538, pages 211–216, Warrendale, PA, 1999. Materials Research Society.

[114] Y. N. Osetsky, D. J. Bacon, and V. Mohles. Atomic modelling of strengthening mechanisms due to voids and copper precipitates in α-iron. *Phil. Mag. A*, 83(31-34):3623–3641, 2003.

[115] R. E. Stoller and S. J. Zinkle. On the relationship between uniaxial yield strength and resolved shear stress in polycrystalline materials. *J. Nucl. Mater.*, 283-287:349–352, 2000.

[116] N.M. Ghoniem, S.-H. Tong, B.N. Singh, and L.Z. Sun. On dislocation interaction with radiation-induced defect clusters and plastic flow localization in fcc metals. *Philos. Mag. A*, 81(11):2743, 2001.